A functional signature of augmented nasal breathing across the cortex

Student: Geet Vashista

2023

Supervisors:

Dr Christian Thoma, Dr Mangor Pederson and Dr Daniel Shepherd

Division: School of public health and interdisciplinary studies

Lodgement statement: A thesis submitted to Auckland University of Technology in fulfilment of the requirements for the degree Master of Health Science (MHSc)

Abstract

Introduction: This investigation examines the impact of technologically augmented nasal breathing (Goodair Nosebuds) on the executive centers of the human brain. The technology emulates humming through pressure oscillations in the tidal air stream, drawing inspiration from evidence that suggests a calming effect of humming.

Methods: 14 healthy participants (nine females) participated in a 30-minute nasal breathing experiment, which included 5-minute wash-in and wash-out periods before and between two 10-minute sham and active conditions, administered in a randomized crossover, single-blind manner. Data were collected using a 64-channel high-density EEG. Brain data were analyzed using a network/graph theoretical approach with a custom Python pipeline that processed raw data into a 3D brain reconstruction.

Results: Sensor space power spectrum analysis and sensor/source space connectivity analysis Identifying unique activity in the somatosensory cortex and inferior parietal lobes. Additionally, the network assessment of connectivity in source space revealed a significant departure from default mode network activity. Visualizations that were not statistically assessed also supported the aforementioned trend.

Conclusion: The findings of this study align with a profile of multimodal integration. Despite the limited sample size, the variety of analytic techniques employed for convergence and the biological plausibility of the findings lend credibility to the results. The source space results of this project are particularly novel. If these findings are replicated in validation studies, devices like the Goodair Nosebuds could be valuable adjuncts in various neuro-therapeutic interventions.

Contents

List of Figures

List of Tables

Table 1

Table of abbreviations

Abbreviations	Definitions
BIDS	Brain Imaging Data Structure
BOLD	Blood oxygen level dependent
CNS	Central nervous system
DMN	Default mode network
DRG	Dorsal respiratory group
EEG	Electroencephalogram
eLORETA	Exact low-resolution electromagnetic tomography
FDC	False discovery correction
fMRI	Functional magnetic resonance imaging
FT	Four transform
GI	Gastrointestinal
HRV	Heart rate variability
ICA	Independent component analysis
LCMV	Linearly constrained minimum variance
MEG	Magnetoencephalography
MRI	Magnetic resonance imaging
NO	Nitric oxide
PLI	Phase lag index
PLV	Phase lock value
PNS	Parasympathetic nervous system
PRG	Pontine respiratory group
RG	Respiratory groups
RNA	Respiratory sinus arrhythmia
sEEG	Scalp electroencephalogram
VRG	Ventral respiratory group
WPLI	Weighted phase lag index

Note. Abbreviations used throughout this report.

Attestation of Authorship

I hereby declare that this submission is my own work and that, to the best of my knowledge and belief, it contains no material previously published or written by another person (except where explicitly defined in the acknowledgements), nor used artificial intelligence tools or generative artificial intelligence tools (unless it is clearly stated, and referenced, along with the purpose of use), nor material which to a substantial extent has been submitted for the award of any other degree or diploma of a university or other institution of higher learning.

Acknowledgement

I would like to acknowledge all my mentors, many of whom are on this project as my supervisors and many more who are not. I consider every single one's contribution, infinite. I would like to acknowledge all the laboratory assistants I have been fortunate to have, particularly Sopha and Ari. Data acquisition in this project took the set-up of over a thousand electrodes, and because of them, I did not have to do them all alone. I need to acknowledge the greater Biodesign lab team, for their experience and mentorship and this includes my office mates. Laura, who personally cooked and fed me every time she saw me working a long day and not eating. Alberto, who was for months my only constant companion, who would be here every day I worked, and every night, and every weekend.

There are many to whom I feel I owe my work, many whose quiet confidence never faded, even though mine always did. Many who might be unsuspecting of my thanks on the matter. My friends, my family, my dog, he's important. To thank them all properly, I would need to double the length of this document and would still have done it no justice. So I won't even try. But to all of them, to all of you. I thank you. There are, however, a few I would like to make a special note off. 4 specifically. My closest mentors and the ones who were the blood of this work with me.

Dr Christian Thoma, my primary supervisor. From whom I learned my criticality, the careful consideration of a scientist and what someone who breathes these things in and out looks like. He is the best scientist I know, and it was his ever-patient eyes that were cast over all the written work I did. As a deeply dyslexic man, I think the fact that anything I write is even remotely readable is a testament to the heroic efforts Dr Christian Thoma committed. Dr Thoma followed me on every wild idea, on every overzealous ambition and only thought of how to make it work. He kept me grounded in the task at

hand as much as anyone could and has now for years been one of the teachers whose tutelage, I have needed the most. For that and much more, Dr Thoma, thank you.

Dr David White, the inventor behind this work, who alongside Dr Thoma was the father of this project. From Dr White, I learned how to think laterally and how profound insight can come from looking at the same things, if one changes how they look at them. More than once, his positivity and experience reassured me with a confidence that I sorely needed. Dr White gave me my place in the Biodesign lab, whenever we were pressed for resources he would find them, whenever problems from far afield would arise he would settle them, each time without a sound or pause. For that and much more, Dr White, thank you.

I was once told that every scientific department needs a wild man, I think certainly every student should have one as a mentor, mine was Dr Daniel Shepherd. From Dr Shepherd I learned the real world of being a scientist. What a real lab was, what it was like to work hour after hour alone, and how much changes when things written on pieces of paper become happenings in the world. I remember watching a monitor with Dr Shepherd as data came in and talking about questions. There I learned how much meaning was in the most trivial of details, how much can be said about so little and how much isn't said even when so much is. I consider Dr Shepherd my first mentor, as he was the first to choose to work with me and the first to bring me onto this project. His experience and bulldog spirit kept me going for all the hours we needed to work through this project. For that and much more, Dr Shepherd, thank you.

I began by saying the contributions of all my teachers are infinite, and I chose this word carefully. I will never know what intellectual roads I would have walked down had it not been for a chance sentence from one here, or a paper shared by another there. As such, each makes an infinite, immeasurable, contribution to my journey, and are thereby

all equals. But even still one stands distinct. He is my first amongst equals, the most important teacher I have ever had, Dr Mangor Pederson. The field I am in, neuroscience, I am in because of Dr Mangor Pederson. For this project, I was able to go from not knowing what “hello world” was, to writing every line of code used, because of Dr Mangor Pederson. Everything I have, every skill, every result, every equation, all of it, in my opinion, should be put at his feet over anyone else's. When I felt truly lost in the analysis for this project, Dr Pederson worked with me till we were out of the woods. Whenever he could, he would let me work in his office with his computer, the only one I had access to that could handle the source localization of this project. He introduced me to connectivity and graph theory. Taught me EEG and how to code. Dr Pederson is every day the scientist I look up to the most. I consider myself the sum of the efforts of my teachers, in this, Dr Pederson joins everyone mentioned, but he is the one who has had an impact on me more than any other. For that and much more, Dr Pederson, thank you.

Ethical approval

Ethical approval was granted by AUT Ethics Committee under code 21/234.

Chapter 1. Introduction

Breathing exerts a profound influence on brain activity. Neuronal tissue has exceptionally high metabolic demands, necessitating energy production through oxidative phosphorylation (Özugur et al., 2020). Consequently, neuronal firing is intimately linked to oxygen and breathing. Additionally, the brain is bathed in cerebrospinal fluid, with its pH largely determined by CO2 levels, which are in turn dependent on breathing. This relationship is so close that chemoreceptors in the brainstem specifically respond to pH changes and directly contribute to the regulation of breathing (Guyenet et al., 2010). The tight coupling between breathing and the brain is evident in functional magnetic resonance imaging (fMRI), where up to 27% of the signal can be breathing-dependent, often representing the second most significant source of noise after movement (Power et al., 2017). Despite the undeniable links between breathing and the brain, our understanding of breathing's influence on the cerebral cortex remains limited.

A recent surge in breathing research has yielded attempts to both deepen our understanding of breathing and translate those insights into practical neuro-breathing-based therapies. The Goodair Nosebuds represent a recent product arising from this growing knowledge base. This device, worn in the nostrils, functions by introducing continuous agitation to inhaled air during breathing. This agitation could potentially stimulate mechanoreceptors present in the nose and/or mobilize endogenous nitric oxide (NO) into respiratory air (Eby, 2006). The principles behind the device draw inspiration from yogic/meditative breathing practices such as Bhramari pranayama (Ushamohan et al., 2020). While the effects of this device on the brain remain unknown, the proposed mechanisms suggest the potential for broad-ranging impacts.

Although the adaptive effects of augmented breathing on the body are well documented, the same cannot be said for its influence on forebrain structures (Zaccaro et al., 2018). Testing the Nosebuds device presents a unique opportunity to delve into the under-investigated relationship between breathing and brain function. This exploration has the potential to significantly contribute to the growing body of literature on this topic (Herrero et al., 2018). Furthermore, the Nosebuds themselves hold promise as a potential neuro-breathing therapeutic tool, making this an exciting avenue of research for several reasons.

Scope of works and Research objectives

Research question

- How does Nosebuds-augmented breathing functionally affect the cerebral cortex in healthy adults?

Objectives:

This thesis will investigate the effects of the Goodair Nosebuds device on brain function in healthy adults. Specifically, the study will focus on:

- **Functional brain connectivity:** We will examine how normal breathing and augmented breathing (using the Nosebuds device) influence functional connectivity within the cerebral cortex, the higher-order processing center of the human brain.
- **Temporal dynamics:** As functional changes are likely to occur over time, we will employ electroencephalography (EEG) to measure brain activity with high temporal resolution.

- **Cortical activity:** Scalp EEG (sEEG) is well-suited for detecting activity in the cerebral cortex due to its proximity to the brain's surface. This aligns with our research question since the cortex is the highest-order brain region.

Autonomic Data Collection (Not Analyzed in This Report):

While not directly analyzed in this report, we will collect autonomic nervous system (ANS) data to potentially inform future research. This data will include:

- Heart rate variability (electrocardiogram)
- Blood volume pulse (finger clip sensor)
- Skin conductance (electrodes on non-dominant hand fingers)
- Ventilation rate (respiratory belt)

Key concepts and literature review

Breathing: from body to the brain

Breathing impacts the body in numerous ways. Changes in breathing rate affect heart rate, lung movements stimulate thoracic organs, and breathing influences metabolism (Zaccaro et al., 2018). Given the brain's sensitivity, it's reasonable to expect breathing to influence its function. While a comprehensive analysis of all potential breathing-brain connections (bodily, parasympathetic nervous system, and autonomic nervous system) is beyond the scope of this report, we can focus on well-established mechanisms.

For example, functional magnetic resonance imaging (fMRI) shows that breathing accounts for up to 27% of the blood-oxygen-level-dependent (BOLD) signal, highlighting the strong link between breathing and brain activity (Power et al., 2017). This doesn't diminish the potential role of the parasympathetic nervous system (PNS) and autonomic

nervous system (ANS) in breathing-brain interactions, but it provides a clear starting point for this investigation.

The biological need for breathing stems from cellular metabolism. Within cells, mitochondria use oxygen to generate energy through oxidative phosphorylation (distinct from cellular respiration) (Özugur et al., 2020). CO2, a waste product of this process, is eliminated through respiration and ventilation (Brinkman et al., 2023). However, CO2 plays a crucial role beyond waste removal. It helps regulate blood pH through the bicarbonate buffer system, which controls respiratory drive (Hopkins et al., 2023). This system maintains acid-base homeostasis by using a weak acid and base to neutralize changes in pH caused by external factors. Chemically, CO2 reacts with water (H2O) to form carbonic acid (H2CO3), which dissociates into bicarbonate (HCO3-) and hydrogen (H+) ions, as represented by the equation:

$$CO_2 + H_2O \rightarrow H2CO_3 \rightarrow HCO_3^- + H^+$$

Critically, CO_2 is one of the two inputs into this system. Subtle changes within and due to this system are detected by central chemoreceptors, located on the medulla oblongata, and peripheral chemoreceptors, located in the carotid and aortic bodies. While the latter is sensitive to blood O_2, CO_2, and overall pH levels, the former is responsive to CO_2 and pH specifically (Nattie & Li, 2012).

Peripheral chemoreceptors, principally those in the carotid body, will detect a decrease in overall pH and signal back to the central nervous system (CNS) via glomus cells and the 9th cranial nerve, the glossopharyngeal nerve (Iizuka, 2001). Conversely, the central chemoreceptors' position at the floor of the ventrolateral aspect of the medulla (4th ventricle), allows them to detect changes in pH in the cerebrospinal fluid. Depending on conditions, in hypercapnia central chemoreceptors arbitrate 50% to 90% of the

ventilation response and in hypercapnia and hyperoxia the response is almost totally driven by central chemoreceptors (Guyenet et al., 2010; Nattie & Li, 2012). Through this chain, CO_2 modulates blood and cerebrospinal fluid pH and thereby respiratory drive.

CO2 and pH play a crucial role in the Bohr effect, which influences how readily hemoglobin binds to oxygen (Benner et al., 2023). Hemoglobin can bind oxygen at any time, but CO2 and pH levels have an inverse relationship with the formation of oxyhemoglobin. Under conditions of stress or in tissues with high oxygen demand, binding of oxygen to free hemoglobin can be detrimental. When oxygen is limited, such binding could lead to oxygen being carried away from tissues that need it most. The Bohr effect prevents this by hindering the scarce oxygen already present in tissues from binding with free or recently freed hemoglobin. This optimizes the offloading of oxygen into tissues that require it for proper function.

This is particularly important for the brain, which has high metabolic demands. At rest, the brain consumes approximately 20% of the body's oxygen, with neuronal tissue specifically accounting for 75-80% of that (Clarke & Sokoloff, 1999). With 18% of all cardiac output dedicated to meeting these needs, the brain's vulnerability to stroke and hypoxia (oxygen deprivation) is understandable (C.-Y. Xing et al., 2017).

While neuronal tissue can engage in glycolysis (energy production without oxygen), its massive energy demands also necessitate oxidative phosphorylation, which relies on oxygen (Özugur et al., 2020). Therefore, breathing directly impacts brain function due to the brain's unique metabolic needs. Breathing mechanics can also affect the brain in less direct ways. For example, diaphragmatic breathing has a relationship with the gut. The diaphragm's movement provides rhythmic stimulation to the gastrointestinal (GI) tract (Hamasaki, 2020; Kocjan et al., 2017).

The gut itself houses the enteric nervous system (ENS), often referred to as the "second brain" due to its similarities to the central nervous system (CNS) in terms of neuronal types and neurotransmitters (Carabotti et al., 2015). However, this term is misleading as the ENS is structurally distinct from the CNS. The gut-brain axis refers to the well-established connection between the gut and the brain (Ochoa-Repáraz & Kasper, 2016). The ENS communicates with the CNS via the vagus nerve (part of the parasympathetic nervous system) and prevertebral ganglia (part of the sympathetic nervous system) (Breit et al., 2018). The diaphragm's location directly above the digestive organs means its movement exerts force on the lower esophagus, stomach, duodenum, liver, and spleen (Hamasaki, 2020; H. Liu et al., 2023). This stimulation is believed to improve GI function, and diaphragmatic breathing is recommended for individuals with various GI issues (Eherer et al., 2011; Halland et al., 2016; Peper et al., 2017).

This suggests a potential indirect pathway from breathing mechanics to the nervous system via the gut-brain axis. While this is beyond the scope of the present report due to its speculative nature, it's an important area for further research (readers can refer to Liu et al., 2023 for more information). If the findings of this report reveal specific physiological profiles, such a mechanism could be one of many contributing factors to the observed effects.

The nose.

Nasal breathing is of importance to this report as it is a key component of adaptive breathing while also being the physical interaction point of the experimental device. The nose forms the base of an anatomically distinct breathing chain separate from that of the chain for food and the mouth (Mankowski & Bordoni, 2023). When ventilating through the nose, air passes through the nose into the pharynx, then to the trachea, and into the bronchi and alveoli (Bilo et al., 2012). When eating, food passes through the mouth and

the back of the throat into the esophagus and to the stomach (Kumar et al., 2020). Although common, with 30 - 50% of adults mouth breathing, it is considered maladaptive, leading to oral/dental issues, and deformities of the craniofacial and stomatognathic system (Nowak et al., 2019).

This is problematic as nasal breathing performs vital functions optimizing respiration. Unlike in mouth breathing, the bones and mucus of the nose provide filtration of particles, protecting the lower airway (Schwab & Zenkel, 1998). The nose also humidifies ventilated air to optimize respiration (Mankowski & Bordoni, 2023). Additionally, the nose controls the temperature of ventilated air, also contributing to respiration optimization (Lindemann et al., 2002). The nose also provides additional adaptive contributions to breathing. For example, during exhalation, nasal breathing increases resistance through friction which slows ventilation, preventing alveoli from collapsing further, thus contributing to respiration optimization (Russo et al., 2017).

The nose also has an intimate relationship with the diaphragm. Travisan et al. (2015) investigated muscle recruitment during nasal vs. mouth breathing in 76 healthy adults. Their findings suggested that mouth breathing resulted in decreased diaphragm amplitude and lower accessory breathing musculature recruitment, particularly during rapid inspiration. This indicates that mouth breathing utilizes less of the total volume of the lungs and is less efficient. An issue with this study, however, is the disregard of posture. Mouth breathers were commonly observed with a forward head posture, which creates a mechanical disadvantage of some accessory breathing musculature. Therefore, this could be causing the failure to recruit the proper musculature for breathing and could be leading to the poor volume utilization observed in mouth breathers. The link between breathing and posture has further been explored by Jung et al. (2016).

The maxillary sinuses of the nose also contain Nitric Oxide (NO). NO is a colorless, water-soluble, and lipid-soluble gas that impacts nearly all the tissues of the body, a property for which it won the "Molecule of the Year" award by the American Association for the Advancement of Science (AAAS journal) in 1992 (Koshland, 1992). NO's odd number of electrons makes it highly reactive, leading to its wide range of impacts on the body (Lancaster, 2015). The synthesis of NO in the body is done through several means, but in the nose, it is primarily done by a lining of endothelial cells in the maxillary sinuses (Lundberg & Weitzberg, 1999). Part of the inspiration for the Goodair Nosebuds was the unique impact of humming on NO in the nose. Air in the peripheral sinuses is typically static, but humming provides a mechanical stimulus that brings static NO into ventilated air, which can then impact and be absorbed by the lower pulmonary system (Eby, 2006; Lundberg & Weitzberg, 1999; Weitzberg & Lundberg, 2002). This occurs to some extent even when not humming. Critically, any effects of inhaled endogenous NO would be absent when orally breathing, as this does not stimulate maxillary NO at all. In the event of an active condition effect, NO therefore forms a particularly interesting possible mechanism of effect both for its direct impact on neuronal tissue and for its wider effects in the body. Additionally, this line of thinking only pertains to gaseous nitric oxide; its solubility means that it may be present in a non-gaseous state, dissolved in tissues in other forms, and this is not accentuated here (Abramson et al., 2001).

The olfactory nerve and the nasal bulb are also sites of interest. The olfactory nerve is the first cranial nerve and one of two originating from the cerebrum (Helwany & Bordoni, 2023, p. 1). Its axons are present on the roof of the nasal cavity, located on the underside of the cribriform plate. On the superior side of the plate, above the nasal cavity is the nasal bulb, which forms the keystone of this neural chain, enabling the perception of scent and flavor (Mori et al., 1999). Along with cranial nerves two and eight, the

olfactory nerve is one of only three cranial nerves considered entirely afferent (Helwany & Bordoni, 2023). It is also only sensitive to chemical stimulation. The nasal bulb itself, unlike other systems such as visual, auditory, and somatosensory perception, is not contralateral but ipsilateral, meaning the two olfactory nerves, one arising from each hemisphere, do not cross and innervate the nasal bulb on the same side of the brain as they arise from. If the experimental condition is found to have an effect, due to proximity, this nerve is one of the first candidates as the likely path of device effect.

Finally, respiratory sinus arrhythmia (RSA) is notable here. While possibly having a mirror in the higher orders of the brain (touched on in later sections), RSA refers to the alteration of heart rate variability (HRV) based on ventilation (Soos & McComb, 2023). This phenomenon is believed to be driven primarily by the Vagus nerve, the tenth cranial nerve. This nerve originates from the brainstem and forms the core of the ANS (Kenny & Bordoni, 2023, p. 10). As such, RSA is a direct example of a known instance of breathing modulating brain function on the temporal scale of seconds. With the utilization of this phenomenon, HRV is considered optimized (most responsive) at a rate of 5 - 6 bpm (van der Zwan et al., 2015). This cadence has since been dubbed resonance breathing (Chaitanya et al., 2022).

Nasal patency may also be of interest to this project. At a given time, in mammals, it is normal for one nostril to be less obstructed than another, with this alternating on the order of hours in humans (Kahana-Zweig et al., 2016). The utility of such a function is debated, with some suggesting it to be important for particulate filtration and others that it is important for infection prevention. What is known is the mechanism behind this phenomenon, which is blood flow, specifically, an increase in blood flow to the erectile tissue of the nasal septum causing enlargement (Proctor & Andersen, 1982). Nasal patency is intimately linked to autonomic function, with a study by Sinha et al. (2021)

finding that pulmonary function and heart rate increased significantly during right nostril breathing. This makes nasal patency interesting as a peripheral impactor of the brain-breathing relationship, but it also has a direct impact on the brain, being linked to lateralization of brain function. The hypothesized link here implicates visuomotor areas of the brainstem, which also communicate with the hypothalamus (Amoroso et al., 1954). Consequently, nasal patency could inform breathing-based neuronal activity higher in the brain, such as the cortex.

Breathing and the brain

The brain can be organized in several ways. Typically, the largest parts of the brain are considered the cerebral cortex, midbrain, cerebellum, and brainstem, laid out from superior to inferior (Nowinski, 2011). These regions each exhibit properties making them both anatomically and functionally distinct. Importantly, however, although often thought of in mechanical terms, like the components of a machine, they are inseparably linked in their function. For this report, the structures in all but the cerebellum are pertinent.

Breathing is primarily driven by the pre-Bötzinger complex (preBötC) in the brainstem (J. C. Smith et al., 1991). This resides in the medulla oblongata, is bilateral, and is believed to be responsible for ventilation in mammals (Muñoz-Ortiz et al., 2019). Damage to this structure is observed to correlate with distortions of breathing to the point of death (McKay & Feldman, 2008). The preBötC is also a member of the greater respiratory group, a series of three regions in the brainstem that exert control over breathing (Ikeda et al., 2017). The group is made up of the ventral respiratory group (VRG), of which the preBötC is a part, the dorsal respiratory group (DRG), and the pontine respiratory group (PRG), which is superior in the pons. In function, all these areas contribute to the respiratory drive and are all necessary for normal human breathing. A

note: occasionally, a fourth group is added to this list, the parafacial respiratory group, however, due to its proximity and congruity with the VRG for this report, these structures, such as the lateral parafacial nucleus and the ventral parafacial nucleus, are considered part of the VRG (Pisanski & Pagliardini, 2019; Powell, 2006).

The location of these three structures is also interesting due to their surroundings. For example, the VRG and DRG are both situated ventral and dorsal, respectively, of the nucleus accumbens (Lucas-Neto et al., 2013). The nucleus accumbens serves as one of the roots of the vagus nerve and is largely responsible for ANS function. One such function is the mediation of HRV and is therefore a key anatomical component of the RSA phenomena. The PRG, conversely, is situated anterior to the 4th ventricle, which houses the aforementioned chemoreceptors of the brainstem (Dutschmann & Dick, 2012). This proximity is reflective of the link between the chemoreceptors and breathing (Nattie & Li, 2012).

There is also clear evidence of higher-order brain structures involved in the breathing process independent of these regions (Schottelkotte & Crone, 2022). The motor cortex, which mediates voluntary movement, was observed by Colle and Massion (1958) as also exerting direct control over the diaphragm. A finding that has since been corroborated (Aminoff & Sears, 1971; Gandevia & Rothwell, 1987; Lipski et al., 1986). Motor cortex control is actioned directly through the phrenic nerve, which originates from C3 to C5 and is the primary driver of diaphragm locomotion (Oliver & Ashurst, 2023). Interestingly, the case may be that these areas of the brain otherwise responsible for skeletomuscular movement are using a phrenic nerve to transfer into the forelimb to exert their control (M.-X. Zheng et al., 2018). In context, diaphragm modulation can be likened to the movement of limbs via continuous thought, and this fact acts precursory to all yogic/breathing techniques where individuals are asked to breathe slowly and into their

bellies (Brown & Gerbarg, 2009). This all occurs independently of the respiratory group structures (Ikeda et al., 2017). It is also interesting that diaphragmatic breathing, more than any other type of breathing, is implicated in RSA and HRV modulation (Russo et al., 2017).

The somatosensory cortex is likewise independently involved in breathing (Schottelkotte & Crone, 2022). Typically, this region of the brain allows for conscious perception and has been shown to be responsive to ventilation likely through mechanoreceptors within the trachea down to the lower airways (Davenport & Vovk, 2009). It is not, however, directly responsive to hypercapnia. This likely results from the location of the CNS chemoreceptors dorsal to the PRG and not near the somatosensory cortex itself. Nevertheless, the importance of the somatosensory cortex in the perception of breathing is undeniable.

Additionally, some qualities of breathing are perceived within the insula and cingulate cortex (Schottelkotte & Crone, 2022). Breathing-based activity in this region has been correlated to low tidal volume/respiration rate, hypercapnia, and mechanoreceptor stimulation (Gehrlach et al., 2020; Peiffer et al., 2008; von Leupoldt & Dahme, 2005). Serving similarly to the somatosensory cortex, these structures contribute to the sensation of feeling breathless (Liotti et al., 2001). The proximity to the somatosensory cortex makes this perhaps unsurprising. Critically, these structures also are part of the limbic system, which plays a role in emotional regulation and sensory information processing (Medford & Critchley, 2010; Rolls, 2019). Other structures of the limbic system are directly projected to form the Respiratory group (Evans, 2010).

There are several projection sites to/from the mid/forebrain to the respiratory group structures (Schottelkotte & Crone, 2022). Notably implicated in this are the

structures of the VRG and the PRG. For example, the VRG has been shown to connect to the extended amygdala via a retrograde and anterograde tracing study (Gaytán & Pásaro, 1998). It has been established by viral tracing experiments that the central nucleus of the amygdala makes a monosynaptic projection directly to the preBotC (Yang et al., 2020). The amygdala's importance to fear perception and behaviour may mean that this is the likely neuronal foundation of the strong link between breathing and personal feelings of distress (Šimić et al., 2021). Furthering this point is the relationship of the hypothalamus to the PRG (Krout et al., 2005; Yokota et al., 2016). The hypothalamus is a large midbrain structure with a range of ANS-related duties such as the assessment of predatory threats, handled by the perifornical hypothalamus, the processing of autonomic changes resultant of stress, handled by the dorsomedial hypothalamus, and behaviour responses particularly to cardiac changes, handled by the posterior hypothalamus (Z. Shahid et al., 2023). Both the perifornical and dorsomedial hypothalamus project into the Kölliker-Fuse

nucleus and the parabrachial nuclei of the PRG (Williams & Burdakov, 2008). Beyond this, the hypothalamus at large projects to the periaqueductal grey, a structure intimately related to the PRG (McGovern et al., 2017). Furthermore, this structure itself has been suggested as important to the perception of breathlessness, a sensical threat assessment task for the already threat-sensitive hypothalamus (Ryan et al., 2014).

The hypothalamus is also the production site of two pertinent neuropeptides. These are orexin and vasopressin (Proczka et al., 2021; Stettner & Kubin, 2013). Neuropeptides are a kind of amino acid-based signaling molecule that exhibits a modulatory effect on neural tissue but also affects other tissues across the body (Merighi, 2017). Neuropeptides are the most common type of signaling molecule in the nervous system and typically, as is the case with orexin and vasopressin, bind to G-protein coupled receptors. Orexin operates exclusively in the CNS and is critical for regulating

wakefulness, homeostasis, proper metabolic functioning, and some motivation-oriented behavior (Kuwaki, 2008; Williams & Burdakov, 2008). It also impacts respiration, likely through orexinergic neurons present in all three regions of the respiratory group including the preBoTC, the KöllikerFuse nucleus, and the nucleus of the solitary tract (Gerber et al., 2016). Additionally, orexin exerts a similar effect on the nucleus of the phrenic nerve, situated inferior to the respiratory group structures in the ventral horn of the cervical spinal cord (Young et al., 2005).

Vasopressin is best known for its contribution to electrolyte and water regulation in the kidneys and circulatory system but also contributes to glucose regulation, cardiovascular operations, as well as breathing (Proczka et al., 2021). Vasopressin, in the nervous system, binds to three G-protein sites; V1a, V1b, and V2. It therefore acts as a hormone in the body and as a neuropeptide within the CNS. V1aR is most relevant to breathing given its presence in the lungs and carotid bodies, and in respiratory group structures of the brainstem such as the preBoTC (Jackson et al., 2005; Kc et al., 2002; Kc & Dick, 2010). Increases in Vasopressin have been correlated with changes in ventilation and are thought to play a role in responses to repetitive stressors. Like the G-protein sites needed for Orexin, V1aR sites are also present at the nucleus of the phrenic nerve (Gerber et al., 2016).

Collectively then, breathing demonstrates a clear signature across all brain levels from the base of the brainstem to the crown of the head. Any of these mechanisms are implacable if a device effect is found. While these brain-to-breathing connections are not exhaustive, this has included some of the most pertinent to the present project. For a further exploration of breathing across different brain structures, see Schottelkotte and Crone (2022). The extent of breathing integration in the brain has recently led Heck et al (2017), to suggest that breathing through several sensory sites acts as a slow oscillation

rhythm that modulates temporal neurodynamics. This would indicate breathing as having a global impact across the whole brain resulting in alterations to cognition, experience perception, and behavior.

Brain organization

To grasp the complexity of the highly interconnected brain, it's important to refer to a contemporary brain organization framework. Up to this point, general references to commonly described brain structures have been made; however, the parcellation of the cerebral cortex, the most critical brain component for this report, poses more difficulty in representation. The cerebral cortex tissue is often divided by its location relative to the skull plate it lies beneath (Qiu et al., 2022). This results in the frontal, temporal, parietal, and occipital lobes. While clear, it also disregards neural anatomy and lacks precision. Brodmann (1909) offered a cortex parcellation based on cytoarchitecture, providing a more nuanced and extensive means of inspecting the brain. Today, there are 52 Brodmenn areas, and several have undergone subdivisions.

An important insight within the Brodmann areas was the concept of lateralization. While similar, the areas are not identical across the two hemispheres of the brain (Brodmann, 1909), reflecting the specialization undertaken by brain regions. Significant to this project is the lateralization of neuronal structures pertinent to breathing. In the brainstem and midbrain, all mentioned structures are lateralized, including the phrenic nerve and nucleus of the phrenic nerve (Rogers, 2021). However, the cortex is asymmetric at the anatomical level as captured by Brodmann's original mapping, and therefore, ideal contemporary parcellation maps should also account for this. Another consideration is the lateralization of function.

Lateralization of function refers to the tendency of functional specialization of cell populations between hemispheres (Rogers, 2021). A classical example of functional

lateralization in the brain is Broca's and Wernicke's areas, responsible for language, typically lateralized to the left hemisphere for most right-handed individuals (Jäncke et al., 2021). However, this pattern does not hold for left-handed individuals, and complications arise with multiple language speakers. This reflects the unique neurodevelopmental processes and can also result from brain injury recovery (Martin et al., 2022). Cognitive lateralization of this type is not always clear. However, lateralization due to sensory input is more predictable. This type of lateralization is due to the anatomy of afferent neural pathways in the brain. An example is sight. The optic nerve, cranial nerve two, carries afferent signals from the eyes to the occipital lobes (A. M. Smith & Czyz, 2023). On its path, it crosses over at the optic chiasm, leading information from one eye to the contralateral brain hemisphere. As a result, signals from the right eye are processed in the left occipital lobe and vice versa. While this holds true for optical perception, the olfactory bulb does not cross its afferent pathways. When input from one side of the body is lateralized to the opposite side of the brain, such as in sight, it's referred to as contralateral activity; when not the case, such as the nasal bulb, it's termed ipsilateral activity.

While the Brodmann areas provide a strong neuroanatomical representation of the cortex, they are now considered antiquated (Qiu et al., 2022). The Human Connectome Project (HCP), launched in 2009 as a multinational effort, aims to create useful maps of the brain (Elam et al., 2021). While originally set as a 5-year project, it has since been extended and is yet to be officially completed. Today, the project offers well over a thousand open-access individual datasets consisting of various data types, including neuroimaging modalities and behavioral data. Based on this extensive work, the HCP has offered its own cortex parcellation options, representing the most complete neuroanatomical segregation of the cortex to date (Glasser et al., 2016). Therefore, implementing this parcellation mapping over the whole cortex would result in 360 distinct

brain regions. It's important to keep in mind, though, that this is simply an organizational choice for practicality and understandability. The cortex always operates as an interconnected whole, and it's inappropriate to ever consider it as truly modular. Brodmann himself stressed that the nervous system should only be thought of as an infinitely complex interconnected whole, and these organizational concepts are merely constructs to which nature is indifferent (Brodmann, 1909). To an extent, this holds true for the whole nervous system, and peripheral nervous system structures should be thought of in similar terms.

Electroencephalography

The core of this project aims to address functional brain activity in the cortex. Therefore, the chosen tool here is electroencephalography (EEG). The modern EEG, as used today, was invented in 1924 by Hans Berger, who built upon existing animal research, most notably conducted by Richard Caton (Haas, 2003). The first human EEG observed an oscillation between 10 to 12 Hz, referred to then as the "Alpha rhythm". Subsequently, other oscillatory patterns, both higher and lower, were discovered, which make up the five defined brain waves known today: Delta (0.5 - 4), Theta (4 - 8), Alpha (8 - 12), Beta (12 - 30), and Gamma (>30) (Teplan, 2002). The clinical adaptation of EEG was rapid, with widespread acceptance by 1938.

In 1934, the first epileptiform spikes were identified, and in 1936, interictal spikes were recognized as the principal signature of epilepsy (Louis et al., 2016). Since then, EEG has become a staple of epileptic diagnosis and research (van Mierlo et al., 2019). Early EEG work also examined profiles correlating with brain tumors and other structural abnormalities (Selvam & Shenbagadevi, 2011). Today, EEG has proven useful in identifying and studying neurodegenerative diseases such as Alzheimer's, sleep disorders like narcolepsy, other brain tissue dysfunctions such as cerebral edema and stroke, and

neurodevelopmental disorders such as autism and attention-deficit/hyperactivity disorder, among others (Buettner et al., 2019; Garcés et al., 2022; Keser et al., 2022; Rossini et al., 2020; Slater et al., 2022).

Effect of breathing on brain electrical activity

Slow breathing has been associated with EEG-measured central nervous system (CNS) changes as well. For example, Fumoto et al. (2004) (n = 22) observed an increase in high Alpha wave (>10 Hz, <13 Hz) activity when participants were directed to pace breathing (PB) at 3 to 4 breaths per minute. The same study also reported an improvement in vigor and decreased state anxiety as assessed by the Profile of Mood (POM) subscale (A. Shahid et al., 2011). Similarly, Yu et al. (2011) (n = 15) reported decreased Theta and increased Alpha activity during paced breathing compared to natural breathing. Near-infrared spectroscopy scans showed increased oxygenated hemoglobin in parts of the anterior prefrontal cortex (Brodmann's areas 9 and 10). Behavioral self-reports captured with the POM and State-Trait Anxiety Inventory showed lowered depression, anxiety, anger/hostility, and confusion. Research such as Park and Park (2012) (n = 58) closely aligns with the present project. Here, Alpha activity increased globally, with local decreases in Theta activity in the left frontal, right temporal, and left parietal areas during 10 breaths per minute. This study also assessed cardiovascular functioning with heart rate variability (HRV), reporting a decrease in the LF/HF ratio via an increase in HF.

There are some important limitations to the work to date. Notably, the proposal by Fumoto et al. (2004) presented PB as associated with vigor, based on participants not becoming sleepy when PB was paired with eyes closed vs. natural breathing paired with eyes closed. However, becoming sleepy when naturally breathing with eyes closed is typical, and the presentation of an active task such as PB would require attention, detectable as increased cortical activity. Therefore, the association of PB with vigor could

result from an active experimental condition being paired against a passive control condition. Park and Park (2012) interpreted their results as indicative of increased inward attention. However, this can be misleading for the same reasons that PB, by nature, demands inward attention relative to natural breathing. Support for this claim from the CNS results of this study is also limited due to the global nature of the changes observed along with enduring limitations in the comprehension of the actual biological meaning of brain signal power.

The experiment in this report aligns closely with research on Bhramari pranayama (Bhramari). Bhramari is a yogic breathing practice involving dedicated nasal breathing, humming during exhalation, and the placement of fingers on at least the tragus and the closed eyelids (Ushamohan et al., 2020). Various studies observed changes within EEG brain waves during Bhramari. For example, Prasad et al. (n.d) found a change from Theta to Alpha activity and an increase in Gamma wave power. Works by Jin et al. (2014), Vazquez et al. (2013), and Vialatte et al. (2009) suggested some kind of lateralization of power spectral density activity within the temporal lobes, with Vialatte et al. (2009) most convincingly championing this point using a LORETA source localization algorithm. Vialatte et al. (2009) also found similar results to Prasad et al. (n.d) regarding Theta activity, additionally observing a drop in wave power. Furthermore, Vazquez et al. (2013) and Vialatte et al. (2009) observed a stabilization of the EEG signal within the cortex during exhalation compared to inhalation. Consequently, this effect is similar to that seen in respiratory sinus arrhythmia (RSA), although this phenomenon is observed above the brainstem, rather than below it. This type of respiration-locked oscillation has since been corroborated by subsequent investigations in both humans and other mammals (Herrero et al., 2018). An issue with that study, however, was the use of a phase lock index, which is vulnerable to the volume conduction problem of EEG, explained more in subsequent

sections. The present project will take steps to address this limitation by using a phase lag index instead, thereby building further on this existing work.

Manipulating EEG data

The gold standard for handling EEG data in a study is the bespoke development of an EEG pipeline. This provides total control over every computational operation necessary to derive meaningful deductions from the dataset, from data preprocessing to noise elimination to the specifics of processing for results. The first notable step within an EEG pipeline, after importing data and setting necessary parameters such as line frequency (the frequency at which electricity is delivered), is the organization of raw data. Here, the Brain Imaging Data Structure (BIDS) standardization system is useful. BIDS is a growing industry standard when working with neuroimaging data, allowing for the uniform organization of every component of raw data, including participant information (Pernet et al., 2019). At the point of BIDS standardization, it is also sensible to convert data into a standard data type such as BrianVision. This is another growing industry standard and allows for ease of computation downstream, as well as external inspection of raw data using other processing and visualization packages if desired. BIDS standardization also represents good practice, as a persistent issue in neuroscience is heterogeneity, which makes peer inspection of work difficult. Therefore, any step to uniform data and results is beneficial to scientific discourse within the field at large.

Next, filtering is performed, a common step in all EEG pipelines used to remove data that can reasonably be suspected to be non-brain in origin or noise (Shoka et al., 2019). All filtering within EEG research aims at attenuation, correcting signal amplitude. There are four types of filters utilized in EEG preprocessing: low pass, high pass, band-pass, and notch. Together, they are utilized to address several non-brain origin artifacts detected within an EEG signal.

One such example is line noise, which refers to the signature generated when the sensitive electrodes of an EEG detect electrical current from power lines within walls and powered devices (Shoka et al., 2019). As power is delivered at a predictable amplitude and voltage in developed nations (230/240V at 50Hz in NZ), this signature is easily identifiable on a power spectral density graph of raw EEG (Travel Adaptor for New Zealand, 2019). Its rhythmic and acute nature makes this an excellent target for a notch filter, which attenuates a specified frequency of a signal while leaving the surrounding frequencies relatively unaffected.

A bandpass filter is another common form of filtration used in EEG. This filter combines both the remaining high-pass and low-pass filters (Lemm et al., 2005). Both filters allow frequencies lower or higher than a set threshold to pass unattenuated. Therefore, a band-pass filter identifies the band of frequencies flanked by high-pass and low-pass filters respectively. A high-pass filter attenuates low-frequency noise, which can manifest as a slow drift of a channel signal at the order of seconds. This type of noise can be caused by perspiration on the scalp, movement of electrode wires, and general head movement (Teplan, 2002). A low-pass filter similarly addresses high-frequency noise, which can originate from muscle movement, particularly of the head and neck (Muthukumaraswamy, 2013). This filter is also important to address the issue of aliasing – when a high-frequency signal is detected as a low-frequency one (Epstein, 2003). An example of how this happens is provided in Figure 1.

Figure 1

Aliasing

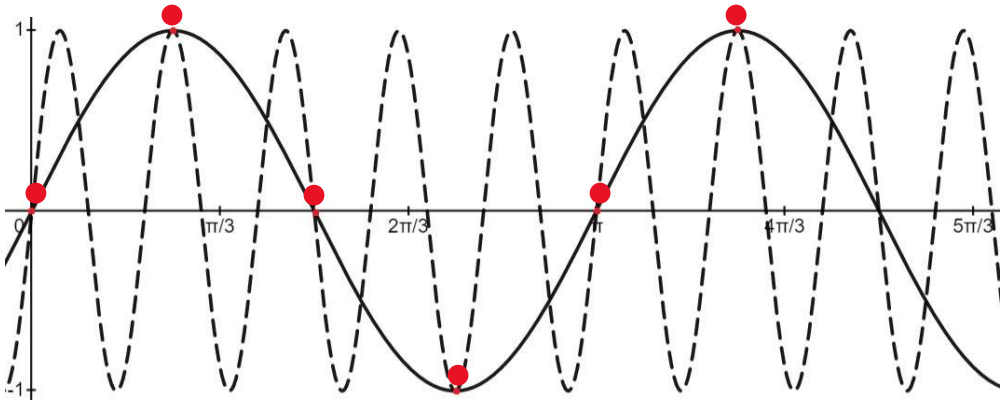

If a hypothetical sampling rate corresponding with the red dots were used, then it is possible that the “real” high-frequency signal represented by the dotted line could be interpreted as a low-frequency signal represented by the solid black line. This is aliasing, and in conjunction with the Nyquist theorem, which states that to accurately interpret a signal it must be sampled at a rate of at least twice that of the target signal, it can be properly accounted for by utilizing low-pass filtering (Por et al., 2019; Teplan, 2002).

EEG filtering typically occurs at two distinct points: at the time of collection, known as offline, and at the time of data preprocessing, known as online. While online filtering is what has been touched on so far, offline filtering is automatic and integrated into EEG amplifiers in the form of a low-pass filter (Shoka et al., 2019). It is important that filtering be one of the first steps performed in the preprocessing phase of data investigation. This is because, for effective filtering, continuous data is advantageous, as more time points can be inspected to determine the particulars of a single. If a high-pass filter is utilized at, for example, 0.5 Hz, this represents a sine wave oscillation of once every 2 seconds, therefore several seconds of data would be required to identify this oscillation accurately.

The next sensible step of a pipeline should be re-referencing. Due to the physics of electricity and current, the electrodes of an EEG detect electrical potentials relative to

a reference point (Lei & Liao, 2017). Consequently, it is important to select this reference point carefully. Typically, during the data collection process, an integrated reference electrode on the EEG cap is used. A somewhat arbitrary choice at the time that is made appropriate by this re-referencing step. The best re-referencing protocol is the use of a virtual average (Yao et al., 2019). This means that the electrical potentials across all electrodes are averaged and then subtracted from each electrode to obtain their specific electric potential values.

Downsampling is also a common necessary step. This is performed primarily to save computational load in later steps of a pipeline (Shoka et al., 2019). This is a late step as the higher temporal resolution is advantageous during filtering and referencing. By downsampling to 200Hz or above, no element of the signal that can be reasonably suspected to be brain activity is lost as this is still well above high gamma frequency, but data is considerably less computationally burdensome. Without such memory management steps, later necessary computations such as for source localization would be different and some, such as whole brain connectivity, impossible.

The primary purpose of preprocessing components of a pipeline is the removal of noise. The core of this task is achieved with an artifact rejection protocol (Shoka et al., 2019). An appropriate tool for this is an independent component analysis (ICA) (Winkler et al., 2011). The principles of this algorithm are best understood with the Fourier transform (FT) (Al-Fahoum & Al-Fraihat, 2014). The FT essentially constitutes any sophisticated spectral signal as a sum of sine waves, see Figure 2.

Figure 2

sum of sine waves

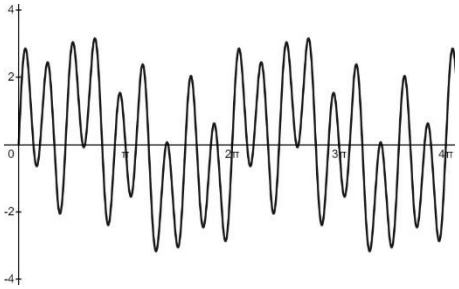

Is the sum of

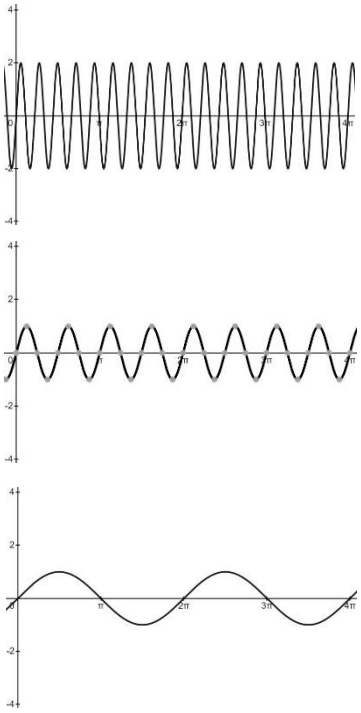

The Fourier Transform (FT) decomposes a signal into its constituent sine and cosine waves of various frequencies. It uses Euler's formula to establish the relationship between a wave's trigonometric and imaginary components, which, when viewed as a clockwise rotation, is accounted for with frequency and time (assuming the signal is time-frequency based). Therefore, expressed as a function, the FT is:

$$\int_{-\infty}^{\infty} g(t)e^{-2\pi ift}\,dt$$

Here, g(t) represents the original signal, e is Euler's constant, f \) is the frequency of the original signal, and t is the time component of the signal of interest. This equation, as written, is the mathematical conceptualization of this transform and is therefore written

for a continuous signal. In practice, however, a signal is discrete, so the equation would be:

$$\frac{1}{t_2 - t_1} \int_{t_1}^{t_2} g(t) e^{-2\pi i f t} \, dt$$

Importantly, the term dt persists, which has the effect of exaggerating the common sinusoidal signals present. This is, in large part, the point of the Fourier transform, but it also leads to errors when not properly accounted for, making appropriate preprocessing critical for proper data interpretation. It's important to note that the Fourier Transform (FT) is distinct from bandpass filtering. While a bandpass filter specifies frequencies of interest, the FT simply identifies what frequencies are present in a signal (Al-Fahoum & Al-Fraihat, 2014).

An Independent Component Analysis (ICA) can utilize an FT or not, but it is always based on these fundamental principles. Acting as a blind source spectrum algorithm, ICA constitutes the spatiotemporal EEG signal as a sum of mathematically independent components (Winkler et al., 2011). By doing this, it is possible for an artifact-specific signal embedded within a recorded signal to be separated. Over time and multiple recording points (electrodes), the artifact will appear with distinct properties as an independent component. Then, this component alone can be excluded without damaging other components. This is a common artifact rejection technique in EEG research, being strong at identifying eye blinks and muscle movement while also providing researchers an opportunity to visually confirm the quality of data (Li & Principe, 2006).

Actual rejection is based on a visual graphical inspection of independent components, scalp topography maps, raster plots, variance over time plots, and phase spectral density plots (Combrisson et al., 2019). Scalp topography maps are inspected for location, particularly around the eyes, and if sources appear outside of the head (Britton et al., 2016). Raster plots are inspected for how commonly appearing a component is across epochs, with sudden and relatively uncommon streaks being likely artifacts. Variance over time is inspected for the quality of the component over the epochs, where isolated variance or high continuous variance could both be indicative of artifacts. Finally, the phase spectral density plot is inspected for the primary frequencies of the IC, where eye blinks likely appear as a low-frequency peak and muscle movement as increasing high-frequency activity.

The final preprocessing step is Epoching, which refers to the separation of the continuous data into discrete sections of interest (Möcks & Gasser, 1984). Usually, this is event or stimulus-locked but can also be done depending on experiment particulars and design. Additionally, good practice at this stage is to visually inspect data as a final sanity check before further processing.

Source localization is necessary to properly address the research question of this project and is relatively uncommon in EEG research (Michel & Brunet, 2019). It can also be thought of as a preprocessing step; however, it is just as often thought of as separate from preprocessing. Here, all the calculations needed to reconstruct the brain signal in a three-dimensional space are performed. This is done through the triangulation of a signal based on the timing between its detection at multiple sensor sites. Consequently, a high-density electrode array, more than 60 electrodes, must be used to have enough sensor sites to triangulate a signal well. Several methods for this exist, with one being a linearly constrained minimum variance (LCMV) beamformer (Hoey et al., 1999). This is a strong

source localization algorithm originally developed for magnetoencephalography (MEG) that yields a relatively high cortex resolution (Bourgeois & Minker, 2009).

The first key element of an LCMV beamformer is its spectral filter. This is the "filter" that inspects an assortment of predefined three-dimensional points to estimate their contribution to a signal at one of the sensor locations moment by moment. To do this, first, a set of spectral weights, a metric corresponding to the particulars of the data inspected in two dimensions (sensor space), must first be prepared. Then, by inverting this matrix and utilizing the predefined voxel volume grid, a time-dependent three-dimensional source localization is produced.

The other component necessary to make this possible is the forward model/operator, which refers to the data required to understand brain tissue within the head volume and the aforementioned predefined voxel volume grid (Miinalainen et al., 2019). This can be done through several means, such as a spherical head model, which represents the layers of the brain as spheres, typically three, within each other (Akalin Acar & Makeig, 2013). Due to the complexity of forward modeling, every approach has critical issues. In the spherical head model, the assumption of the brain as a perfect sphere is known to be incorrect as this is not the actual shape of the brain. It also typically assumes uniform conductivity across every layered sphere, which is also not reflective of real neural tissue. The latter point here is also pertinent to the problem of volume conductivity, which will be touched on shortly.

The best practice when determining a forward operator for an individual is to use a structural, such as an MRI, neuroimage to create a bespoke account of neural anatomy (Henson et al., 2009). When this is not possible or available, an average brain volume can be calculated. This is done by using a set of MRI scans from an open-source repository (fsaverage) to create a template brain (French & Paus, 2015). This can then serve as a

forward operator for all participants and make up the second component needed for source localization. With this and the spectral filter weights, it is possible to create an LCMV filter. For more information on LCMV beamformer construction, see Hoey et al. (1999) and Bourgeois and Minker (2009).

A challenging issue with source reconstruction is attempting to account for volume conductivity (van den Broek et al., 1998). The volume conductivity problem in EEG refers to the issues created by attempting to record charge potentials at a distance from their source. In EEG, this refers to the neuronal potential energies being looked for. Charges that are close to a sensor are referred to as near-field, and distant charges are far-field. Far-field charges reach the sensor through several layers of cell populations with varying conductivity profiles, and this can skew the timing of when a signal from a single source is detected at different sensor locations, the difference between these timings being key for source reconstruction. This is the main issue with attempting to determine subcortical brain activity with an sEEG.

For the present project, while an LCMV beamformer construction is relatively robust against this issue, a few additional steps can be taken to further account for it (Bourgeois & Minker, 2009). Firstly, the EEG tool is not being extended beyond its reasonable means. While EEG can make deeper brain (far-field) estimates of charge (neuronal) activity, the deeper the charge, the more difficult volume conductivity becomes to account for (van den Broek et al., 1998). As such, in this project, the line of inquiry is constrained to the cortex, with that part of the brain, as it represents near-field signals, being well suited for robust data acquisition. Second and more significantly, connectivity is determined by the phase lag index (PLI).

PLI is a popular choice for determining brain connectivity (Stam et al., 2007). “Phase” as a concept pertains to a difference of time between two sinusoidal functions.

"Lag" refers to when a waveform is relatively delayed relative to another waveform, the opposite being referred to as a "lead". The phase lag index within EEG then, is a measure of the phasing lag for an EEG signal over time and sensor locations. It is mathematically written as:

$$PLI = \left| \frac{1}{n} \sum_{t=1}^{n} sgn(Im(e^{i(\phi^j - \phi^k)t})) \right|$$

Here, a signal is represented on the complex plane as a vector, where ϕ^j and ϕ^k represent the vector angle of the sinusoidal functions being inspected. In the case of EEG, this represents the signal at different electrodes. Im represents the transform necessary to extract simply the imaginary component of this vector, sgn represents the sign function which returns a simple pulse or minus 1. The remainder of the equation pertains to the steps necessary for deriving an average across time, and importantly, an absolute value is returned, meaning that the product of this equation is always either 1 or 0.

A key feature of this equation as written is that it ignores the presence of instantaneous phasing (phase lag of 0) or perfect phasing. The reasoning for this is the possibility of the volume conductivity problem. These two types of phasing are ignored by the utilization of the sgn function primarily. For example:

Figure 3

PLI imaginary components

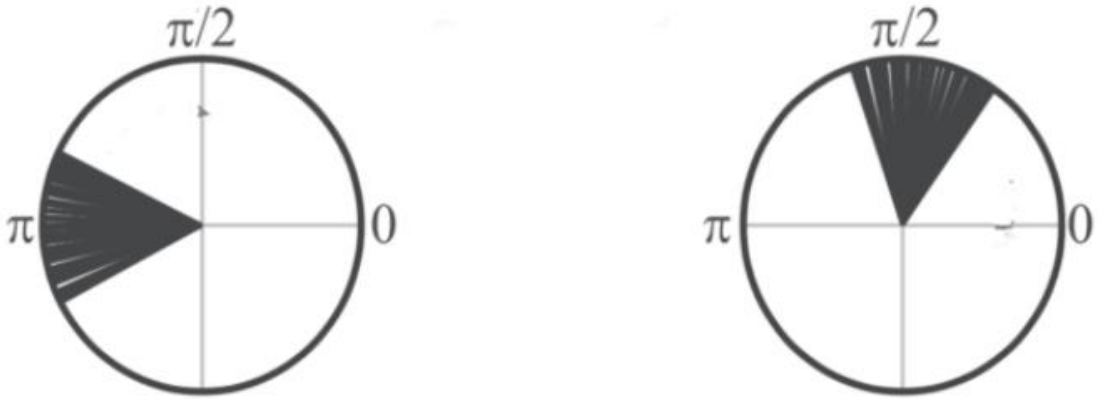

Note. This figure was taken from Cohen (2015) with permission for reuse in this thesis. License data: October 16th, 2023. License number: 5650590948037.

When complex phase vectors are oriented around the real axis (x-axis on a Cartesian plane) as in the first circle, representing their imaginary components as either 1 or negative 1 and then summing this will likely return a 0. In contrast, when these vectors are not oriented around the real axis, such as in the second circle, this effect would not occur, and the return would be 1. It's important to note that since PLI is an absolute value, regardless of the negativity or positivity of the summation of the return of the sign function, when PLI is not 0, it will only ever be 1. PLI's insensitivity to phasing around the real axis (0 and π) is part of what distinguishes it from other phase metrics such as phase locking value (PLV) (Stam et al., 2007).

In practice, however, the weighted phase lag index (WPLI) is arguably more suitable. This allows for the preservation of cross-spectrum data by returning a non-absolute value based solely on imaginary componentry, which is not possible with the binary PLI (Stam et al., 2007). The alternative would be to threshold and use PLI; however, this creates fundamental limitations of its own (Adamovich et al., 2022). The equation for WPLI therefore reads as:

$$wPLI = \frac{\left|\frac{1}{n}\sum_{t=1}^{n} sgn(Im(e^{i(\phi^j-\phi^k)t}))\right|}{\frac{1}{n}\sum_{t=1}^{n}\left|sgn(Im(e^{i(\phi^j-\phi^k)t}))\right|}$$

Where all variables are the same as *PLI* with only the addition of w which refers to weighting (Vinck et al., 2011). wPLI, when applied to brain neuroscience datasets, reflects the communications happening within different parts of the brain. This is then useful when attempting to answer questions such as those proposed in this project. Beyond this, a powerful interpretation tool for wPLI is graph theory.

Graph theory

Mathematically, a graph refers to a representation of a collection of interconnected objects (Sporns, 2016). These objects are termed vertices or nodes, and the interconnections between them are termed edges. A graph, therefore, can be used to represent a range of different data types and real-world systems. The study of these graph objects is designated graph theory and focuses on deciphering the relations emergent in different types of graphs. The implementation of graph theory is used today in computer sciences, economics, psychology, transport logistics, telecommunications, physics, and the modeling of biological systems (Pirzada, 2007).

Graph theory originates from the work of Leonhard Euler (Biggs et al., 1986). In the early 18th century, he provided an analysis of a mathematical problem referred to as the seven bridges of Konigsberg. This problem asks to prove logically if it is or is not possible for a person to return to the mainland of Konigsberg after walking onto its two main islands, having crossed each of the city's seven bridges only once. The logical proof that shows this to be impossible by Euler is the first theorem of graph theory. Euler referred to it as a problem of the geometry of position, which has since both birthed graph

theory and network theory (Mason & Verwoerd, 2006). Critically, the insight Euler showed was that only the relationship between a system's objects was necessary to deduce many complex functions of the greater system without granularly understanding each component individually. This is what makes graph theory a compelling tool to use in biological and brain modeling.

Brain networks naturally lend themselves to representations as graphs (Sporns, 2016). The precise nature of these graphs is, however, contingent on the scale and the biological line of questioning. For example, at the microscale, neurons are a natural fit as nodes and synaptic transmission between them as edges. In contrast, at the global scale, anatomically distant areas are nodes and the relative coherence of a collective signal between such areas, as illustrated through WPLI, for example, are edges. This also pairs well with the point on understanding a system through the relationship of its components rather than exhaustively understanding each component. Collectively then, graph theory allows for the analysis of complex components of the brain, anatomical or physiological, and offers a promise of deep insight even with current technological constraints. Evidence for the brain behaving as a network can be seen in Bassett et al (2018). A brief note: the term graph is the formal designation of these objects in mathematics, but when applied to a real-world system, the term network is often used. This has led to the creation of network theory, which is a large subset of the purer mathematical graph theory. While somewhat distinct from each other, for this report, these terms, graphs, and networks, both refer to brain networks and will be used interchangeably.

Brain networks, as well as networks at large, have several internal properties. For a deeper exploration of this, see Sporns (2016). A few of particular interest are path length and graph topology. A path length refers to the number of steps (edges) needed to bridge two given points in a network. This concept forms the basis of a few graph metrics used

in the present report. Closely linked is topology, which refers to the organization of nodes and edges. The key here is that its topology ignores all other elements of a system save for the relationship of the links between them. A practical example in a brain network can be thought of with a neuronal population that is distinct and communicating with a distant neuronal population through projection pathways, versus a distinct neuronal population communicating to an anatomically adjacent neuronal population. Because in both cases, neuronal populations are communicating directly, they are considered topologically adjacent in both scenarios. What is required, though, for processed data computations is an adjacency matrix. An adjacency matrix is a square matrix of all pairwise connections used to define a finite graph. Therefore, a connectivity matrix is by definition very close to an adjacency matrix and in most neuroscience investigations these two are the same; however, a true adjacency matrix may have been driven from a connectivity matrix by additional steps such as filtering. The present report will adhere to the neuroscience norm, though, and take the WPLI connectivity matrix as the adjacency matrix.

The first notable metrics are Degree and node strength. In theoretical purity, degree represents the number of edges a given node has. As such, it is written mathematically as:

$$k_i = \sum_{j \in N} \alpha_{ij}$$

Where N is the set of all nodes within the network, and α is the connection/s (edge/s) between two nodes. This measure gives a crude overview of interconnectivity within a network (Rubinov & Sporns, 2010). A key issue of this function as presented is that it will count all edges twice, once for α_{ij} and once for α_{ji}. \). But this is easily dealt with using a logical constraint. Here, however, such a step is not necessary because of the

use of WPLI for our connectivity analysis; node strength is a more appropriate metric. Closely correlated with Degree, it represents the sum of edge weights, not just the presence or lack thereof of edges around a node. As such, it is ideal for implementation on our connectivity data. Degree itself is a metric constrained to use only in a binary undirected graph, a limitation shared by node strength, which will not outright destroy the spectral data by forcing a binary input like PLI.

$$k_i^w = \sum_{j \in N} w_{ij}$$

Where all variables are the same as Degree with only the addition of w which refers to weighting.

The next metrics look to address questions of Centrality within a network. First introduced by Bavelas (1950) in the context of social networks, centrality now refers to a quality possessed by a node that provides some topological information regarding its position within a network. Specifically, how "central" it is. For example, a node of high Degree that is situated as to be easily reached (with a short path) from another node would be considered relatively more central. Consequently, such a node would also be a likely stop on many paths taken within the network. This is the property of centrality and its formal constitution of it can be summarized in Freeman (1978) who stated the properties of the central node in a simple 5 node 4-edged hub and spoke graph as being:

1. That the central node has the highest degree possible (connected to all other nodes).

2. It is situated at the shortest path possible between all other nodes.

3. It is situated as close, that is being reachable by the smallest path, to all other nodes as possible.

The application of this concept to real-world networks has birthed several measurements of centrality. Two interesting metrics of centrality are betweenness centrality and eigenvector centrality. Betweenness centrality was first proposed by Freeman (1977), with the intent of capturing how likely a node with the intent of capturing how likely a node (α) will be on the shortest path between a random node pair (β, γ) where the initial node is not part of the pair (α ≠ β or γ). If information in a network travels via the shortest path, then this node, or nodes with high betweenness centrality, exert a disproportionate effect on information following within the network. The mathematical representation of betweenness centrality is:

$$b_i = \frac{1}{(n-1)(n-2)} \sum_{h,j \in N, h \neq j, h \neq i, j \neq i} \frac{\rho_{hj}^{(i)}}{\rho_{hj}}$$

Where ρ is the total steps on the shortest path between to nodes (Rubinov & Sporns, 2010). The use of Betweenness centrality in neuroscience can be seen in (Goodale et al., 2020; Lohmann et al., 2010; Makarov et al., 2018; Pedersen et al., 2023; Soman et al., 2023).

Eigenvector centrality is another measure of centrality. As such, this also measures the influence of a node within a network but whereas Betweenness centrality is entirely contingent on node degree, eigenvector centrality incorporates the degree of adjacent nodes in its assessment of centrality. For example, if a node has only two edges, but both its adjacent nodes each have relatively high degrees, the node will have a high eigenvector centrality.

Eigenvector centrality can therefore be considered a proxy for a node's importance in bridging paths across a network. The mathematical representation of eigenvector centrality is:

$$C_i^E = \frac{1}{\lambda_n} \sum_{j \in N} \alpha_{ij} x_j$$

Where λ is the eigenvalue of a node (Fornito et al., 2016; Newman & Newman, 2018). The use of eigenvector centrality in neuroscience can be seen in (Lohmann et al., 2010; Lorenzini et al., 2023; Oldham et al., 2019; Roberts et al., 2016; Suarez et al., 2022).

Both Betweenness and Eigenvector centrality are revealing of hub nodes. Hub nodes are generally defined as nodes which exert a disproportionate impact on a network. At its simplest, this could be nodes with higher-than-average degrees, however, in real-world networks, having many edges is not informative of the importance of those edges to pathing within the network as a whole. In the present study, this is why both the aforementioned metrics of centrality are being used.

The presence of hubs within a brain network is easily interpretable. Generally, it is neural populations, in the case of this report as defined by regions with high centrality, that are somehow critical for the flow of information through the brain (Freeman, 1978). These areas often act as modulators to the rest of the brain such as the prefrontal/parietal cortex, cingulate gyrus, and the temporal cortex (Zuo et al., 2012). Hubs can also be further specified into types such as connector or provincial hubs (Sporns et al., 2007). For this investigation, such granularity is outside its scope; however, interested readers can turn to Guimera and Amaral (2005), and Rubinvo & Sporns (2010). What is alluded to by this concept is the interplay between network integration vs modularity/segregation.

Separate from hub nodes and measures of centrality is the concept of integration. In both brain networks and as a concept, this refers to the ability of a network to quickly incorporate distributed populations of nodes into a global whole (Rubinov & Sporns, 2010). Typically, this can be assessed by metrics such as global efficiency or characteristic path length. Here, however, the assessment of hub nodes will indicate integration itself, as at the scales expected here (58*58 and 360*360), high centrality nodes are acting as integration sites themselves. The relatively small networks also mean that typical measures of integration may be insensitive and therefore uninformative at this scale. The counter concept of integration is segmentation, which can also independently be assessed for.

Segmentation refers to the performances of tasks within distinct locally interconnected groups of nodes. In a brain network, this can be thought of as an assessment of functionally discrete populations of neurons performing tasks such as in the sensory-motor cortex (Kulkarni et al., 2022). Such groups of cells or node populations are referred to as clusters or modules. Clusters of this type can be assessed using the clustering coefficient. The clustering coefficient (at the nodal level) is essentially a count of closed triads, which is a situation where a node (A) is connected to two nodes (B, G) where those two are also directly connected (Fornito et al., 2016). The mathematical representation of the clustering coefficient is:

$$C^{w} = \frac{1}{n} \sum_{j \in N} \frac{2t_{i}^{w}}{k_{i}(k_{i} - 1)}$$

Where t is the number of triangles around a node, see Rubinov and Sporns et al (2010). The use of the clustering coefficient in neuroscience can be seen in (Binnewijzend et al., 2014; Joyce et al., 2010; Lohmann et al., 2010).

High levels of clustering in the brain regions reflect local information processing and are typical in sensory processing regions such as the sensory-motor cortex (Kulkarni et al., 2022). Clustering is also thought of as a kind of network motif. Network motifs are recurring patterns within a large network, sometimes thought of as subgraphs, that occur more frequently than by chance. The inspection of such motifs is thought to represent the fundamental properties of a network and its function. The latter point makes this concept particularly interesting to neuroscience. The clustering coefficient is also closely linked to small-worldness. Small-worldness is a property first proposed by Watts and Strogatz (1998), which proposes a kind of network where the average path length increases proportionately to the log of the number of nodes within the network:

$$L \propto log\ N$$

This concept is highly applicable to the brain as it is constrained by biological costs such as finite metabolic resources, spatial embedding, and the need to provide robust function in the face of possible network damage (Fornito et al., 2016). The brain was demonstrated to be a small-world network as well by Bassett and Bullmore (2006).

To summarize, graph theory provides a sensible means of describing brain activity. It has a history in neuroscience already, and while the different properties of a network are complex, this investigation will make a relatively simple investigation of brain networks created through breathing experimentation. More complex properties than inspected here, while not pertinent to this study, may be of interest to future studies depending on experiment findings.

Study design underpinning

Design

To answer the research question proposed, this study will take the form of a sham-controlled randomized crossover design (Sibbald & Roberts, 1998). This will be further explained in the methods section; however, this project will also require eligibility/exclusion criteria. Exclusion criteria are commonly used in scientific research to ensure ethical proceedings and the elimination of confounding variables. For this report, confounding variables will be anything that could reasonably be suspected to impact breathing and nasal function. As the device augments nasal breathing, an acute respiratory sickness such as the flu or SARS-CoV-2 may adversely impact mechanisms of effect. For similar reasons, any chronic anatomical or functional nasal issues that impede nasal breathing at all would also be confounding. Finally, the research question also specifies healthy individuals. While all the aforementioned may be grounds to exclude people on this point as well, this additionally means individuals with cardiovascular, metabolic, or autonomic disorders would also be ineligible. Each of these disorder categories represents a form of unhealthy function which could affect collected data. While relatively distant from the CNS data, these have a direct impact on ANS data and are therefore not allowable for inclusion. Furthermore, as ANS data is reflective of homeostasis within the body, some effort to assess the basic metabolic and endocrine profiles of participants at the time of testing would also be sensible.

Statistics

Although this study will generate some statistical output, this should be treated and thought of as only a secondary outcome. Due to both the multimodal data as well as the novel nature of the device being tested, there are no examples of studies that can be taken as proxies to acquire expectant standard deviations or mean differences between

test conditions. Therefore, it is not possible to calculate power for true hypothesis testing. These facts collectively mean that the present project is, by nature, exploratory science and will also mean no hypotheses are proposed here. Instead, the utility of the statistics performed will be to provide some loose context for the interpretation of results.

Chapter 2. Methods

Research question

- How does Nosebuds-augmented breathing functionally affect the cerebral cortex in healthy adults?

The null hypothesis of this investigation was that there was no difference between the connectivity profiles of sham and augmented (experiment) breathing of participants. Importantly, as this study could not be properly powered, there was no test of the null; however, one could still be presented as the negation of the hypothesis.

Study design

This was a randomized crossover double-blind sham controlled experimental study. Blinding was enforced using an “A” and “B” device labeling system at the level of the experiment and by a “condition 1” and “condition 2” labeling system at the level of data. Randomization was done using a simple randomization algorithm written in Python by the primary researcher of this study. This returned a total proportionate AB and BA protocols over the given sample group, with half AB and half BA. The sham control was in dimensionality and upon visual inspection the same as the active device. Rotation of small motors in the active device did, however, create an audible humming which was a property not shared by the sham.

Table 2

Demographics

Total	n =14 (F = 9)
Age	25.6 (SD 7.71)
Handedness	L = 1

Note. With one exception, ID 487, all participants were under 30 and if excluded, the average age becomes 23.86 (SD = 3.86). n = number of participants, SD = standard deviation, L = left-handed.

Recruitment procedure

Participants were sought through digital posts on social media sites, physical poster advertising, and word of mouth. All physical advertisements were placed on the AUT north compass on 90 Akoranga Drive Northcote Auckland 0627. Contact information for this project included the email of the primary researcher for any questions or concerns potential participants might have. Once initial contact was made and interest established, a participation form outlining eligibility criteria and experiment particulars was sent. Following this, if the individual wished to participate, they were made aware of available slots and one at their convenience was selected. This process from participant information sheet to booking data took a minimum of two weeks to ensure proper informed consent.

Eligibility criteria

Required eligibility for this project revolved around the necessity to control for confounding variables that could affect possible mechanisms of effect. With the nose and nasal functioning on this list, no upper respiratory tract infections (including SARS-CoV-2) two weeks before data collection were required. Beyond this, for similar reasons, all

types of smokers were also ineligible, including vape smokers. Finally, all instances of chronic respiratory issues such as asthma were also grounds for exclusion. But a sole exception was being made for mild asthma, because of its sheer population prevalence and widely available effective treatment options often leading to no functional respiratory impairment. Physical nasal impairment due to injury or otherwise also resulted in ineligibility. Similarly, to mild asthma, however, an exception was being made for mild to moderate deviated septum. Also, like asthma, this was because typically a deviated septum does not lead to any functional impairment, the phenomenon is present to some degree in much of the population and intervention is only required in extreme cases. Finally, cardiovascular, metabolic, or autonomic disorders also led to exclusion, these collectively along with the aforementioned satisfied the "health" specification of the research question. All eligibility was based on self-reports and was specified to potential participants as part of the participant information sheet.

Active Device condition

The prototype active Nosebuds was a battery-powered wearable that inserted into the nostrils to deliver humming-like pressure oscillations into the tidal nasal air stream using motor-driven rotating airflow shutters that cyclically partially occluded the incoming air stream at a frequency rate replicating that found during low-frequency humming (100 Hz to 450 Hz). Airflow shuttering occurred during inhalation and exhalation. The active device alternated sides every 90 seconds. See figure 4 for device images.

Figure 4

Device images

Note. Image of NoseBuds. Individual in images is a researcher on this project and consented to use of image.

Session procedure

Each session booking lasted for 3 hours and took place in the psychophysiology laboratory of the AUT north campus at the physical address of 90 Akoranga Drive, Northcote, Auckland 0627, room AR151. Upon arrival at a session, participants were greeted by no less than two researchers, and the eligibility criteria were reconfirmed. Basic information on how they slept the previous night as well as caffeine consumption on the day was then noted.

Once this was complete, participants were reminded of the study protocol, which was first presented on the participant information form. They were shown the devices utilized for the testing and the ventilated sound-attenuated chamber where data collection would take place. Participants were then measured for an EEG cap, asked if they would like to use the restroom before entering the test booth, and then invited to take a seat on a large recliner facing a blank wall within the chamber. A camera in the corner of the booth was pointed out and explained to not be recording, but only to be present for

monitoring the participant throughout the experiment. Next to the recliner was a sole monitor, which would be used by researchers to set up testing instrumentation. Participants had been advised within the data collection session confirmation email to bring a device or any material of some kind to relax with while the setup process was carried out. Once seated, participants were provided a small table should they wish to work or keep material such as a laptop on during setup.

Chiefly, this was in the form of a Neuroscan Quik-Cap Silicone Electrode Array run from Neuroscan's Curry 7. This cap used an integrated reference electrode and ground electrode along with additional channels such as an electrooculogram (EOG), although these latter additional channels were unused for this study. First, the cap was fitted and plugged in, and then a demonstration with one of the syringes used for the necessary filling of electrodes with conductive gel was performed. This included a showing of the dullness of the syringe on a researcher's arm. Next, ground and reference electrodes were set up while taking time to check in with the participant about pressure and possible discomfort. Once this was complete, a channel electrode was set up and detected at an acceptable impedance, and the participant was comfortable with the process, the full cap was set up with one of two researchers taking a hemisphere each.

The cap set-up was expected to take between 40 to 50 minutes. If more researchers were present, a circuit was used with researchers shifting in and out, keeping two on set up at all times. Regular check-ins regarding the comfort of the participant continued to be made throughout, with it being stressed to participants that a full stop would happen should that ever be requested. Additionally, at least one researcher during data collection was always female to ensure set-up could occur while observing any participant-specific cultural requests. Once set-up was complete, all researchers left the testing booth where the primary researcher instructed the participant to recline the chair and relax breathing

solely through their nose. Finally, the proceedings of the experiment itself were mentioned for a final time, and after the participant indicated their comfort, the researcher left the room, and the experiment began.

Experiment proceedings

1) Participants were asked to breathe normally through their nose for 5 minutes.

2) Participants were given an experiment device (sham or active depending on randomization), directed to don it, and asked to continue breathing nasally for 10 minutes.

3) Participants had the device taken from them and were asked to breathe nasally for 5 minutes.

4) Participants were given the final device (sham or active depending on randomization) for a final 10 minutes and once again asked to breathe nasally.

EEG pipeline and data preparation

Best practice in EEG processing was to construct a bespoke pipeline that would clean and integrate the data from raw. This allowed for complete control over every computational decision that must be made when investigating complex data such as with an EEG. Here, the bespoke pipeline in question can be seen in figure 5.

Figure 5

Full EEG pipeline

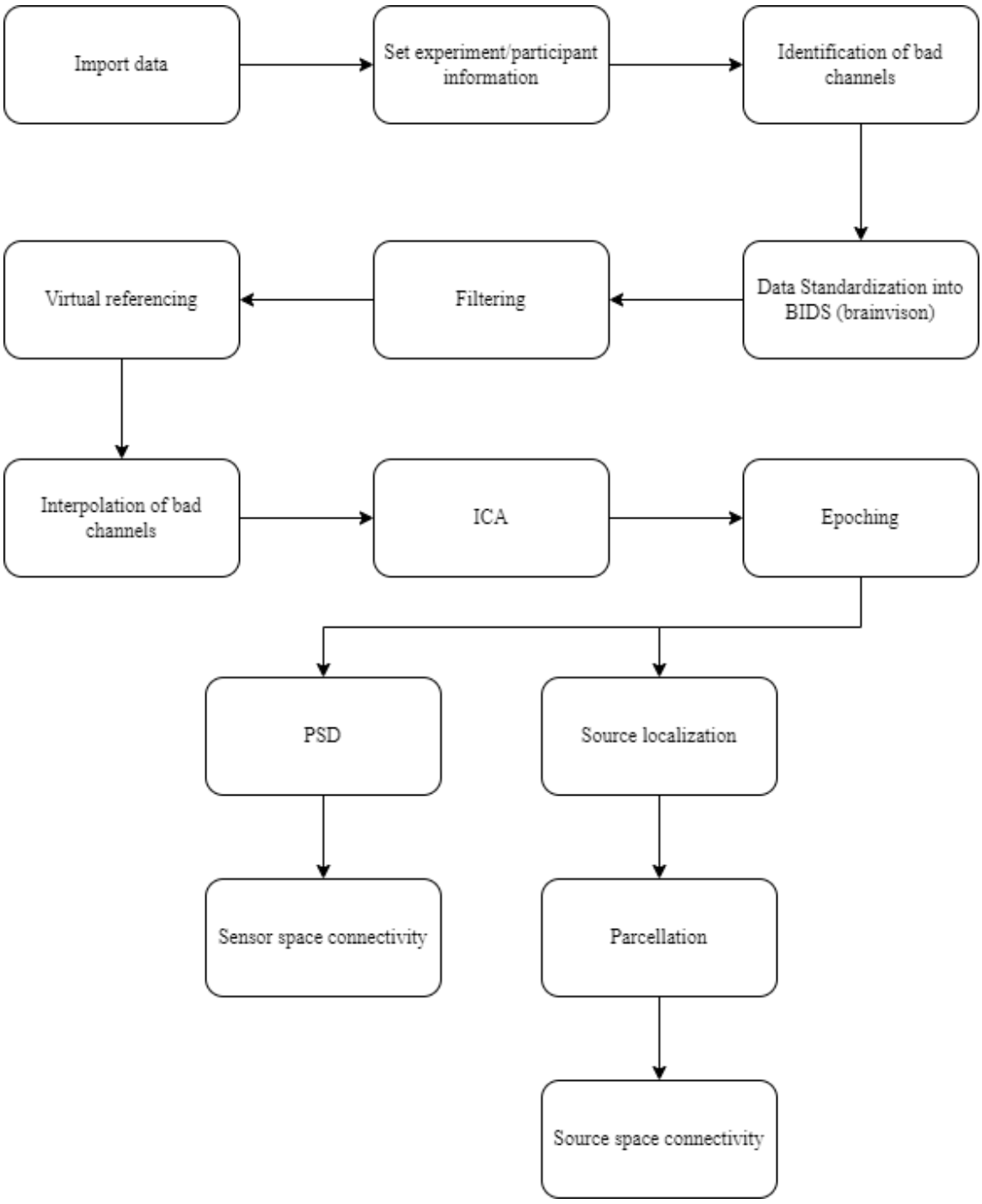

Note. Flow chart of the complete EEG pipeline. BIDS = brain imaging data structure, ICA = independent component analysis, PSD = power spectrum density.

The Python-MNE package was selected to build most of the EEG pipeline. This represented a suite of cutting-edge functions and data structures that allowed for internal consistency and functionality. It also enabled data to be produced at a high contemporary quality. Offline filtering in the project was set at 1000 Hz. Line noise was configured at 50 Hz, and a bandpass filter of 1 and 100 Hz was implemented. Re-referencing was done using a virtual average reference, and downsampling to 250 Hz was performed. ICA generated 32 components, all of which were inspected by the primary researcher. Screenshots of Topoplot components post-rejection and cleaned data segments were kept and independently cross-checked by the project's senior researcher. The final step of conventional preprocessing involved epoching, which was done manually on cleaned data to avoid residual movement artifacts.

From this stage onward, sensor space processing involved generating a power spectral density plot before transitioning to connectivity analysis. This was computed using wPLI and resulted in a connectivity matrix of 58 channels by 58 channels. This is not 64 due to the removal of unneeded channels such as electrooculography (EOG) channels. In our study, no additional cleaning was applied to the connectivity matrix, making it interchangeable with an adjacency matrix. Source space processing began with an LCMV beamformer, for which filter weights were prepared using a Freesurfer average. As the average head volume was utilized, there was no need to conduct a head morph. Subsequently, parcellation was performed using the aforementioned human connectome cortical map before calculating connectivity once again with wPLI. This yielded the final output of a 360 by 360 region of interest connectivity matrix (also synonymous with adjacency matrix). Finally, statistics were computed for the outputs of both processing streams.

Chapter 3. Results

Data were collected for 15 participants, along with two pilots. The pilots were necessary to determine the particulars of a practical study design that would yield high data quality. This involved determining the total experiment length and the physical positioning of participants. Initially, only one pilot was thought necessary, but ultimately two were required to produce the study design as outlined. Additionally, one participant's data, identified as ID 323, was excluded in its entirety upon inspection under ICA. Both the primary researcher and the senior researcher determined it to be unrecoverable. Screenshots for this and other datasets are included in the appendices. Typically, 10 to 15 ICA components were rejected for participants under a conservative exclusion scheme, with the most common artifacts being located at the back of the head, likely due to kinetic stimulation from contact of electrodes with the chair headrest. Of the 14 included participants, 8 went through the A-B stream and 6, originally 7 with participant 323, through the B-A stream.

The experiment setup typically took 70 minutes with two researchers preparing equipment. During the experiment, device donning proceeded smoothly for all participants except ID 679. This participant had an injury to the left arm (a right-handed participant) which was in a cast, allowing limited finger movement. Consequently, ANS sensors were placed on the right hand, and this meant that the participant had to be assisted by a researcher to don the sham and active devices. After this point, participants typically settled quickly in the sham condition but took considerably longer in the active condition. Participants were observed smiling, laughing, and responding initially to the novel device and its sound, mentioning after the experiment its pleasantness and similarity to a white noise machine. They became settled enough to begin acquiring an epoch between 30 to 60 seconds after beginning the active condition. For the Sham condition, this was

approximately 10 to 20 seconds. Once data were acquired and pre-processed, the first output computed was spectral power density, and results can be seen in figure 6.

Figure 6

Power spectrum findings

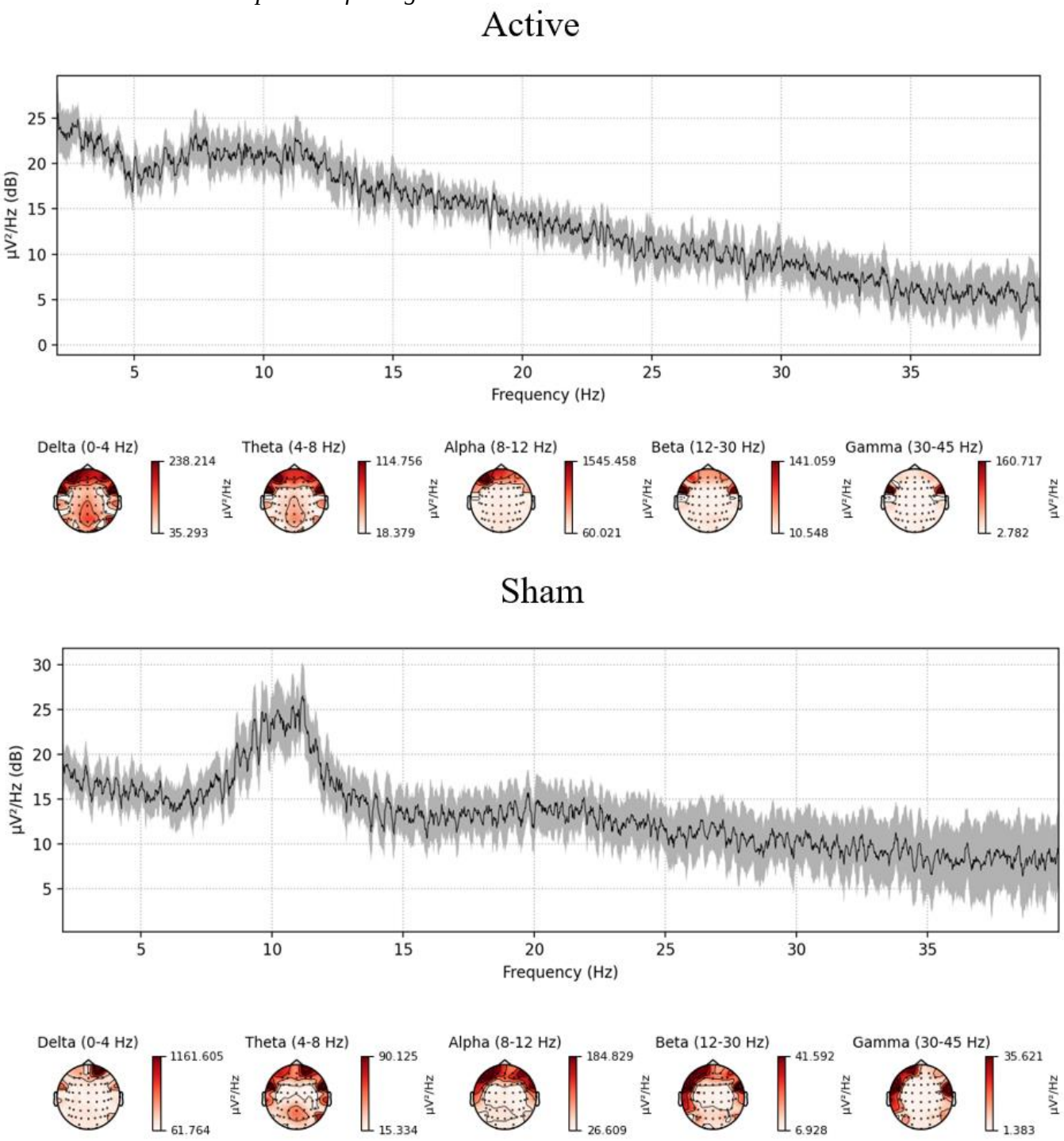

Note. Power spectrum plotted with standard deviation. Calculated across all participants using a cleaned 60-second epoch that began at the introduction of a stimulus.

Power spectral density was calculated both as an independent outcome and as a data validation check. Consequently, as observed in the Topoplots of Figure 6, it was determined that the results of the delta and gamma bands across both conditions were nonsensical. Therefore, the focus moving into connectivity would be on the Theta, Alpha, and Beta bands. Results for significance testing for spectral power are presented in Table 3, and sensor WPLI connectivity is depicted in Figures 7 through 9.

Table 3

Power spectrum statistics

	Beta			
Electrode	Sham	Buds	P val	FDC val
CZ	-2.11E-10	1.27E-10	3.70E-02	4.58E-01
CP1	-3.16E-10	5.36E-11	4.89E-02	4.58E-01
CPZ	-2.54E-10	9.38E-11	4.41E-02	4.58E-01
TP8	3.20E-10	-3.27E-10	4.16E-02	4.58E-01
M1	4.23E-10	-2.54E-10	3.78E-02	4.58E-01
PO8	2.77E-10	-3.25E-10	3.98E-02	4.58E-01

Note. Statistical results from a sensor power spectrum calculation via a paired t-test and false detection correction algorithm (FDC). Only significant nodes (channels) and wave bands are shown. Significance threshold set at 0.05.

Figure 7

Sensor space Theta connectivity

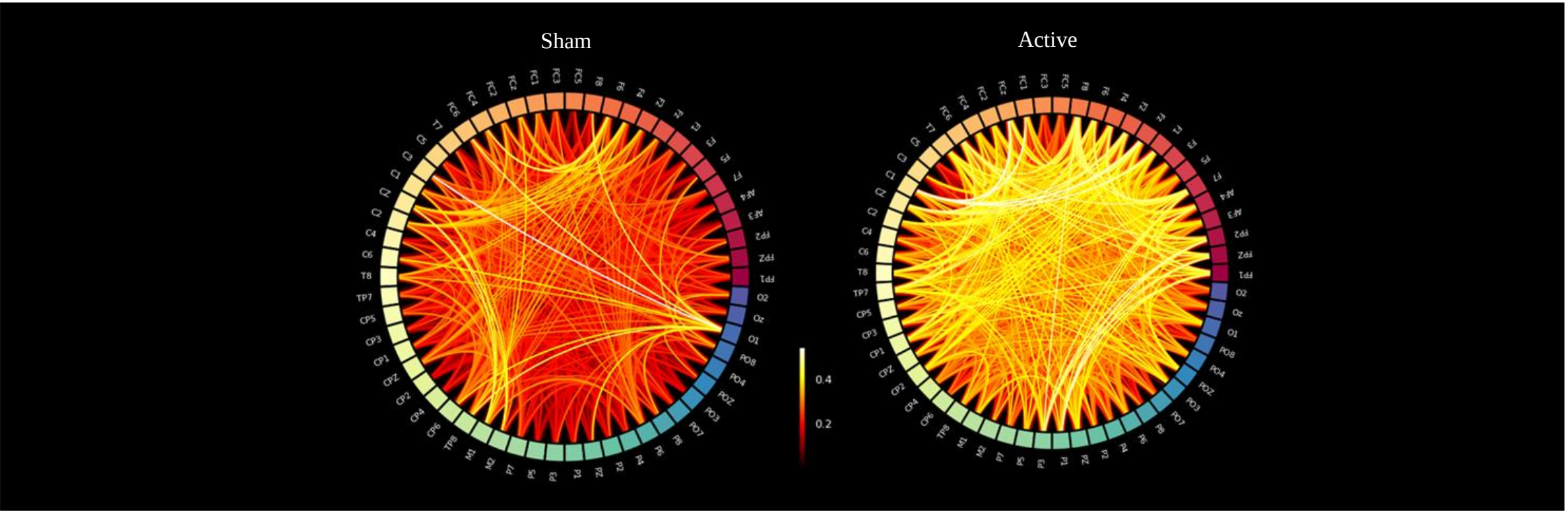

Note. A crucial plot visualization of Theta sensor space wPLI connectivity matrix. The 64 points around each circumference correspond to 64 EEG channels, with the intensity of their connection representing the wPLI value. A fully connected graph is assumed, so each node has 63 connections (the number of channels minus one for self-connection).

Figure 8

Alpha sensor space connectivity

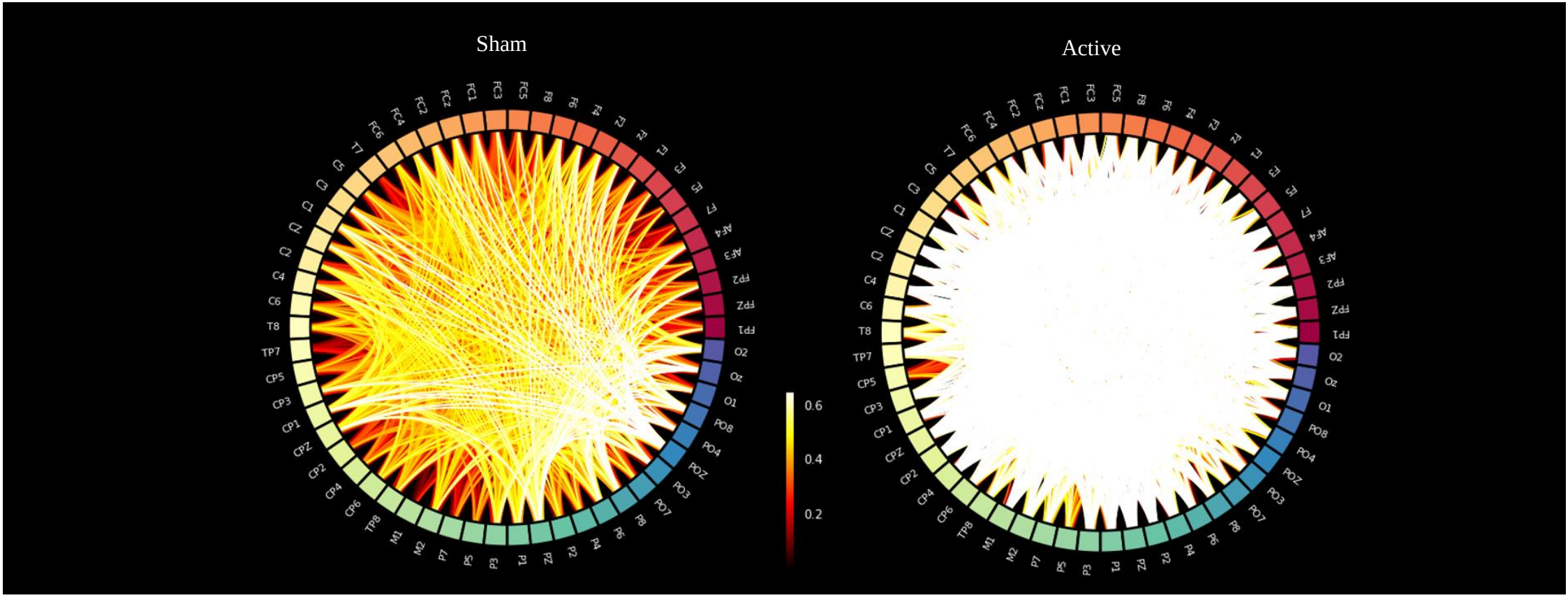

Note. A crucial plot visualization of Alpha sensor space wPLI connectivity matrix. The 64 points around each circumference correspond to 64 EEG channels, with the intensity of their connection representing the wPLI value. A fully connected graph is assumed, so each node has 63 connections (the number of channels minus one for self-connection).

Figure 9

Beta sensor space connectivity

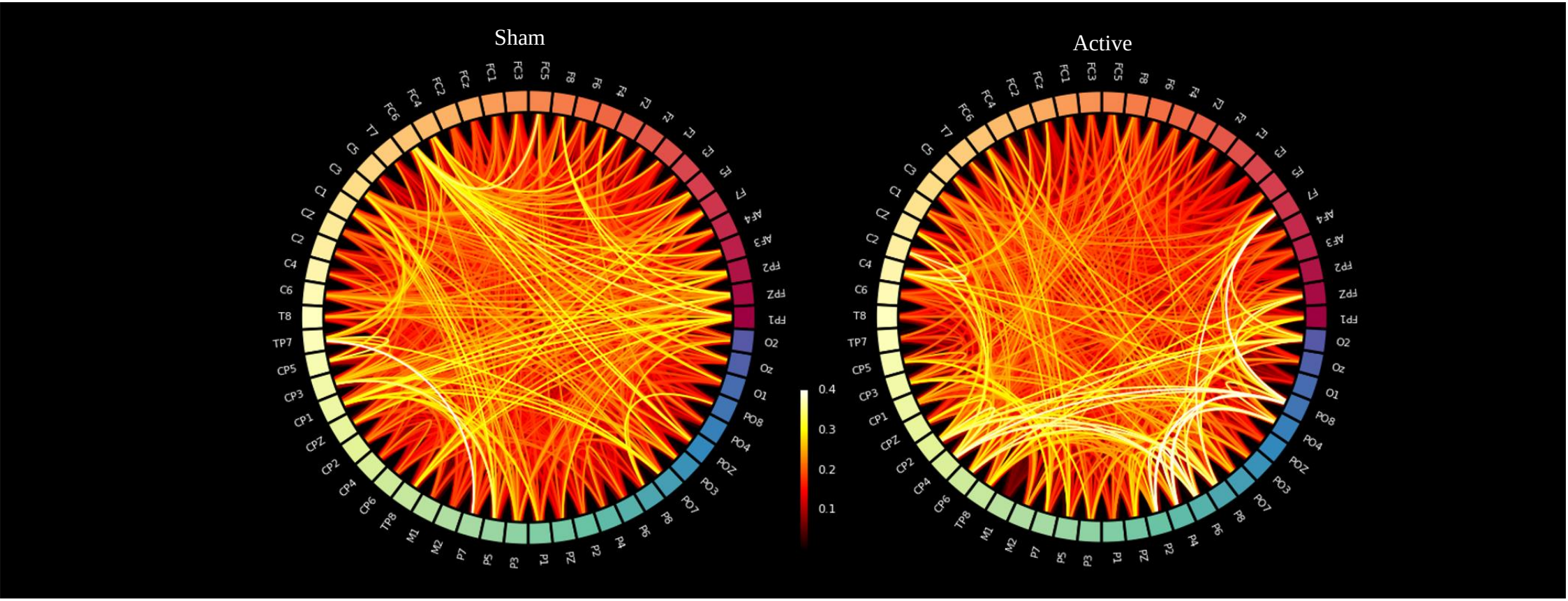

Note. A crucial plot visualization of Beta sensor space wPLI connectivity matrix. The 64 points around each circumference correspond to 64 EEG channels, with the intensity of their connection representing the wPLI value. A fully connected graph is assumed, so each node has 63 connections (the number of channels minus one for self-connection).

Figures 7-9 are direct visualizations of the connectivity/adjacency matrix. A final step in preprocessing before the power analysis was the dropping of peripheral and uninformative electrodes such as the CB (cerebellum electrodes), which brings the total matrix size to 58 by 58. In this context, a fully connected graph is assumed, with electrodes forming nodes and connectivity weights between them forming edges. The majority of values fall between 0.4 to 0.65, except for Alpha Buds connectivity, which demonstrated unusually high connectivity. Once discussed, the research team agreed that this reflects an artifact and was further filtered using a bespoke filter algorithm. The results of this can be seen in supplementary material. It is not included here as it would not maintain the uniformity of a connectivity matrix being an adjacency matrix, as is the paradigm of this project. Therefore, while interesting, that figure represents data that falls outside the purview of the present project, and all sensor space visualizations are representative of the network analysis input used. These results can be seen in Tables 6 and 5.

Table 4

Sensor node strength

		Theta		
Eectrodes	Sham	Active	P val	FDC val
C6	4.76E+00	3.56E+00	2.11E-02	8.51E-01
		Alpha		
Eectrodes	Sham	Buds	P val	FDC val
C5	9.54E+00	7.15E+00	2.86E-02	9.34E-01
		Beta		
Eectrodes	Sham	Active	P val	FDC val
PO7	1.68E+00	2.07E+00	4.88E-02	9.57E-01
O1	4.38E-01	6.16E-01	2.05E-02	9.57E-01

Note. Statistical results from a paired t-test of node strength calculated using sensor connectivity matrices. Significance verified using a false detection algorithm (FDC). Only significant nodes (channels) and bands are listed. Significance set at 0.05.

Table 5

Sensor betweenness

Theta				
Eectrodes	Sham	Active	P val	FDC val
C6	2.98E+01	9.49E+01	4.22E-02	4.89E-01
CP1	4.61E+01	1.62E+01	1.45E-02	4.89E-01
P7	2.27E+01	5.03E+01	3.61E-02	4.89E-01
PO8	2.50E+00	1.66E+01	1.74E-02	4.89E-01
Oz	1.71E+00	1.43E-01	3.34E-02	4.89E-01
Alpha				
Eectrodes	Sham	Active	P val	FDC val
PO7	1.11E+01	3.11E+01	2.63E-02	6.94E-01

Note. Statistical results from a paired t-test of betweenness calculated using sensor connectivity matrices. Significance verified using a false detection algorithm (FDC). Only significant nodes (channels) and bands are listed. Significance set at 0.05.

No meaningful eigenvector betweenness or clustering coefficient calculations could be performed due to the small size of the sensor space networks, so they were excluded at this stage. At this point, the LCMV beamformer was run, and source reconstruction results can be seen in Figure 7.

Figure 10

Source space visualization

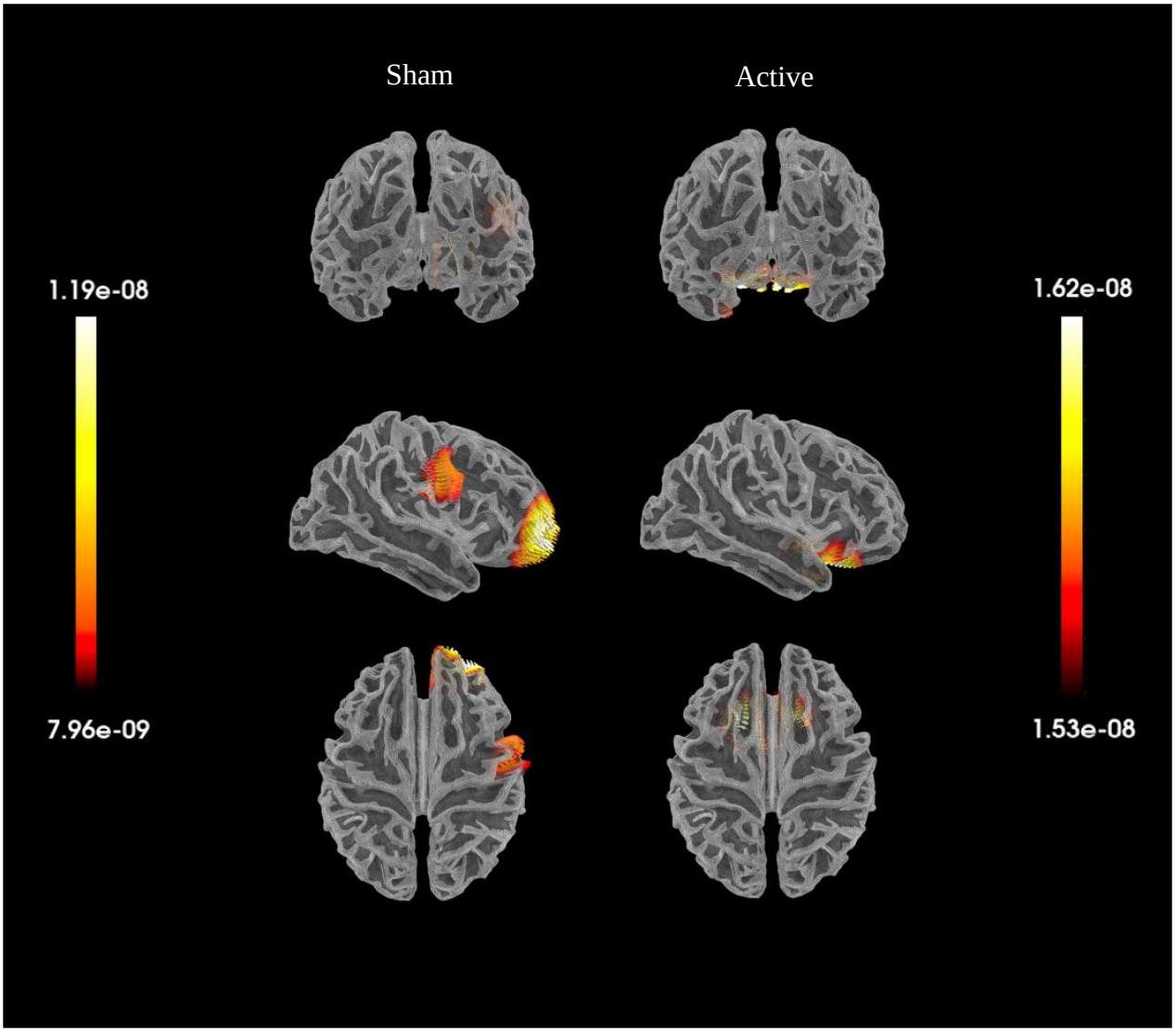

Note. Full brain volume projection of average epoch activity across all participants. Brain volume is represented as an averaged FreeSurfer mesh, and activity value is calculated using an LCMV beamformer. For visualization purposes, only a vector value is represented.

Key activity in the active condition manifested in a manner that, while discernible in conventional brain views, remained somewhat ambiguous. Therefore, an additional supplementary figure has been included to provide a clearer presentation of this activity, particularly around the longitudinal fissure when viewed ventrally. Additionally, due to the initially constrained representation of activity power, the visualization scales were adjusted downwards to allow for a more extensive inspection of activity across the cortex in both conditions. This adjustment is illustrated in Figure 8. Moreover, this revealed a distinct pattern of lateralization, which was subsequently correlated with nasal patency, as depicted in Figure 9.

Figure 11

Adjusted source space activity

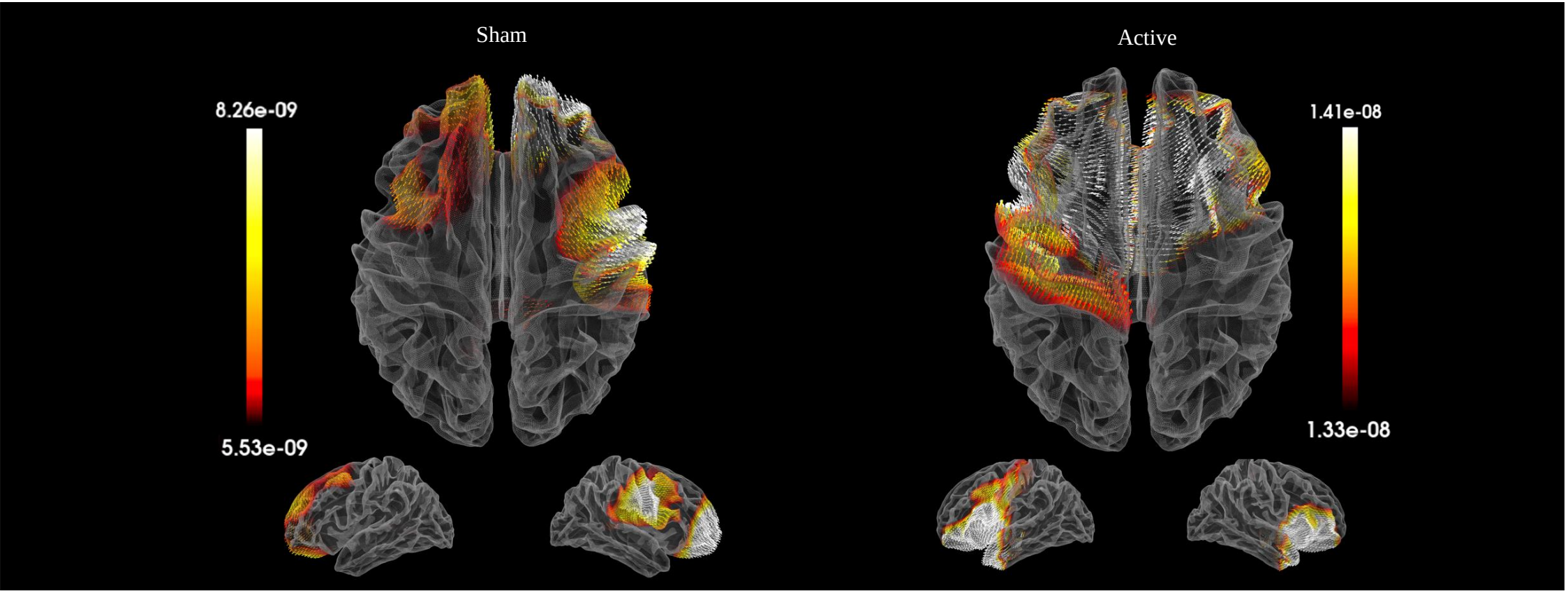

Note. Full brain volume projection of scaled average epoch activity across all participants. Brain volume is represented as an averaged FreeSurfer mesh, and activity value is calculated using an LCMV beamformer. For visualization purposes, only a vector value is represented.

Figure 12.

Source space activity relative to nasal patency

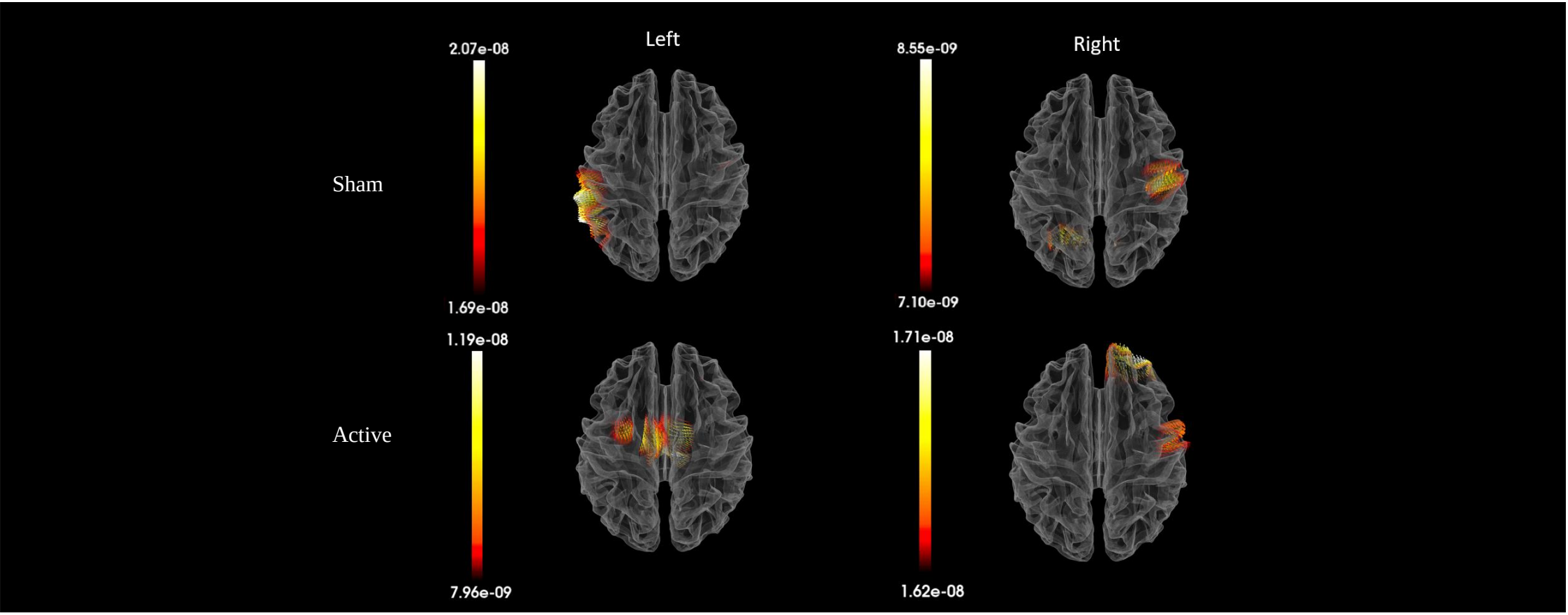

Note. Full brain volume projection of average epoch activity across all participants by nasal patency. Brain volume is represented as an averaged FreeSurfer mesh, and activity value is calculated using an LCMV beamformer. For visualization purposes, only a vector value is represented.

All source space visualizations were generated using a vector LCMV beamformer, while the data input for the source space WPLI was generated using a scalar LCMV beamformer with a 'max-power' method. This approach was chosen to preserve current direction, enabling the figures to be more informative and intuitively representative of the flow of brain charges. The 'max-power' method optimizes for power and serves as the input for the WPLI calculator after parcellation into 360 regions using the MMP HCP atlas. These results are depicted in Figure 9, with the network analysis presented in Tables 6 to 9. Additionally, the significance threshold was reduced from 0.05 to 0.01 to accommodate the large number of tests conducted.

Figure 13

Source space matrix

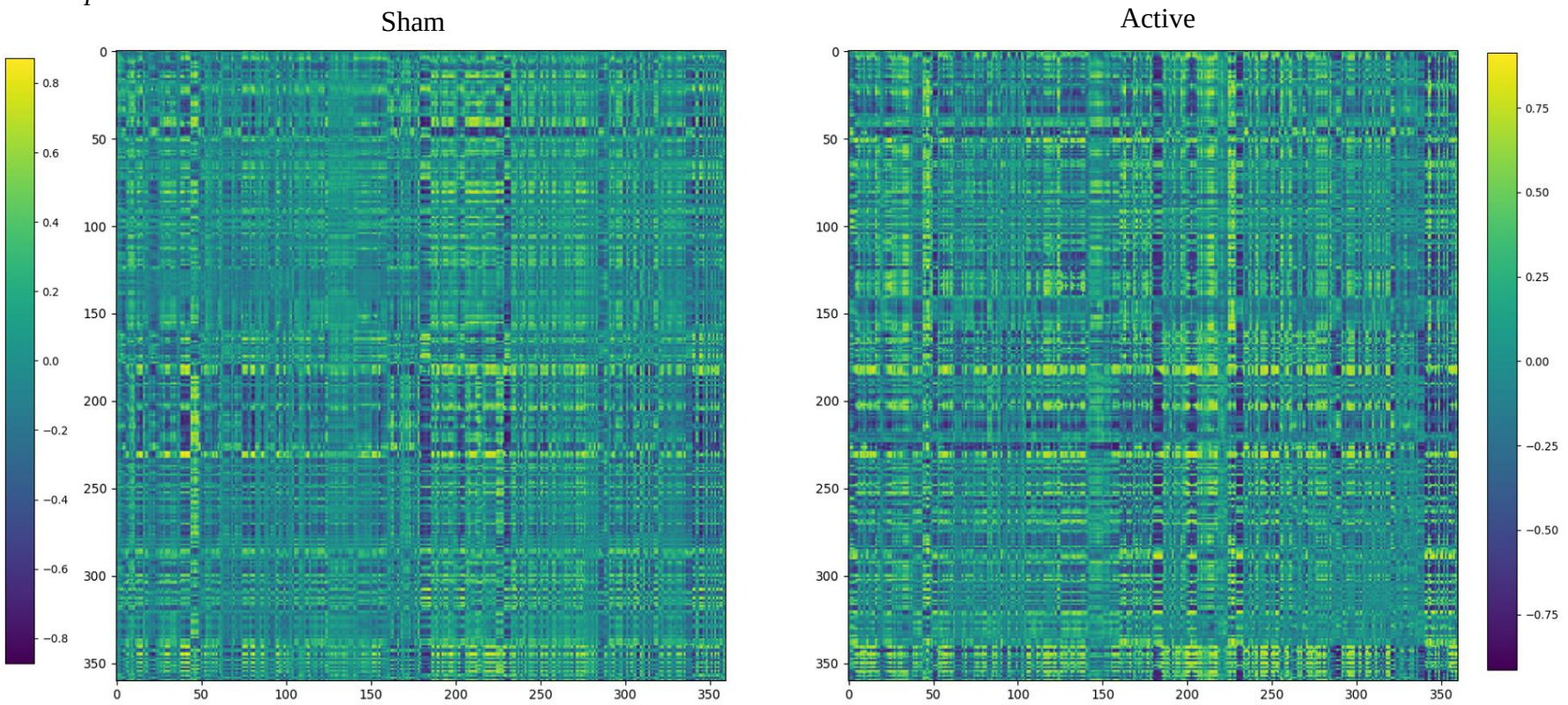

Note. Average source space matrices for each condition after parcellation. Connectivity matrix calculated with wPLI, outputting a 360 region of interest by 360 region of interest matrix, with each interesting point representing the magnitude of the wPLI value.

Table 6

Source space node strength

Theta					
Area [index]	Anatomical name	Sham	Active	P val	FDC val
L_V8	Ventral_Stream_Visual	2.51E+01	6.10E+01	8.04E-03	5.98E-01
Beta					
Area [index]	Anatomical name	Sham	Active	P val	FDC val
L_23d	Posterior_Cingulate	1.14E+01	4.38E+01	9.39E-03	9.92E-01
L_PGs	Inferior_Parietal	7.23E+00	4.74E+01	3.48E-03	9.92E-01
R_d23ab	Posterior_Cingulate	1.48E+01	3.44E+01	9.35E-03	9.92E-01

Note. Statistical results from a paired t-test of node strength calculated using source connectivity matrices. Significance verified using a false detection algorithm (FDC). Only significant nodes (regions of interest) and bands are listed. Significance set at 0.01.

Table 7

Source space betweenness

Theta					
Area [index]	Anatomical name	Sham	Active	P val	FDC val
L_STSva	Auditory_Association	1.24E+04	1.87E+03	0. 9.55E-03	0. 9.24E-01
Alpha					
Area [index]	Anatomical name	Sham	Active	P val	FDC val
L_FOP4	Insula_FrontalOperc	2.05E+04	5.09E+03	0. 8.87E-03	0. 9.38E-01
Beta					
Area [index]	Anatomical name	Sham	Active	P val	FDC val
L_PFm	Inferior_Parietal	1.01E+05	7.61E+04	2.53E-03	4.55E-01
L_PGp	Inferior_Parietal	3.10E+04	6.89E+04	5.43E-03	6.52E-01
R_Ig	Insula_FrontalOperc	3.34E+04	7.93E+04	2.63E-05	9.47E-03

Note. Statistical results from a paired t-test of betweenness calculated using source connectivity matrices. Significance verified using a false detection algorithm (FDC). Only significant nodes (regions of interest) and bands are listed. Significance set at 0.01.

Table 8

Source space eigenvector centrality

Theta					
Area [index]	Anatomical name	Sham	Active	P val	FDC val
L_IFSa	Inferior_Frontal	1.15E-02	2.66E-02	6.75E-03	7.57E-01
L_p24pr	AntCing_MedPFC	2.82E-02	1.17E-02	6.57E-03	7.57E-01
R_d32	AntCing_MedPFC	1.41E-02	1.41E-02	2.18E-03	7.57E-01
Beta					
Area [index]	Anatomical name	Sham	Active	P val	FDC val
L_31pv	Posterior_Cingulate	3.60E-02	1.42E-02	8.39E-03	7.87E-01
R_MST	MT+_Complex	1.03E-02	3.14E-02	7.28E-03	7.87E-01

Note. Statistical results from a paired t-test of eigenvector centrality calculated using source connectivity matrices. Significance verified using a false detection algorithm (FDC). Only significant nodes (regions of interest) and bands are listed. Significance set at 0.01.

Table 9

Source space clustering

Theta					
Area [index]	Anatomical name	Sham	Active	P val	FDC val
R_10d	OrbPolaFrontal	9.55E-04	-2.41E-03	9.49E-03	8.54E-01
R_24dv	ParaCentral_MidCing	1.76E-03	-2.03E-03	7.41E-03	8.54E-01
R_31pd	Posterior_Cingulate	-2.00E-03	8.20E-04	4.88E-03	8.54E-01
R_s32	AntCing_MedPFC	1.64E-03	-1.78E-03	8.43E-03	8.54E-01
Alpha					
Area [index]	Anatomical name	Sham	Active	P val	FDC val
L_8BL	Dorsolateral_Prefrontal	1.87E-03	-1.04E-03	7.24E-03	7.29E-01
L_STSva	Auditory_Association	1.47E-03	-2.03E-03	2.96E-03	5.34E-01
R_5L	ParaCentral_MidCing	1.80E-03	-2.21E-03	8.11E-03	7.29E-01
R_ProS	Posterior_Cingulate	8.83E-04	-2.80E-03	2.66E-03	5.34E-01
Beta					
Area [index]	Anatomical name	Sham	Active	P val	FDC val
L_3a	SomaSens_Motor	8.85E-04	-6.63E-04	8.93E-03	6.43E-01
L_7Pm	Superior_Parietal	-4.76E-04	1.32E-03	8.73E-03	6.43E-01
L_TE2a	Lateral_Temporal	-9.78E-04	1.48E-03	6.26E-04	2.25E-01
R_PFm	Inferior_Parietal	-6.09E-04	9.26E-04	6.56E-03	6.43E-01
R_PGp	Inferior_Parietal	-1.00E-03	9.30E-04	7.55E-03	6.43E-01

Note. Statistical results from a paired t-test of clustering calculated using source connectivity matrices. Significance verified using a false detection algorithm (FDC). Only significant nodes (regions of interest) and bands are listed. Significance set at 0.01.

Chapter 4. Discussion

Interpretations

This is the first study to examine the profile of functional brain activity within the cortex during technologically augmented nasal breathing (GoodAir Nosebuds). The two conditions compared were an active device condition (Nosebuds) and a sham. The sham was identical to the active condition except for its lack of rotors; thus, it produced no sound upon ventilation and no oscillation of ventilated air. The findings of this project are rich and make a meaningful contribution to breathing neuroscience at large. The first notable finding here is that statistical significance was most consistently found in the Beta band. With only the exception of betweenness in sensor space connectivity, Beta activity was found to be significant in every metric (network and power) and in both sensor and source space. Next, the location of this activity should be considered, which is primarily in the somatosensory area at the crown of the head and the inferior parietal gyrus. Both structures are known to play a role in multimodal sensory processing and integration. There is also evidence that this type of activity in these regions is specifically correlated to Beta oscillations. Therefore, the cortical effects of the active condition are most consistent with those of multimodal sensory integration.

This line of thought is supported by a clear mid-range change in spectral power as seen in Figure 6 between active and sham conditions. Spectral power represents the amplitude of changes across frequencies (Bazanova & Vernon, 2014). When electrodes were tested for significance independently and within specific frequency bands, significance was only found in sensorimotor/somatosensory electrodes (CZ, CPZ, and CP1) and right temporal lobe electrodes (TP8, PO8, M1) within the Beta band. The somatosensory cortex is responsible for physical perception across the body (Nowinski,

2011). It is also closely linked to the primary motor cortex, both in proximity and in function. The primary motor cortex is largely responsible for the executive execution of movement. Both the somatosensory and the primary motor cortex are predominantly contralaterally afferent and efferent.

The temporal lobe is often considered responsible for auditory processing. An important consideration because, while the active condition produced sound via its rotors, the sham's lack of rotors meant that it produced no sound at all. This then constitutes a true confining variable. However, the activity profile present here in this area remains most consistent with that of multimodal sensory integration. While it is reasonable to suspect that the temporal lobes' involvement is likely due to the sham imperfection, as in it producing no sound, this offers a less compelling explanation as to why somatosensory areas would also appear significant. It is also important to consider that activity is significant in specifically the Beta band and not both the Beta and Alpha bands. Often, Alpha activity makes up some component of audio-processing in this part of the brain (Bazanova & Vernon, 2014; Strauß et al., 2014; Weisz et al., 2011). A recent study by Cao et al (2022) asserted that in activity associated with linguistic processing in the temporal lobes, Alpha and Beta wave activity did not spatially dissociate and this is distinct from "classic" Alpha or Beta sensorimotor power oscillations in the area. Accordingly, our temporal lobe results are most in line with power activity brought on by multimodal integration, as all power changes are in a specific power band, Beta, and not spread between both Alpha and Beta.

Beyond this, activity can also be considered likely synchronous based on source space findings. The continued significance of the Beta band activity across every metric in source space represents its continued importance to connectivity. It is important to stress that this is wholly different from spectral power. Where the former concerns itself

with changes in amplitude across frequencies, the latter concerns itself with waveform phasing (Stam et al., 2007). The areas implemented at the level of source space were the inferior parietal lobe and the posterior cingulate gyrus. The source reconstruction algorithm in this project has allowed for increased anatomical precision. The convergence onto the same areas in both a power and connectivity assessment, particularly in the same wave band suggests that not only is the activity observed exhibiting meaningful changes in power independently in those regions, but that these changes are synchronous. This being an aforementioned known property of specifically multimodal sensory integration, this lends strong evidence to this explanation of the results.

Even so, a deeper exploration of the network statistics is meaningful, as it provides insight into how activity is behaving overall. Beginning with node strength, which is itself a relatively crude metric, showed the most significant regions within the Beta band. The limited number of significant points is not a property shared by the other network metrics, likely reflecting their sophistication. All significant areas independent of the wave band demonstrated a relative increase in node strength in the active condition. Two of the three regions correspond to the posterior cingulate gyrus (L_23d, R_d23ab) and the third corresponds to the inferior parietal gyrus (L_PGs). The latter mimics the significant results found in the same region as part of the sensor power analysis of this report, demonstrating convergence in both power and connectivity. The Posterior cingulate gyrus, conversely, is a key structure of the default mode network (DMN), a collection of brain areas responsible for the brain's true wakeful resting state, and has known connections to breathing (Schottelkotte & Crone, 2022). Furthermore, the regulatory effects of the cingulate gyrus as a whole, and its inclusion in the limbic system, may indicate that there are some greater effects present on the regulatory system in the device condition. What those may be, this report is not designed to discern, but the possibility of such an effect can be considered feasible.

Betweenness and eigenvector centrality, in this context, are measures of integration as they represent areas that act as bridges within the network, allowing it to become a cohesive whole. They both also represent more sophisticated network metrics than node strength and show considerably more significant areas in all wavebands accordingly. In both betweenness and eigenvector Beta centrality, the posterior cingulate gyrus and the inferior parietal gyrus are again represented. Unlike with node strength, however, their significance here suggests that they are acting either more so, in the case of an increase, or less so, in the case of a decrease, as key integration sites engaged during the active condition. The inferior parietal lobe findings here are interesting as the two specific locations within the lobe demonstrate both an increase and decrease in betweenness as seen in Table 7 and 8.

At face value, this could be seen as contradictory, but this also configures to the emergent Multimodal sensory integration pattern. The site of increase (PGp) is located relatively posterior to the rest of the lobe and is a known contributor to task-related performance and multimodal sensory integration specifically when paired with the somatosensory cortex (de Haan & Dijkerman, 2020). This is in contrast to the site of decrease (PFm) which is located relatively superior within the lobe close to the great longitudinal fissure and is often associated with the DMN (Sandhu et al., 2021). A lowering of integration in the DMN indicates a true departure from a resting state of the brain, which is consistent with other findings. If the brain is engaged in the aforementioned integration efforts, this does not represent a resting state, so a drop in DMN integration is sensible. This is further supported by the findings within the posterior cingulate gyrus which also saw a drop in eigenvector centrality as seen in Table 8. The posterior cingulate gyrus is also a part of the DMN, is anatomically very close to the superior inferior parietal lobe section PFm and is therefore also consistent with its functional profile. This means there are two DMN structures both with consistent

decreases in integration and thereby evidence of a departure from a resting state. Conversely, the inferior parietal section that is linked not to the DMN but to active task performance and specifically multimodal sensory integration, did show an increase in integration. Collectively then, this remains consistent with other findings.

Clustering coefficient findings continue to represent the aforementioned areas. The same areas of the inferior parietal gyrus are represented again with an increase in their clustering coefficient, a reasonable expectation considering their likely involvement in multimodal sensory integration. However, the representation of the somatosensory cortex here is peculiar as this shows a drop in its clustering coefficient. This is an interesting finding as this area of the brain typically is very clustered in function (Kulkarni et al., 2022). Such a property might be biologically advantageous because the brain is constantly performing sensory perception so it would be economical to organize the apprentice to perform general perception locally, but when more complex perception tasks are presented, the local system would need to integrate with other parts of the brain (Fornito et al., 2016). Therefore, the drop in clustering coefficient here could be reflective of this, a shift away from simple sensory perception, such as is being constantly performed, to a more complex globally integrated perception task. If so, this would be further evidence for multimodal sensory integration, with the additional integration sites being those found in the inferior parietal lobe. This is speculative, however, and while possible, should be considered a tentative explanation of observations.

A notable addition within this metric is the inferior temporal gyrus with an increase in clustering as seen in Table 9. This is consistent with its known role in auditory processing and multimodal sensory integration and likely provides a similar function in this context as the inferior parietal gyrus (Onitsuka et al., 2004). Additionally, as seen in Tables 6 - 9, some other interesting areas that were consistently represented in multiple

network metrics and multiple wave bands were the auditory association areas. Again, an addition likely represents the processing requirements of the active device conditions' humming sound as opposed to the sham conditions' silence.

A counter-interpretation of this report's findings would likely assert that observed activity was contingent purely on the mechanical simulation of the device placed in the nostrils and the disparity in sound between sham and active conditions. This, however, is dubious. Setting aside the evidence presented that makes sensible contributions to multimodal integration interpretation of data, there are fundamental issues with this other line of thought. As mentioned, significant activity within the inferior parietal lobe was specific primarily to the Beta band, with Alpha only being represented relatively sparsely in some network metrics. However, as Cao et al (2022) mentioned, activity in this region not relating to multimodal integration did not appear spatially distinct. If then, the observed findings are simply representative of auditory processing it would be expected that more significance be seen within the Alpha band; however, this is not the case for either power or connectivity in the region at any level of organization. This is again, in contrast to multimodal activity as pointed out, which is specific to the Beta band.

Another issue arises if Figure 10 representing signal-to-source space reconstruction is considered, which shows clear sham activity in the somatosensory cortex. This suggests that the act of simply inserting the novel device into the nostrils provides some level of regional activation. The activity appears lower in the region, however, than the significant activity aforementioned, making it more in line with activation due to sensations coming from the face. As a result, this is likely the mechanoreceptor stimulation by the sham device, something that is both reasonable to see as well as notably distant from previous activity. This then further suggests that said previous activity reflects at least the addition of some other kinds of stimulation.

Importantly, the significance of any of this cannot be spoken for as no statistical testing on source space figures has been performed as of yet. This represents preliminary evidence that the somatosensory cortex is affected regardless of active or sham condition. However, it should at least be concerning if the interpretation of our data suggests findings based on simple cutaneous stimulation.

The point on statistical significance also further adds to the effect observed being due to something other than just mechanical stimulation of the nostrils. This is precisely because this experiment was sham-controlled. Mechanical stimulation should therefore be consistent between conditions. As such, the statistical comparison between conditions should not detect significance in this part of the somatosensory cortex, and it does not, which suggests that the mechanical stimulation is there in both conditions, but there is a significant difference elsewhere in the somatosensory cortex. It is likely that the only reason that the face's mechanically stimulated area of the somatosensory cortex is not represented in source space visualizations is because of the huge power disparity between the active and sham conditions as seen in Figure 10. As can be seen in Figures 11 where this disparity is altered, more of the somatosensory cortex does become involved in both conditions. This does deserve meaningful verification nevertheless, so a further research suggestion is the statistical interaction of power in source space in its integrity.

The replicability of at least the connectivity results should also be considered briefly, which also showed congruence with source space findings. Little significance was found in node strength across any wave band as seen in Table 4. But two (C5, C6) of the four nodes found significant could be related to the somatosensory cortex. These were both in Theta and Alpha and showed a drop in node strength suggesting a shift away from true resting ready state again (Clements et al., 2021). This then further implies that this area is genuinely responsive to the active condition in some biologically feasible way.

The remaining nodes (O1 and PO7) point to the temporal and occipital regions respectively; these too then fit with multimodal sensory integration as other findings have. Additionally, O1 and PO7 are both in line with findings of significance in source space for the PGp inferior parietal lobe. Again showing a convergence into this area, this time across levels of organization and thereby, further verifying the legitimacy of its contribution to the active condition activity profile. Beyond this, the lack of more extensive interesting significant findings within node strength is again a reflection of node strength as a crude network assessment tool.

The strongest evidence for the observed findings reflecting simple auditory processing comes from sensor space betweenness. This metric revealed more significant nodes than sensor node strength but largely showed mixed results, as seen in Table 5. PO7 is the only electrode present that appeared to have a significant increase for both betweenness and node strength, albeit in two different wave bands favoring the active device. This convergence not only occurs in both sensor space network metrics but also, in a sense, in the power analysis results as it appears in the posterior temporal to occipital lobe, albeit contralaterally to the area significant in power. The Alpha band represents the other major known oscillatory activity in the region linked to somatosensory cortex function as well (Cao et al., 2022). So, this area is further implicated in some sort of active device-related effect. In the remaining five nodes (C6, CP1, P7, PO8, OZ), all but one (CP1) represent a site around the rim of the head and posterior to the midline, and are therefore likely sensitive to temporal to occipital activity. Paired with being specific to the Theta wave band, this could once again be due to the humming sound of the active condition. Theta synchronization activity of this kind in the temporal lobe, albeit the frontotemporal lobe, has been observed when listening to pleasant music (Ara & Marco-Pallarés, 2021). Therefore, it stands that these findings of significance here reflect rhythmic device sound and not some other bodily response.

Even so, these findings are relatively limited compared to the substantial data suggesting the multimodal integration interpretation. On that front, a final consideration should also be that of biological feasibility. The active device does present all the necessary stimuli required to elicit this response. It certainly presents more than the sham condition with the confounding variable of sound, which could still be responsible for observed activity, but might not be solely responsible for the results of this investigation. If the results depended on just mechanical stimulation and sound, the active condition could reasonably be suspected to simulate the bulk of the temporal lobe and the part of the somatosensory cortex responsible for cutaneous stimulation of the face, as mentioned. As the findings of this report are not so straightforward, it remains possible that although the observed findings could be due to the confounding sound variable, they may, as the data suggest, not solely be due to this. Finally, the biological feasibility also suggests that the pipeline developed for this project did function correctly. While not an explicit goal of this investigation, it has thereby created a useful tool that could be utilized in further studies, both on this subject matter and others.

Although due to methodological limitations of this investigation, more speculation on figures and findings should only tentatively be performed, an inspection of visualizations might also be informative of both patterns in the data that did not meet significance and possible avenues for future research. This should all be taken, however, as pure statistically unsubstantiated speculation at this point. Beginning with Theta band WPLI then, in Figure 7, a clear difference in magnitude is present favoring the device condition. This activity appears relatively global, involving most of the brain to some extent. Theta connectivity of this kind has been observed in altered states of consciousness as a result of physiological/neurological disorders or neural damage in the form of traumatic brain injury (Chennu et al., 2014). It has also been observed in generalized social anxiety disorder and here it has specifically been linked to increased

information processing and introspective thought (M. Xing et al., 2016). In the context of this experiment, this could therefore reflect the self-focus of thought. The act of wearing a novel, noisy, and ventilation-responsive device within an experiment would be a natural prompt to introspection. The lack of a clear pattern of connectivity in this band would also be expected in this scenario, as such a cognitive change would appear in a relatively global manner involving many brain regions.

Alpha band activity also shows a substantial favoring of connectivity towards the active condition as seen in Figure 8. In this context, however, such a finding is likely not biologically feasible and reflective of noise in the data. For this report, as outlined in the introduction, the connectivity matrix will be considered synonymous with an adjacency matrix, so this formed the basis of network analysis input. This was done in the hope that while the visual inspection of the data might have been unproductive, perhaps some meaning can be determined when considered as a network. Whatever findings emerge, however, should be considered very carefully as a consequence. Furthermore, although further processing of data was outside the scope of this project, a fitter for this dataset was designed and implemented, as can be seen in the appendices. The Sham condition, conversely, appeared clear enough and showed a proclivity for Alpha synchronicity in the occipital lobe and general posterior of the brain. This is a sensible finding as Alpha oscillations in this part of the brain are generally considered part of its default functioning (Clements et al., 2021). Therefore, this suggests that the sham condition is closer to a true rest brain state.

The Beta band connectivity profile is similarly difficult to interpret but most certainly appears real, as seen in Figure 9. Here there does seem to be a clear pattern of increased phasing within the device condition localized to the left parietal to occipital lobes. While literature on activity of this type is available, it is largely in a clinical

population and therefore limited in its applicability to this experiment (X. Liu et al., 2022; Shah-Basak et al., 2019; Tewarie et al., 2013). Interestingly, the areas in question here also capture the areas in which significant spectral power activity was found. Evidence does exist implicating Beta band connectivity in this region to attentive motion and perception (Chung et al., 2017). This could be a sensible explanation for the results found. Again, the active device condition does create noise, so it is reasonable to suspect that participants would take notice of this novel phenomenon and be acutely aware of both their breathing and the sensation of the device, possibly more so than in the sham condition.

Again, no statistical investigation was made at this level though, so these findings can only be considered as simple curiosities. Statistical testing here would make for an interesting project and therefore be considered for future research. In the same unsubstantiated but interesting vein, the findings of the source space visualizations may also be considered. As seen in Figure 10, it is immediately clear that there is a regional difference between conditions. The active condition demonstrates activity in the inferior frontal gyrus, a part of the prefrontal cortex, which is responsible for language processing and several cognitive functions such as attention and response inhibition (Hartwigsen et al., 2019; Ishkhanyan et al., 2020). Consequently, it may be tempting to place this activity as audio processing, which is a distinct possibility, however it may not be. Audio processing typically involves the temporal lobes, and

the lack of their activation in this figure suggests that the activation observed originates from elsewhere (Onitsuka et al., 2004). While not more plausible, another explanation of this activity could be olfactory stimuli of the olfactory bulb as the left and right inferior frontal gyri are situated on either side of its housing (Mori et al., 1999). It then remains that this activity could be a reflection of olfactory nerve activation brought

on by the active device condition. This would also explain why both the gyri are for the most part equally activated.

The sham device appears to be creating activation in the somatosensory cortex, as has previously been mentioned, but it also appears to create activity in the frontopolar cortex, as seen in Figure 10. This area of the brain deals with cognitive engagement and the redistribution of cognitive resources (Mansouri et al., 2015). It is also considered part of the DMN. The DMN is closely linked to the cingulate gyrus, which was consistently significant within the network analysis of source space reconstruction (Sandhu et al., 2021). Activation in this area could reflect the natural cognitive allocation of resources to novel circumstances, as would be expected in both experimental conditions. The lack of activation in this area during the device condition is perhaps contrary to this point but could also be reflective of the substantial differences in magnitude present between conditions.

When these magnitude disparities were adjusted, as shown in figures 11, all prior patterns largely held. Even in these figures, the charge power scales have not been matched, as doing so would result in either one empty brain or a brain totally white with activity. At this adjusted scale, though, the somatosensory cortex becomes clearly active in the device condition, and more of the frontal cortex is involved in the sham condition. The continuing disparity in charge power and activity in the frontal lobe further suggests that there are possibly legitimate differences across the cortex. Another evident pattern in figures 12 is that of lateralization.

The lateralization of these findings led to the generation of figures 12, which divided data by nasal patency, which is itself alternative and lateralized (Kahana-Zweig et al., 2016; Sinha et al., 2021). Here, an ipsilateral trend became visible. At its face, this suggests that there may be structures driving observed activity trends within the nose

itself, the most obvious of these being the olfactory nerve and the nasal bulb. This would line up neatly with figures 10 with its activity in the olfactory sulcus and would also rationalize the ipsilateral activity as the olfactory nerve is ipsilaterally oriented. The olfactory nerve is also only stimulated chemically, which means if it does have a role in observed neuronal activity, the most plausible chemical stimulus for it to be responding to would be NO (Gage & Nighorn, 2014). It is tempting to suggest, therefore, that NO is a strong possible mechanism of effect for observations within the findings; however, this would not explain the same lateralization pattern in the sham condition. While NO could still have a role in the activity observed, this pattern may be better explained by different afferent pathways stimulated by both experimental conditions.

Once again, particularly the disparities in the location of activity are speculative. They do represent genuine patterns present within the data collected; however, the epistemological implications of the phrase "absence of evidence is not evidence of absence" need to be considered. While the observed could be due to chance, no statistical assessment is even made at this level because the paradigm of brain activity held in this report is that of network systems and this does not yet represent a network. All the same, the core of this project is that of an exploratory study, and within this respect, these findings are not only interesting unto themselves even without statistical significance, but by their presence, offer a clear avenue for further research. Finally, this concept is double-sided though; for example, a point made earlier dependent on the lack of Alpha significance relative to Beta significance indicating multimodal integration might itself be a misleading finding. With a larger sample size, or different statistical metrics, perhaps Alpha activity would become significant, and the aforementioned point be debunked. All the same, the presentation of evidence and its interpretation within this report can only be done on the data it has generated, and here the findings stand as they have been presented.

Limitations, strengths and further research

A fundamental limitation of this project was its crude statistical assessments. As an exploratory study, the intention at the onset was not to perform hypothesis testing; as such, no calculations were made for power or Alpha. Even if statistical significance were widely found, it would, at best, have to be considered tentative. This led to the adoption of a T-test assessment scheme, which was only applied to network outcomes and sensor power. Sensor power was included as it serves as a sanity check in this report, as well as an outcome. Not performing a statistical analysis of power within source space is then a missed opportunity and offers an avenue for further analysis. Additionally, a T-test setup may be inappropriate for the context of this experiment. As the focus of statistical scrutiny was on connectivity, it would have been advantageous to use a specialized statistical assessment such as the aforementioned network-based statistics (Zalesky et al., 2010). Such metrics account for errors emerging from the types of mass testing involved in network statistical assessments, beyond that which could be offered by false detection algorithms. This makes them more suitable for assessments such as those performed in this report. Furthermore, outside of connectivity assessment, the spectral power assessment of this project could have benefited from more sophisticated statistical approaches such as clustered permutation testing (Meyer et al., 2021). This technique first randomizes the traits of conditions, then generates a statistic, then repeats these steps to generate a permutation and then determines where in the distribution the original data's statistic falls. As such, this method constitutes a nonparametric test and is a popular and effective statistical tool utilized in neuroscience (Candia-Rivera & Valenza, 2022). Its utilization is also an avenue for further research both with the data acquired as part of this project and neuroimaging data acquired on the present topics henceforth.

Additionally, a similar argument can be made about the use of the false discovery control (FDC) algorithm. Classical FDCs are often thought of as overly conservative when applied to network data due to their simplistic handling of high volumes of hypothesis tests (Fornito et al., 2016). Contemporary FDC algorithms have attempted to account for such shortcomings by incorporating supplementary metrics along with p-values to increase power (Korthauer et al., 2019). However, the algorithm (from SciPy. Stats) used here did not. The general failure of the specifically utilized FDC to find significance within this project then likely reflects its inappropriateness given the subject matter and the low participant number.

In contrast, an overt strength of this project was its use of sequential analysis. By first verifying the biological feasibility of power spectrum findings, further interpretation of data could be done with increased confidence. This element of analysis served both as an independent metric of interest, with findings as explored, and an extremely robust sanity check. This ties neatly into another strength of this project, which comes from its multi-scale and multi-analysis approach to its data. The components of all spectral time series signals, EEG included, are made up of power (amplitude), phase, and frequency. This project's approach has meant that all of these properties were analyzed or integrated into its investigation. Spectral power served as a classical EEG analysis technique investigating power and provided a rigorous data validation check. Phase is by definition the concern of connectivity and frequency is integrated by using traditional wave bands at all points of analysis. This was further built upon for connectivity by analysis in both source and sensor space. While such an effort is rare, none of the techniques used are novel independently. What is unique is for all of them to be done as part of a single project.

Here, as mentioned, this has allowed for convergent patterns to emerge in wave bands, for example, Beta, and in areas, for example, the somatosensory cortex and the inferior parietal lobe. The interpretation that Goodair Nosebuds activity in the somatosensory cortex and the inferior parietal lobe is not only significant in Beta power, but also in connectivity, suggests synchronous activity between these areas. Such an activity profile would be expected in multimodal sensory integration, a sensible task undertaken by the brain in response to the experiment condition. This example captures all three of the components of a time series signal and illustrates how together, they can contribute to the detection and constitution of a biologically feasible phenomenon. Such insight would not have been possible if the project had adopted a less comprehensive approach. While either significance of power or connectivity would have indicated activation patterns, convergence onto it from independent metrics across multiple organizational levels raises confidence and clarity of an emergent happening. This is a particularly desirable trait in an exploratory study.

Clear limitations also existed intrinsic to the experiment's design. Already touched on is the sham device’s imperfection in that it produces no ventilation-responsive audio, something that the active condition does. This was an unfortunate material restriction that provided a difficult-to-mitigate, serious confounding variable. However, as audio processing remains a likely contributor to the driving mechanism of at least some of the significant activation effects observed, it may not be the sole contributor. As mentioned, this would not by itself result in multimodal processing, which is a better functional fit for the findings here than pure audio processing (Y. E. Cohen, 2009; Onitsuka et al., 2004). This more complete constitution of observed activity is once again thanks to the variety of approaches utilized in this project, an aforementioned strength that somewhat allows for the possibility of working around the confounding variable of sound. Nevertheless, it remains a confounding variable which has profoundly affected

confidence in result interpretations. Particularly when considered that the audio stimuli were not random or rhythmic, but enterally responsive to a participant's own ventilation. This could thereby bring attention to the breath itself. While a simple audio stimulus might not be enough to elicit multimodal sensory integration, this might. As such a key correction to be made in subsequent validation and replication studies is the elimination of this confounding variable. Another avenue for further research.

Epoching within analysis can also be considered restricting. Firstly, only the first clean 60-second period after device insertion, both sham and active, was acquired. A necessity to preserve data quality, it also meant that the first instances of device effect regardless of condition are not represented in processed data. From the time of insertion to a participant becoming settled once more (not moving to adjust the device or respond to it with large motion) was up to 60 seconds. If, for instance, hypothetically, NO does contribute to observed effects in some way, it is notable that the majority of static NO in the maxillary sinus will have been expelled by the start of an epoch (Weitzberg & Lundberg, 2002). Such an effect would be extremely pertinent, but this report is unable to provide any note on possible effects present in data that were impossible to analyze. Adding additional complexity to issues with epoching is that the active device alternates open nostrils every 90 seconds. For most participants then, the epoched data likely represents the stimulation of air in only one nostril, the right, which limits the interpretability of results once again. This also has an impact on lateralization. The points on lateralization during interpretations were noted as highly speculative, partly for this reason, this restriction could offer evidence explicitly to the contrary of the points made there. While it was suggested that those patterns present could be due to NO in some capacity, the limitation of air stimulation to only one nostril would likely suggest otherwise. Therefore, the observed patterns may be less dependent on any property of any

experiment condition and more so intrinsically linked to nasal patency itself. Regardless, this offers another interesting avenue for further research.

While not precisely a design limitation, the stringent exclusion criteria should also be mentioned. The exclusion of several common chronic disorders, as well as smoking including vaping, resulted in a distinct population that may be considered overly healthy to be generalizable to the public. Such a population may not represent the best use cases for a therapeutic effect either, as in this case, it is likely no therapeutic effect is needed, so one will not occur. While this is not always the case with treatments, for example, an opioid will always cause an effect but it being adaptive depending on circumstance, others such as walking to improve cardio health will have a diminishing effect the closer a person is to a healthy cardiac output (Murtagh et al., 2010). This creates a distinction between types of therapeutic effects and a disparity in safety profiles (Naci & Ioannidis, 2015). Although the Nosebuds are a hitherto untested technology, it is likely that their effect is analogous to that of the latter example as opposed to the former. Hence the issue with testing in a healthy population sample. This point however will be better assessed by the ANS metrics collected as part of this project, but not analyzed here.

Several technical limitations also exist. For example, a virtual average was used as part of preprocessing, a widely well-regarded technique to perform the required task (Teplan, 2002). But recent literature has suggested that a standardized infinity zero reference may be more suitable, particularly when working with network metrics. Zheng et al (2018) utilized a high-density (64-channel) EEG array, the same as this project, and found that differences in connectivity profiles of behavior states as well as small-worldness in music listing was significantly higher when using an infinity zero reference scheme vs a virtual average. There were also disparities between the referencing modalities for power, although these were not quite as clear as those for connectivity.

Nevertheless, this represents a technological development that could have a profound impact on all the findings of this report and offers additional possibilities for further research.

Something else that carries a series of technical considerations is the use of the Beamformer source localization algorithm. The use of any source localization algorithm first constitutes a strength of this project due to the several insights made by the addition of source space data. Examples of this come from the specificity of activity to region and the identification of otherwise difficult-to-implicate structures, such as the posterior cingulate gyrus. However, the findings of a recent study by Halder et al (2019) suggests that an LCMV beamformer could be outperformed by an eLORETA within at least false detection resistance. Due to its exploratory nature, this project has chosen to operate as conservatively as possible, on this principle an eLORETA could be argued as more appropriate for the present project. This is not to discredit LCMV Beamformers however as the same study pointed out that they were also successful at every task presented, so the validity and reliability of the technique is not in question, simply its relative resistance to type one error. The use of an eLORETA would also dramatically drop voxel resolution, from over 20,000 in this project, to likely less than 7,000. An undesirable outcome as this could have compromised the specificity of activity to region that is a key strength of this project. An avenue for further research then might be the development of an eLORETA algorithm to provide a cross-verification step within source space supplementary to the now-existent Beamformer scripts.

An additional technical limitation regarding the beamformer arises from its data covariance matrix. In MEG research, this is calculated with an ambient room measurement (Singh, 2014). In EEG research, this is calculated over a non-task-related epoch (Hoey et al., 1999). In this project, this was done using a clean 60-second epoch

from the wash-in period, as this represents dedicated nasal breathing free from both the sham and active devices. However, it remains a wash-in and not a true baseline (Laursen et al., 2019). The participants were likely aroused at the beginning of this period as it comes directly after up to an hour of equipment application in a small uniformly dark EEG booth. This is why it constitutes a wash-in rather than a baseline, as during this time it is hoped that any effects that are contingent on this arousal are allowed to fade. Therefore, by calculating a covariance matrix over an epoch within this period, it could arguably be capturing some effect of this arousal if present, which could change source space findings. While this is unlikely to be substantial, it bears mentioning as a limitation all the same.

Another strength of this project comes from its use of WPLI. The volume conductivity problem remains a challenge when working with EEG/MEG data. Here this was addressed in part by the LCMV Beamformer, but also by the use of a PLI metric for connectivity. In past studies, such as Herrero et al (2018), metrics such as PLV have been used, which is sensitive to volume conductivity and therefore dubious to interpret. PLI and WPLI do not share this issue as they are both relatively resistant to volume conductivity at the cost of sensitivity to noise and a propensity for type 2 errors. The former was also why rigorous data cleaning and validation, made possible by the bespoke pipeline developed for this project, was critical for this project. Additionally, WPLI, while simultaneously representing a fuller account of data than would be possible within a thresholded PLI, has been demonstrated to outperform PLI in real local field potentials in coherence and imaginary coherence (Stam et al., 2007). Collectively, this report represents a step forward for connectivity breathing investigations.

PLI/WPLI's propensity for type 2 errors is a meaningful limitation, however. Due to their mathematical particulars, naturally occurring phenomena of simulation phasing

are excluded. This is an issue because neuronal activation can fairly be modeled as a dipole, sets of simultaneous opposite charges separated by space (Niedermeyer, 1996). What affords this metric its resistance to volume conductivity then also ensures that genuine neurological activity is also rejected, making this metric extremely conservative. This was deemed appropriate for this project due to its exploratory nature and objective to find valid biologically feasible phenomena, but further research should consider supplementing with less conservative metrics to assess valid data that is undoubtedly being under-represented within present findings.

Finally, other research avenues include further graph theoretical explorations inspecting yet more sophisticated data patterns. The network paradigm of this project has been insightful so this may continue to be a fruitful line of inquiry. Although several network matrices were a part of this project, no account of motifs or cores was made (Sporns, 2016). For example, a sensible research suggestion might be an investigation of giant components between conditions to better illuminate what key structures may be acting within and between breathing conditions. Additionally, while betweenness and eigenvector centrality were both used here as proxies for graph integration, dedicated metrics for this do exist such as global efficacy (Rubinov & Sporns, 2010). Therefore, further investigations can also improve upon metric fundamentals as well. An ideal brain graph would capture spatial embedding, node heterogeneity, connectivity weights, connectivity directionality, edge heterogeneity, and dynamic organizational changes (Fornito et al., 2016). Despite the extent of investigation in this project, only two, spatial embedding and connectivity, were accounted for here, and even these only tentatively. This leaves several options for further network-oriented projects. Some of the aforementioned properties could be uniquely challenging but reasonable next steps from here could be the generation of directed graphs (accounting for connectivity

directionality) and a small-worldness assessment (attempting a better account for graph organization) as this is a known property of the brain (Bassett & Bullmore, 2006).

Conclusion

Key findings

· Significant activity appeared primarily in the Beta wave band.

· Both power and connectivity analyses in sensor space activity in the somatosensory cortex and the inferior parietal lobe showed significant activity.

· Source localization further narrowed down specificity to these regions and also implicated structures associated with the default mode network (DMN).

· These findings, even when assessed extremely conservatively, are consistent with activity observed during multimodal sensory integration and a shift away from a true resting state.

The aim of this project was to explore the functional cortical profile of augmented breathing using Goodair Nosebuds. This involved a custom EEG pipeline processing 14 raw datasets through preprocessing, sensor power, sensor connectivity, source space reconstruction, parcellation, source space connectivity, and network assessments of connectivity. Despite conservative analyses, each modality revealed a consistent and biologically plausible effect, all pointing towards a similar activation pattern: multimodal sensory integration. This was evidenced by significant activity in both power and network connectivity observed in the somatosensory and inferior parietal lobes. Further network connectivity findings indicated significant changes in Default Mode Network (DMN) structures, suggesting a departure from a true resting state, which aligns with the interpretation of results regarding multimodal integration. Despite methodological constraints and a limited sample size, the consistent convergence of results instills

confidence in the validity of the observed effects. While validation and replication are necessary, these findings strongly suggest a genuine response to the active condition. These results open up exciting new research avenues, offering the potential for deeper insights into cortical breathing mechanisms and the development of innovative neuro-breathing therapeutic interventions.

References

Abramson, S. B., Amin, A. R., Clancy, R. M., & Attur, M. (2001). The role of nitric oxide in tissue destruction. *Best Practice & Research. Clinical Rheumatology*, *15*(5), 831–845. https://doi.org/10.1053/berh.2001.0196

Adamovich, T., Zakharov, I., Tabueva, A., & Malykh, S. (2022). The thresholding problem and variability in the EEG graph network parameters. *Scientific Reports*, *12*, 18659. https://doi.org/10.1038/s41598-022-22079-2

Akalin Acar, Z., & Makeig, S. (2013). Effects of Forward Model Errors on EEG Source Localization. *Brain Topography*, *26*(3), 378–396. https://doi.org/10.1007/s10548-012-0274-6

Al-Fahoum, A. S., & Al-Fraihat, A. A. (2014). Methods of EEG Signal Features Extraction Using Linear Analysis in Frequency and Time-Frequency Domains. *ISRN Neuroscience*, *2014*, 730218. https://doi.org/10.1155/2014/730218

Aminoff, M. J., & Sears, T. A. (1971). Spinal integration of segmental, cortical and breathing inputs to thoracic respiratory motoneurones. *The Journal of Physiology*, *215*(2), 557–575. https://doi.org/10.1113/jphysiol.1971.sp009485

Amoroso, E. C., Bell, F. R., & Rosenberg, H. (1954). The relationship of the vasomotor and respiratory regions in the medulla oblongata of the sheep. *The Journal of Physiology*, *126*(1), 86–95. https://doi.org/10.1113/jphysiol.1954.sp005194

Ara, A., & Marco-Pallarés, J. (2021). Different Thata connectivity patterns underlie pleasantness evoked by familiar and unfamiliar music. *Scientific Reports*, *11*(1), Article 1. https://doi.org/10.1038/s41598-021-98033-5

Bassett, D. S., & Bullmore, E. (2006). Small-World Brain Networks. *The Neuroscientist*, *12*(6), 512–523. https://doi.org/10.1177/1073858406293182

Bassett, D. S., Zurn, P., & Gold, J. I. (2018). On the nature and use of models in network neuroscience. *Nature Reviews. Neuroscience*, *19*(9), 566–578. https://doi.org/10.1038/s41583-018-0038-8

Bavelas, A. (1950). Communication Patterns in Task-Oriented Groups. *Journal of the Acoustical Society of America*, *22*, 725–730.

Bazanova, O. M., & Vernon, D. (2014). Interpreting EEG Alpha activity. *Neuroscience & Biobehavioral Reviews*, *44*, 94–110. https://doi.org/10.1016/j.neubiorev.2013.05.007

Benner, A., Patel, A. K., Singh, K., & Dua, A. (2023). Physiology, Bohr Effect. In *StatPearls*. StatPearls Publishing. http://www.ncbi.nlm.nih.gov/books/NBK526028/

Biggs, N., Lloyd, E. K., & Wilson, R. J. (1986). *Graph Theory, 1736-1936*. Clarendon Press.

Bilo, G., Revera, M., Bussotti, M., Bonacina, D., Styczkiewicz, K., Caldara, G., Giglio, A., Faini, A., Giuliano, A., Lombardi, C., Kawecka-Jaszcz, K., Mancia, G., Agostoni, P., & Parati, G. (2012). Effects of Slow Deep Breathing at High Altitude on Oxygen Saturation, Pulmonary and Systemic Hemodynamics. *PLoS ONE*, *7*(11), e49074. https://doi.org/10.1371/journal.pone.0049074

Binnewijzend, M. A. A., Adriaanse, S. M., Van der Flier, W. M., Teunissen, C. E., de Munck, J. C., Stam, C. J., Scheltens, P., van Berckel, B. N. M., Barkhof, F., & Wink, A. M. (2014). Brain network alterations in Alzheimer's disease measured by Eigenvector centrality in fMRI are related to cognition and CSF biomarkers. *Human Brain Mapping*, *35*(5), 2383–2393. https://doi.org/10.1002/hbm.22335

Bourgeois, J., & Minker, W. (Eds.). (2009). Linearly Constrained Minimum Variance Beamforming. In *Time-Domain Beamforming and Blind Source Separation: Speech Input in the Car Environment* (pp. 27–38). Springer US. https://doi.org/10.1007/978-0-387-68836-7_3

Breit, S., Kupferberg, A., Rogler, G., & Hasler, G. (2018). Vagus Nerve as Modulator of the Brain–Gut Axis in Psychiatric and Inflammatory Disorders. *Frontiers in Psychiatry*, *9*, 44. https://doi.org/10.3389/fpsyt.2018.00044

Brinkman, J. E., Toro, F., & Sharma, S. (2023). Physiology, Respiratory Drive. In *StatPearls*. StatPearls Publishing. http://www.ncbi.nlm.nih.gov/books/NBK482414/

Britton, J. W., Frey, L. C., Hopp, J. L., Korb, P., Koubeissi, M. Z., Lievens, W. E., Pestana-Knight, E. M., & St. Louis, E. K. (2016). *Electroencephalography (EEG): An Introductory Text and Atlas of Normal and Abnormal Findings in Adults, Children, and Infants* (E. K. St. Louis & L. C. Frey, Eds.). American Epilepsy Society. http://www.ncbi.nlm.nih.gov/books/NBK390354/

Brodmann, K. (1909). Vergleichende Lokalisationslehre der Grosshirnrinde in ihren Prinzipien dargestellt auf Grund des Zellenbaues. Barth.

Brown, R. P., & Gerbarg, P. L. (2009). Yoga Breathing, Meditation, and Longevity. *Annals of the New York Academy of Sciences*, *1172*(1), 54–62. https://doi.org/10.1111/j.1749-6632.2009.04394.x

Buettner, R., Fuhrmann, J., & Kolb, L. (2019). Towards high-performance differentiation between Narcolepsy and Idiopathic Hypersomnia in 10 minute EEG recordings using a Novel Machine Learning Approach. *2019 IEEE International Conference*

on E-Health Networking, Application & Services (HealthCom), 1–7. https://doi.org/10.1109/HealthCom46333.2019.9009608

Candia-Rivera, D., & Valenza, G. (2022). Cluster permutation analysis for EEG series based on non-parametric Wilcoxon–Mann–Whitney statistical tests. *SoftwareX*, *19*, 101170. https://doi.org/10.1016/j.softx.2022.101170

Cao, Y., Oostenveld, R., Alday, P. M., & Piai, V. (2022). Are Alpha and beta oscillations spatially dissociated over the cortex in context-driven spoken-word production? *Psychophysiology*, *59*(6), e13999. https://doi.org/10.1111/psyp.13999

Carabotti, M., Scirocco, A., Maselli, M. A., & Severi, C. (2015). The gut-brain axis: Interactions between enteric microbiota, central and enteric nervous systems. *Annals of Gastroenterology : Quarterly Publication of the Hellenic Society of Gastroenterology*, *28*(2), 203–209.

Chaitanya, S., Datta, A., Bhandari, B., & Sharma, V. K. (2022). Effect of Resonance Breathing on Heart Rate Variability and Cognitive Functions in Young Adults: A Randomised Controlled Study. *Cureus*, *14*(2), e22187. https://doi.org/10.7759/cureus.22187

Chennu, S., Finoia, P., Kamau, E., Allanson, J., Williams, G. B., Monti, M. M., Noreika, V., Arnatkeviciute, A., Canales-Johnson, A., Olivares, F., Cabezas-Soto, D., Menon, D. K., Pickard, J. D., Owen, A. M., & Bekinschtein, T. A. (2014). Spectral signatures of reorganised brain networks in disorders of consciousness. *PLoS Computational Biology*, *10*(10), e1003887. https://doi.org/10.1371/journal.pcbi.1003887

Chung, J. W., Ofori, E., Misra, G., Hess, C. W., & Vaillancourt, D. E. (2017). Beta-band activity and connectivity in sensorimotor and parietal cortex are important for

accurate motor performance. *NeuroImage*, *144*(Pt A), 164–173. https://doi.org/10.1016/j.neuroimage.2016.10.008

Clarke, D. D., & Sokoloff, L. (1999). Regulation of Cerebral Metabolic Rate. In *Basic Neurochemistry: Molecular, Cellular and Medical Aspects. 6th edition*. Lippincott-Raven. https://www.ncbi.nlm.nih.gov/books/NBK28194/

Clements, G. M., Bowie, D. C., Gyurkovics, M., Low, K. A., Fabiani, M., & Gratton, G. (2021). Spontaneous Alpha and Thata Oscillations Are Related to Complementary Aspects of Cognitive Control in Younger and Older Adults. *Frontiers in Human Neuroscience*, *15*. https://www.frontiersin.org/articles/10.3389/fnhum.2021.621620

Cohen, M. X. (2015). Effects of time lag and frequency matching on phase-based connectivity. *Journal of Neuroscience Methods*, *250*, 137–146. https://doi.org/10.1016/j.jneumeth.2014.09.005

Cohen, Y. E. (2009). Multimodal activity in the parietal cortex. *Hearing Research*, *258*(1–2), 100–105. https://doi.org/10.1016/j.heares.2009.01.011

Colle, J., & Massion, J. (1958). [Effect of motor cortex stimulation on the electrical activity of the phrenic and median nerves]. *Archives Internationales De Physiologie Et De Biochimie*, *66*(4), 496–514. https://doi.org/10.3109/13813455809084226

Combrisson, E., Vallat, R., O'Reilly, C., Jas, M., Pascarella, A., Saive, A., Thiery, T., Meunier, D., Altukhov, D., Lajnef, T., Ruby, P., Guillot, A., & Jerbi, K. (2019). Visbrain: A Multi-Purpose GPU-Accelerated Open-Source Suite for Multimodal Brain Data Visualization. *Frontiers in Neuroinformatics*, *13*. https://www.frontiersin.org/articles/10.3389/fninf.2019.00014

Davenport, P. W., & Vovk, A. (2009). Cortical and subcortical central neural pathways in respiratory sensations. *Respiratory Physiology & Neurobiology*, *167*(1), 72–86. https://doi.org/10.1016/j.resp.2008.10.001

de Haan, E. H. F., & Dijkerman, H. C. (2020). Somatosensation in the Brain: A Theoretical Re-evaluation and a New Model. *Trends in Cognitive Sciences*, *24*(7), 529–541. https://doi.org/10.1016/j.tics.2020.04.003

Dutschmann, M., & Dick, T. E. (2012). Pontine Mechanisms of Respiratory Control. *Comprehensive Physiology*, *2*(4), 2443–2469. https://doi.org/10.1002/cphy.c100015

Eby, G. A. (2006). Strong humming for one hour daily to terminate chronic rhinosinusitis in four days: A case report and hypothesis for action by stimulation of endogenous nasal nitric oxide production. *Medical Hypotheses*, *66*(4), 851–854. https://doi.org/10.1016/j.mehy.2005.11.035

Eherer, A., Netolitzky, F., Högenauer, C., Puschnig, G., Hinterleitner, T., Scheidl, S., Kraxner, W., Krejs, G., & Hoffmann, K. (2011). Positive Effect of Abdominal Breathing Exercise on Gastroesophageal Reflux Disease: A Randomized, Controlled Study. *The American Journal of Gastroenterology*, *107*, 372–378. https://doi.org/10.1038/ajg.2011.420

Elam, J. S., Glasser, M. F., Harms, M. P., Sotiropoulos, S. N., Andersson, J. L. R., Burgess, G. C., Curtiss, S. W., Oostenveld, R., Larson-Prior, L. J., Schoffelen, J.-M., Hodge, M. R., Cler, E. A., Marcus, D. M., Barch, D. M., Yacoub, E., Smith, S. M., Ugurbil, K., & Van Essen, D. C. (2021). The Human Connectome Project: A retrospective. *NeuroImage*, *244*, 118543. https://doi.org/10.1016/j.neuroimage.2021.118543

Epstein, C. M. (2003). Aliasing in the visual EEG: A potential pitfall of video display technology. *Clinical Neurophysiology*, *114*(10), 1974–1976. https://doi.org/10.1016/S1388-2457(03)00168-8

Evans, K. C. (2010). Cortico-limbic circuitry and the airways: Insights from functional neuroimaging of respiratory afferents and efferents. *Biological Psychology*, *84*(1), 13–25. https://doi.org/10.1016/j.biopsycho.2010.02.005

Fornito, A., Zalesky, A., & Bullmore, E. (2016). *Fundamentals of Brain Network Analysis*. Academic Press.

Freeman, L. C. (1977). A Set of Measures of Centrality Based on Betweenness. *Sociometry*, *40*(1), 35–41. https://doi.org/10.2307/3033543

Freeman, L. C. (1978). Centrality in social networks conceptual clarification. *Social Networks*, *1*(3), 215–239. https://doi.org/10.1016/0378-8733(78)90021-7

French, L., & Paus, T. (2015). A FreeSurfer view of the cortical transcriptome generated from the Allen Human Brain Atlas. *Frontiers in Neuroscience*, *9*. https://www.frontiersin.org/articles/10.3389/fnins.2015.00323

Fumoto, M., Sato-Suzuki, I., Seki, Y., Mohri, Y., & Arita, H. (2004). Appearance of high-frequency Alpha band with disappearance of low-frequency Alpha band in EEG is produced during voluntary abdominal breathing in an eyes-closed condition. *Neuroscience Research*, *50*(3), 307–317. https://doi.org/10.1016/j.neures.2004.08.005

Gage, S. L., & Nighorn, A. (2014). The role of nitric oxide in memory is modulated by diurnal time. *Frontiers in Systems Neuroscience*, *8*. https://www.frontiersin.org/articles/10.3389/fnsys.2014.00059

Gandevia, S. C., & Rothwell, J. C. (1987). Activation of the human diaphragm from the motor cortex. *The Journal of Physiology*, *384*, 109–118. https://doi.org/10.1113/jphysiol.1987.sp016445

Garcés, P., Baumeister, S., Mason, L., Chatham, C. H., Holiga, S., Dukart, J., Jones, E. J. H., Banaschewski, T., Baron-Cohen, S., Bölte, S., Buitelaar, J. K., Durston, S., Oranje, B., Persico, A. M., Beckmann, C. F., Bougeron, T., Dell'Acqua, F., Ecker, C., Moessnang, C., … The EU-AIMS LEAP group authorship. (2022). Resting state EEG power spectrum and functional connectivity in autism: A cross-sectional analysis. *Molecular Autism*, *13*(1), 22. https://doi.org/10.1186/s13229-022-00500-x

Gaytán, S. P., & Pásaro, R. (1998). Connections of the rostral ventral respiratory neuronal cell group: An anterograde and retrograde tracing study in the rat. *Brain Research Bulletin*, *47*(6), 625–642. https://doi.org/10.1016/s0361-9230(98)00125-7

Gehrlach, D. A., Weiand, C., Gaitanos, T. N., Cho, E., Klein, A. S., Hennrich, A. A., Conzelmann, K.-K., & Gogolla, N. (2020). A whole-brain connectivity map of mouse insular cortex. *eLife*, *9*, e55585. https://doi.org/10.7554/eLife.55585

Gerber, K. J., Squires, K. E., & Hepler, J. R. (2016). Roles for Regulator of G Protein Signaling Proteins in Synaptic Signaling and Plasticity. *Molecular Pharmacology*, *89*(2), 273–286. https://doi.org/10.1124/mol.115.102210

Glasser, M. F., Coalson, T. S., Robinson, E. C., Hacker, C. D., Harwell, J., Yacoub, E., Ugurbil, K., Andersson, J., Beckmann, C. F., Jenkinson, M., Smith, S. M., & Van Essen, D. C. (2016). A multi-modal parcellation of human cerebral cortex. *Nature*, *536*(7615), 171–178. https://doi.org/10.1038/nature18933

Goodale, S. E., González, H. F. J., Johnson, G. W., Gupta, K., Rodriguez, W. J., Shults, R., Rogers, B. P., Rolston, J. D., Dawant, B. M., Morgan, V. L., & Englot, D. J. (2020). Resting-State SEEG May Help Localize Epileptogenic Brain Regions. *Neurosurgery*, *86*(6), 792–801. https://doi.org/10.1093/neuros/nyz351

Guimerà, R., & Nunes Amaral, L. A. (2005). Functional cartography of complex metabolic networks. *Nature*, *433*(7028), Article 7028. https://doi.org/10.1038/nature03288

Guyenet, P. G., Stornetta, R. L., & Bayliss, D. A. (2010). Central respiratory chemoreception. *The Journal of Comparative Neurology*, *518*(19), 3883–3906. https://doi.org/10.1002/cne.22435

Haas, L. (2003). Hans Berger (1873–1941), Richard Caton (1842–1926), and electroencephalography. *Journal of Neurology, Neurosurgery, and Psychiatry*, *74*(1), 9. https://doi.org/10.1136/jnnp.74.1.9

Halder, T., Talwar, S., Jaiswal, A. K., & Banerjee, A. (2019). Quantitative Evaluation in Estimating Sources Underlying Brain Oscillations Using Current Source Density Methods and Beamformer Approaches. *eNeuro*, *6*(4), ENEURO.0170-19.2019. https://doi.org/10.1523/ENEURO.0170-19.2019

Halland, M., Parthasarathy, G., Bharucha, A. E., & Katzka, D. A. (2016). Diaphragmatic breathing for rumination syndrome: Efficacy and mechanisms of action. *Neurogastroenterology & Motility*, *28*(3), 384–391. https://doi.org/10.1111/nmo.12737

Hamasaki, H. (2020). Effects of Diaphragmatic Breathing on Health: A Narrative Review. *Medicines (Basel, Switzerland)*, *7*(10), 65. https://doi.org/10.3390/medicines7100065

Hartwigsen, G., Neef, N. E., Camilleri, J. A., Margulies, D. S., & Eickhoff, S. B. (2019). Functional Segregation of the Right Inferior Frontal Gyrus: Evidence From Coactivation-Based Parcellation. *Cerebral Cortex (New York, N.Y.: 1991)*, *29*(4), 1532–1546. https://doi.org/10.1093/cercor/bhy049

Heck, D. H., McAfee, S. S., Liu, Y., Babajani-Feremi, A., Rezaie, R., Freeman, W. J., Wheless, J. W., Papanicolaou, A. C., Ruszinkó, M., Sokolov, Y., & Kozma, R. (2017). Breathing as a Fundamental Rhythm of Brain Function. *Frontiers in Neural Circuits*, *10*. https://www.frontiersin.org/articles/10.3389/fncir.2016.00115

Helwany, M., & Bordoni, B. (2023). Neuroanatomy, Cranial Nerve 1 (Olfactory). In *StatPearls*. StatPearls Publishing. http://www.ncbi.nlm.nih.gov/books/NBK556051/

Henson, R. N., Mattout, J., Phillips, C., & Friston, K. J. (2009). Selecting forward models for MEG source-reconstruction using model-evidence. *NeuroImage*, *46*(1), 168–176. https://doi.org/10.1016/j.neuroimage.2009.01.062

Herrero, J. L., Khuvis, S., Yeagle, E., Cerf, M., & Mehta, A. D. (2018). Breathing above the brain stem: Volitional control and attentional modulation in humans. *Journal of Neurophysiology*, *119*(1), 145–159. https://doi.org/10.1152/jn.00551.2017

Hoey, G. V., de Walle, R. V., Vanrumste, B., D'Have, M., Lemahieu, I., & Boon, P. (1999). *Beamforming Techniques Applied in EEG Source Analysis*.

Hopkins, E., Sanvictores, T., & Sharma, S. (2023). Physiology, Acid Base Balance. In *StatPearls*. StatPearls Publishing. http://www.ncbi.nlm.nih.gov/books/NBK507807/

Iizuka, M. (2001). Respiratory activity in glossopharyngeal, vagus and accessory nerves and pharyngeal constrictors in newborn rat in vitro. *The Journal of Physiology*, *532*(Pt 2), 535–548. https://doi.org/10.1111/j.1469-7793.2001.0535f.x

Ikeda, K., Kawakami, K., Onimaru, H., Okada, Y., Yokota, S., Koshiya, N., Oku, Y., Iizuka, M., & Koizumi, H. (2017). The respiratory control mechanisms in the brainstem and spinal cord: Integrative views of the neuroanatomy and neurophysiology. *The Journal of Physiological Sciences*, *67*(1), Article 1. https://doi.org/10.1007/s12576-016-0475-y

Ishkhanyan, B., Michel Lange, V., Boye, K., Mogensen, J., Karabanov, A., Hartwigsen, G., & Siebner, H. R. (2020). Anterior and Posterior Left Inferior Frontal Gyrus Contribute to the Implementation of Grammatical Determiners During Language Production. *Frontiers in Psychology*, *11*, 685. https://doi.org/10.3389/fpsyg.2020.00685

Jackson, K., Silva, H. M. V., Zhang, W., Michelini, L. C., & Stern, J. E. (2005). Exercise training differentially affects intrinsic excitability of autonomic and neuroendocrine neurons in the hypothalamic paraventricular nucleus. *Journal of Neurophysiology*, *94*(5), 3211–3220. https://doi.org/10.1152/jn.00277.2005

Jäncke, L., Liem, F., & Merillat, S. (2021). Are language skills related to structural features in Broca's and Wernicke's area? *European Journal of Neuroscience*, *53*(4), 1124–1135. https://doi.org/10.1111/ejn.15038

Jin, J., Dauwels, J., Vialatte, F. B., & Cichocki, A. (2014). Synchrony analysis of paroxysmal gamma waves in meditation EEG. *2014 IEEE International Conference on Acoustics, Speech and Signal Processing (ICASSP)*, 4703–4707. https://doi.org/10.1109/ICASSP.2014.6854494

Joyce, K. E., Laurienti, P. J., Burdette, J. H., & Hayasaka, S. (2010). A New Measure of Centrality for Brain Networks. *PLOS ONE*, *5*(8), e12200. https://doi.org/10.1371/journal.pone.0012200

Jung, S. I., Lee, N. K., Kang, K. W., Kim, K., & Lee, D. Y. (2016). The effect of smartphone usage time on posture and respiratory function. *Journal of Physical Therapy Science*, *28*(1), 186–189. https://doi.org/10.1589/jpts.28.186

Kahana-Zweig, R., Geva-Sagiv, M., Weissbrod, A., Secundo, L., Soroker, N., & Sobel, N. (2016). Measuring and Characterizing the Human Nasal Cycle. *PLOS ONE*, *11*(10), e0162918. https://doi.org/10.1371/journal.pone.0162918

Kc, P., & Dick, T. E. (2010). Modulation of cardiorespiratory function mediated by the paraventricular nucleus. *Respiratory Physiology & Neurobiology*, *174*(1–2), 55–64. https://doi.org/10.1016/j.resp.2010.08.001

Kc, P., Haxhiu, M. A., Trouth, C. O., Balan, K. V., Anderson, W. A., & Mack, S. O. (2002). CO(2)-induced c-Fos expression in hypothalamic vasopressin containing neurons. *Respiration Physiology*, *129*(3), 289–296. https://doi.org/10.1016/s0034-5687(01)00321-8

Kenny, B. J., & Bordoni, B. (2023). Neuroanatomy, Cranial Nerve 10 (Vagus Nerve). In *StatPearls*. StatPearls Publishing. http://www.ncbi.nlm.nih.gov/books/NBK537171/

Keser, Z., Buchl, S. C., Seven, N. A., Markota, M., Clark, H. M., Jones, D. T., Lanzino, G., Brown, R. D., Worrell, G. A., & Lundstrom, B. N. (2022). Electroencephalogram (EEG) With or Without Transcranial Magnetic Stimulation (TMS) as Biomarkers for Post-stroke Recovery: A Narrative Review.

Frontiers in Neurology, *13*. https://www.frontiersin.org/articles/10.3389/fneur.2022.827866

Kocjan, J., Adamek, M., Gzik-Zroska, B., Czyżewski, D., & Rydel, M. (2017). Network of Breathing. Multifunctional Role of the Diaphragm: A Review. *Advances in Respiratory Medicine*, *85*(4), Article 4. https://doi.org/10.5603/ARM.2017.0037

Korthauer, K., Kimes, P. K., Duvallet, C., Reyes, A., Subramanian, A., Teng, M., Shukla, C., Alm, E. J., & Hicks, S. C. (2019). A practical guide to methods controlling false discoveries in computational biology. *Genome Biology*, *20*(1), 118. https://doi.org/10.1186/s13059-019-1716-1

Koshland, D. E. (1992). The molecule of the year. *Science (New York, N.Y.)*, *258*(5090), 1861. https://doi.org/10.1126/science.1470903

Krout, K. E., Mettenleiter, T. C., Karpitskiy, V., Nguyen, X. V., & Loewy, A. D. (2005). CNS neurons with links to both mood-related cortex and sympathetic nervous system. *Brain Research*, *1050*(1–2), 199–202. https://doi.org/10.1016/j.brainres.2005.04.090

Kulkarni, V., Joshi, Y., & Manthalkar, R. (2022). A Clustering Approach for Sensory-Motor Cortex Signal Classification Using Electroencephalogram Signal for Brain-Computer Interface. In A. Dhawan, R. A. Mishra, K. V. Arya, & C. R. Zamarreño (Eds.), *Advances in VLSI, Communication, and Signal Processing* (pp. 277–291). Springer Nature. https://doi.org/10.1007/978-981-19-2631-0_26

Kumar, D., Zifan, A., Ghahremani, G., Kunkel, D. C., Horgan, S., & Mittal, R. K. (2020). Morphology of the Esophageal Hiatus: Is It Different in 3 Types of Hiatus Hernias? *Journal of Neurogastroenterology and Motility*, *26*(1), 51–60. https://doi.org/10.5056/jnm18208

Kuwaki, T. (2008). Orexinergic modulation of breathing across vigilance states. *Respiratory Physiology & Neurobiology*, *164*(1–2), 204–212. https://doi.org/10.1016/j.resp.2008.03.011

Lancaster, J. R. (2015). Nitric oxide: A brief overview of chemical and physical properties relevant to therapeutic applications. *Future Science OA*, *1*(1). https://doi.org/10.4155/fso.15.59

Laursen, D. R. T., Paludan-Müller, A. S., & Hróbjartsson, A. (2019). Randomized clinical trials with run-in periods: Frequency, characteristics and reporting. *Clinical Epidemiology*, *11*, 169–184. https://doi.org/10.2147/CLEP.S188752

Lei, X., & Liao, K. (2017). Understanding the Influences of EEG Reference: A Large-Scale Brain Network Perspective. *Frontiers in Neuroscience*, *11*, 205. https://doi.org/10.3389/fnins.2017.00205

Lemm, S., Blankertz, B., Curio, G., & Muller, K.-R. (2005). Spatio-spectral filters for improving the classification of single trial EEG. *IEEE Transactions on Biomedical Engineering*, *52*(9), 1541–1548. https://doi.org/10.1109/TBME.2005.851521

Li, R., & Principe, J. C. (2006). Blinking artifact removal in cognitive EEG data using ICA. Conference Proceedings: ... Annual International Conference of the IEEE Engineering in Medicine and Biology Society. IEEE Engineering in Medicine and Biology Society. Annual Conference, 2006, 5273–5276. https://doi.org/10.1109/IEMBS.2006.260605

Lindemann, J., Leiacker, R., Rettinger, G., & Keck, T. (2002). Nasal mucosal temperature during respiration. *Clinical Otolaryngology and Allied Sciences*, *27*(3), 135–139. https://doi.org/10.1046/j.1365-2273.2002.00544.x

Liotti, M., Brannan, S., Egan, G., Shade, R., Madden, L., Abplanalp, B., Robillard, R., Lancaster, J., Zamarripa, F. E., Fox, P. T., & Denton, D. (2001). Brain responses associated with consciousness of breathlessness (air hunger). *Proceedings of the National Academy of Sciences of the United States of America*, *98*(4), 2035–2040. https://doi.org/10.1073/pnas.98.4.2035

Lipski, J., Bektas, A., & Porter, R. (1986). Short latency inputs to phrenic motoneurones from the sensorimotor cortex in the cat. *Experimental Brain Research*, *61*(2), 280–290. https://doi.org/10.1007/BF00239518

Liu, H., Wiedman, C. M., Lovelace-Chandler, V., Gong, S., & Salem, Y. (2023). Deep Diaphragmatic Breathing—Anatomical and Biomechanical Consideration. *Journal of Holistic Nursing*, 08980101221149866. https://doi.org/10.1177/08980101221149866

Liu, X., Liu, S., Li, M., Su, F., Chen, S., Ke, Y., & Ming, D. (2022). Altered gamma oscillations and beta–gamma coupling in drug-naive first-episode major depressive disorder: Association with sleep and cognitive disturbance. *Journal of Affective Disorders*, *316*, 99–108. https://doi.org/10.1016/j.jad.2022.08.022

Lohmann, G., Margulies, D. S., Horstmann, A., Pleger, B., Lepsien, J., Goldhahn, D., Schloegl, H., Stumvoll, M., Villringer, A., & Turner, R. (2010). Eigenvector centrality mapping for analyzing connectivity patterns in fMRI data of the human brain. *PloS One*, *5*(4), e10232. https://doi.org/10.1371/journal.pone.0010232

Lorenzini, L., Ingala, S., Collij, L. E., Wottschel, V., Haller, S., Blennow, K., Frisoni, G., Chételat, G., Payoux, P., Lage-Martinez, P., Ewers, M., Waldman, A., Wardlaw, J., Ritchie, C., Gispert, J. D., Mutsaerts, H. J. M. M., Visser, P. J., Scheltens, P., Tijms, B., … Wink, A. M. (2023). Eigenvector centrality dynamics are related to

Alzheimer's disease pathological changes in non-demented individuals. *Brain Communications*, *5*(3), fcad088. https://doi.org/10.1093/braincomms/fcad088

Louis, E. K. S., Frey, L. C., Britton, J. W., Frey, L. C., Hopp, J. L., Korb, P., Koubeissi, M. Z., Lievens, W. E., Pestana-Knight, E. M., & Louis, E. K. S. (2016). Appendix 6. A Brief History of EEG. In *Electroencephalography (EEG): An Introductory Text and Atlas of Normal and Abnormal Findings in Adults, Children, and Infants [Internet]*. American Epilepsy Society. https://www.ncbi.nlm.nih.gov/books/NBK390348/

Lucas-Neto, L., Neto, D., Oliveira, E., Martins, H., Mourato, B., Correia, F., Rainha-Campos, A., & Gonçalves-Ferreira, A. (2013). Three dimensional anatomy of the human nucleus accumbens. *Acta Neurochirurgica*, *155*(12), 2389–2398. https://doi.org/10.1007/s00701-013-1820-z

Lundberg, J., & Weitzberg, E. (1999). Nasal nitric oxide in man. *Thorax*, *54*(10), 947–952.

Makarov, V. V., Zhuravlev, M. O., Runnova, A. E., Protasov, P., Maksimenko, V. A., Frolov, N. S., Pisarchik, A. N., & Hramov, A. E. (2018). Betweenness centrality in multiplex brain network during mental task evaluation. *Physical Review E*, *98*(6), 062413. https://doi.org/10.1103/PhysRevE.98.062413

Mankowski, N. L., & Bordoni, B. (2023). Anatomy, Head and Neck, Nasopharynx. In *StatPearls*. StatPearls Publishing. http://www.ncbi.nlm.nih.gov/books/NBK557635/

Mansouri, F. A., Buckley, M. J., Mahboubi, M., & Tanaka, K. (2015). Behavioral consequences of selective damage to frontal pole and posterior cingulate cortices.

Proceedings of the National Academy of Sciences, *112*(29), E3940–E3949. https://doi.org/10.1073/pnas.1422629112

Martin, K. C., Ketchabaw, W. T., & Turkeltaub, P. E. (2022). Plasticity of the language system in children and adults. *Handbook of Clinical Neurology*, *184*, 397–414. https://doi.org/10.1016/B978-0-12-819410-2.00021-7

Mason, O., & Verwoerd, M. (2006). *Graph Theory and Networks in Biology* (arXiv:q-bio/0604006). arXiv. http://arxiv.org/abs/q-bio/0604006

McGovern, A. E., Ajayi, I. E., Farrell, M. J., & Mazzone, S. B. (2017). A neuroanatomical framework for the central modulation of respiratory sensory processing and cough by the periaqueductal grey. *Journal of Thoracic Disease*, *9*(10), 4098–4107. https://doi.org/10.21037/jtd.2017.08.119

McKay, L. C., & Feldman, J. L. (2008). Unilateral Ablation of Pre-Bötzinger Complex Disrupts Breathing during Sleep but Not Wakefulness. *American Journal of Respiratory and Critical Care Medicine*, *178*(1), 89–95. https://doi.org/10.1164/rccm.200712-1901OC

Medford, N., & Critchley, H. D. (2010). Conjoint activity of anterior insular and anterior cingulate cortex: Awareness and response. *Brain Structure & Function*, *214*(5–6), 535–549. https://doi.org/10.1007/s00429-010-0265-x

Merighi, A. (2017). Neuropeptides and Coexistence☆. In *Reference Module in Neuroscience and Biobehavioral Psychology*. Elsevier. https://doi.org/10.1016/B978-0-12-809324-5.02310-5

Meyer, M., Lamers, D., Kayhan, E., Hunnius, S., & Oostenveld, R. (2021). Enhancing reproducibility in developmental EEG research: BIDS, cluster-based permutation

tests, and effect sizes. *Developmental Cognitive Neuroscience*, *52*, 101036. https://doi.org/10.1016/j.dcn.2021.101036

Michel, C. M., & Brunet, D. (2019). EEG Source Imaging: A Practical Review of the Analysis Steps. *Frontiers in Neurology*, *10*. https://www.frontiersin.org/articles/10.3389/fneur.2019.00325

Miinalainen, T., Rezaei, A., Us, D., Nüßing, A., Engwer, C., Wolters, C. H., & Pursiainen, S. (2019). A realistic, accurate and fast source modeling approach for the EEG forward problem. *NeuroImage*, *184*, 56–67. https://doi.org/10.1016/j.neuroimage.2018.08.054

Möcks, J., & Gasser, T. (1984). How to select epochs of the EEG at rest for quantitative analysis. *Electroencephalography and Clinical Neurophysiology*, *58*(1), 89–92. https://doi.org/10.1016/0013-4694(84)90205-0

Mori, K., Nagao, H., & Yoshihara, Y. (1999). The olfactory bulb: Coding and processing of odor molecule information. *Science (New York, N.Y.)*, *286*(5440), 711–715. https://doi.org/10.1126/science.286.5440.711

Muñoz-Ortiz, J., Muñoz-Ortiz, E., López-Meraz, L., Beltran-Parrazal, L., & Morgado-Valle, C. (2019). The pre-Bötzinger complex: Generation and modulation of respiratory rhythm. *Neurología (English Edition)*, *34*(7), 461–468. https://doi.org/10.1016/j.nrleng.2018.05.006

Murtagh, E. M., Murphy, M. H., & Boone-Heinonen, J. (2010). Walking – the first steps in cardiovascular disease prevention. *Current Opinion in Cardiology*, *25*(5), 490–496. https://doi.org/10.1097/HCO.0b013e32833ce972

Muthukumaraswamy, S. D. (2013). High-frequency brain activity and muscle artifacts in MEG/EEG: A review and recommendations. *Frontiers in Human Neuroscience*, *7*, 138. https://doi.org/10.3389/fnhum.2013.00138

Naci, H., & Ioannidis, J. P. A. (2015). Comparative effectiveness of exercise and drug interventions on mortality outcomes: Metaepidemiological study. *British Journal of Sports Medicine*, *49*(21), 1414–1422. https://doi.org/10.1136/bjsports-2015-f5577rep

Nattie, E., & Li, A. (2012). Central Chemoreceptors: Locations and Functions. *Comprehensive Physiology*, *2*(1), 221–254. https://doi.org/10.1002/cphy.c100083

Newman, M., & Newman, M. (2018). *Networks* (Second Edition, Second Edition). Oxford University Press.

Niedermeyer, E. (1996). Dipole theory and electroencephalography. *Clinical EEG (Electroencephalography)*, *27*(3), 121–131. https://doi.org/10.1177/155005949602700305

Nowak, A., Christensen, J., Mabry, T., Townsend, J., & Wells, M. (2019). *Pediatric Dentistry* (6th ed.). Elsevier. https://doi.org/10.1016/B978-0-323-60826-8.00106-1

Nowinski, W. L. (2011). Introduction to Brain Anatomy. In K. Miller (Ed.), *Biomechanics of the Brain* (pp. 5–40). Springer. https://doi.org/10.1007/978-1-4419-9997-9_2

Ochoa-Repáraz, J., & Kasper, L. H. (2016). The Second Brain: Is the Gut Microbiota a Link Between Obesity and Central Nervous System Disorders? *Current Obesity Reports*, *5*(1), 51–64. https://doi.org/10.1007/s13679-016-0191-1

Oldham, S., Fulcher, B., Parkes, L., Arnatkevičiūtė, A., Suo, C., & Fornito, A. (2019). Consistency and differences between centrality measures across distinct classes of networks. *PLOS ONE*, *14*(7), e0220061. https://doi.org/10.1371/journal.pone.0220061

Oliver, K. A., & Ashurst, J. V. (2023). Anatomy, Thorax, Phrenic Nerves. In *StatPearls*. StatPearls Publishing. http://www.ncbi.nlm.nih.gov/books/NBK513325/

Onitsuka, T., Shenton, M. E., Salisbury, D. F., Dickey, C. C., Kasai, K., Toner, S. K., Frumin, M., Kikinis, R., Jolesz, F. A., & McCarley, R. W. (2004). Middle and Inferior Temporal Gyrus Gray Matter Volume Abnormalities in Chronic Schizophrenia: An MRI Study. *The American Journal of Psychiatry*, *161*(9), 1603–1611. https://doi.org/10.1176/appi.ajp.161.9.1603

Özugur, S., Kunz, L., & Straka, H. (2020). Relationship between oxygen consumption and neuronal activity in a defined neural circuit. *BMC Biology*, *18*(1), 76. https://doi.org/10.1186/s12915-020-00811-6

Park, Y.-J., & Park, Y.-B. (2012). Clinical utility of paced breathing as a concentration meditation practice. *Complementary Therapies in Medicine*, *20*(6), 393–399. https://doi.org/10.1016/j.ctim.2012.07.008

Pedersen, M., Pardoe, H. R., Mito, R., Sethi, M., Vaughan, D. N., Carney, P. W., & Jackson, G. D. (2023). *Anti-Seizure Medications Alter the Brain's Network Topology* (p. 2023.09.01.23294923). medRxiv. https://doi.org/10.1101/2023.09.01.23294923

Peiffer, C., Costes, N., Hervé, P., & Garcia-Larrea, L. (2008). Relief of dyspnea involves a characteristic brain activation and a specific quality of sensation. *American*

Journal of Respiratory and Critical Care Medicine, *177*(4), 440–449. https://doi.org/10.1164/rccm.200612-1774OC

Peper, E., Mason, L., & Huey, C. (2017). Healing Irritable Bowel Syndrome with Diaphragmatic Breathing. *Biofeedback*, *45*(4), 83–87. https://doi.org/10.5298/1081-5937-45.4.04

Pernet, C. R., Appelhoff, S., Gorgolewski, K. J., Flandin, G., Phillips, C., Delorme, A., & Oostenveld, R. (2019). EEG-BIDS, an extension to the brain imaging data structure for electroencephalography. *Scientific Data*, *6*(1), 103. https://doi.org/10.1038/s41597-019-0104-8

Pirzada, S. (2007). Applications of graph theory. *PAMM*, *7*(1), 2070013–2070013. https://doi.org/10.1002/pamm.200700981

Pisanski, A., & Pagliardini, S. (2019). The parafacial respiratory group and the control of active expiration. *Respiratory Physiology & Neurobiology*, *265*, 153–160. https://doi.org/10.1016/j.resp.2018.06.010

Por, E., van Kooten, M., & Sarkovic, V. (2019). *Nyquist–Shannon sampling theorem*.

Powell, F. L. (2006). VENTILATION | Control. In G. J. Laurent & S. D. Shapiro (Eds.), *Encyclopedia of Respiratory Medicine* (pp. 438–446). Academic Press. https://doi.org/10.1016/B0-12-370879-6/00426-9

Power, J. D., Plitt, M., Laumann, T. O., & Martin, A. (2017). Sources and implications of whole-brain fMRI signals in humans. *NeuroImage*, *146*, 609–625. https://doi.org/10.1016/j.neuroimage.2016.09.038

Prasad, R., Bakardjian, H., Cichocki, A., & Matsuno, F. (2007). Source localization with EEG data for BP shows major activities in the frontal areas of the brain. In

Proceedings of the SICE Annual Conference (p. 778). https://doi.org/10.1109/SICE.2007.4421087

Prasad, R., & Matsuno, F. (2007). Hummgenic changes in large scale temporal correlation of EEG in BP. *Proceedings of the SICE Annual Conference*. https://doi.org/10.1109/SICE.2007.4421328

Prasad, R., Matsuno, F., Bakardjian, H., Vialatte, F., & Cichocki, A. (2006). *EEG Changes After Bhramari Pranayama*.

Proctor, D. F., & Andersen, I. H. P. (1982). *The Nose, Upper Airway Physiology and the Atmospheric Environment*. Elsevier Biomedical Press.

Proczka, M., Przybylski, J., Cudnoch-Jędrzejewska, A., Szczepańska-Sadowska, E., & Żera, T. (2021). Vasopressin and Breathing: Review of Evidence for Respiratory Effects of the Antidiuretic Hormone. *Frontiers in Physiology*, *12*, 744177. https://doi.org/10.3389/fphys.2021.744177

Qiu, W., Ma, L., Jiang, T., & Zhang, Y. (2022). Unrevealing Reliable Cortical Parcellation of Individual Brains Using Resting-State Functional Magnetic Resonance Imaging and Masked Graph Convolutions. *Frontiers in Neuroscience*, *16*. https://www.frontiersin.org/articles/10.3389/fnins.2022.838347

Roberts, J. A., Perry, A., Lord, A. R., Roberts, G., Mitchell, P. B., Smith, R. E., Calamante, F., & Breakspear, M. (2016). The contribution of geometry to the human connectome. *NeuroImage*, *124*(Pt A), 379–393. https://doi.org/10.1016/j.neuroimage.2015.09.009

Rogers, L. J. (2021). Brain Lateralization and Cognitive Capacity. *Animals : An Open Access Journal from MDPI*, *11*(7), 1996. https://doi.org/10.3390/ani11071996

Rolls, E. T. (2019). The cingulate cortex and limbic systems for emotion, action, and memory. *Brain Structure & Function*, *224*(9), 3001–3018. https://doi.org/10.1007/s00429-019-01945-2

Rossini, P. M., Di Iorio, R., Vecchio, F., Anfossi, M., Babiloni, C., Bozzali, M., Bruni, A. C., Cappa, S. F., Escudero, J., Fraga, F. J., Giannakopoulos, P., Guntekin, B., Logroscino, G., Marra, C., Miraglia, F., Panza, F., Tecchio, F., Pascual-Leone, A., & Dubois, B. (2020). Early diagnosis of Alzheimer's disease: The role of biomarkers including advanced EEG signal analysis. Report from the IFCN-sponsored panel of experts. *Clinical Neurophysiology*, *131*(6), 1287–1310. https://doi.org/10.1016/j.clinph.2020.03.003

Rubinov, M., & Sporns, O. (2010). Complex network measures of brain connectivity: Uses and interpretations. *NeuroImage*, *52*(3), 1059–1069. https://doi.org/10.1016/j.neuroimage.2009.10.003

Russo, M. A., Santarelli, D. M., & O'Rourke, D. (2017). The physiological effects of slow breathing in the healthy human. *Breathe*, *13*(4), 298–309. https://doi.org/10.1183/20734735.009817

Ryan, R., Spathis, A., Clow, A., Fallon, M., & Booth, S. (2014). The biological impact of living with chronic breathlessness—A role for the hypothalamic-pituitary-adrenal axis? *Medical Hypotheses*, *83*(2), 232–237. https://doi.org/10.1016/j.mehy.2014.04.011

Sandhu, Z., Tanglay, O., Young, I. M., Briggs, R. G., Bai, M. Y., Larsen, M. L., Conner, A. K., Dhanaraj, V., Lin, Y.-H., Hormovas, J., Fonseka, R. D., Glenn, C. A., & Sughrue, M. E. (2021). Parcellation-based anatomic modeling of the default mode network. *Brain and Behavior*, *11*(2), e01976. https://doi.org/10.1002/brb3.1976

Schottelkotte, K. M., & Crone, S. A. (2022). Forebrain control of breathing: Anatomy and potential functions. *Frontiers in Neurology*, *13*. https://www.frontiersin.org/articles/10.3389/fneur.2022.1041887

Schwab, J. A., & Zenkel, M. (1998). Filtration of particulates in the human nose. *The Laryngoscope*, *108*(1 Pt 1), 120–124. https://doi.org/10.1097/00005537-199801000-00023

Selvam, V. S., & Shenbagadevi, S. (2011). Brain tumor detection using scalp eeg with modified Wavelet-ICA and multi layer feed forward neural network. *2011 Annual International Conference of the IEEE Engineering in Medicine and Biology Society*, 6104–6109. https://doi.org/10.1109/IEMBS.2011.6091508

Shah-Basak, P. P., Dunkley, B. T., Ye, A. X., Wong, S., da Costa, L., & Pang, E. W. (2019). Altered beta-band functional connectivity may be related to 'performance slowing' in good outcome aneurysmal subarachnoid patients. *Neuroscience Letters*, *699*, 64–70. https://doi.org/10.1016/j.neulet.2019.01.053

Shahid, A., Wilkinson, K., Marcu, S., & Shapiro, C. M. (2011). Profile of Mood States (POMS). In A. Shahid, K. Wilkinson, S. Marcu, & C. M. Shapiro (Eds.), *STOP, THAT and One Hundred Other Sleep Scales* (pp. 285–286). Springer New York. https://doi.org/10.1007/978-1-4419-9893-4_68

Shahid, Z., Asuka, E., & Singh, G. (2023). Physiology, Hypothalamus. In *StatPearls*. StatPearls Publishing. http://www.ncbi.nlm.nih.gov/books/NBK535380/

Shoka, A., Dessouky, M., el-sherbeny, A., & El-Sayed, A. (2019). Literature Review on EEG Preprocessing, Feature Extraction, and Classifications Techniques. *Menoufia Journal of Electronic Engineering Research*, *28*, 292–299. https://doi.org/10.21608/mjeer.2019.64927

Sibbald, B., & Roberts, C. (1998). Understanding controlled trials Crossover trials. *BMJ : British Medical Journal*, *316*(7146), 1719–1720.

Šimić, G., Tkalčić, M., Vukić, V., Mulc, D., Španić, E., Šagud, M., Olucha-Bordonau, F. E., Vukšić, M., & R. Hof, P. (2021). Understanding Emotions: Origins and Roles of the Amygdala. *Biomolecules*, *11*(6), 823. https://doi.org/10.3390/biom11060823

Singh, S. P. (2014). Magnetoencephalography: Basic principles. *Annals of Indian Academy of Neurology*, *17*(Suppl 1), S107–S112. https://doi.org/10.4103/0972-2327.128676

Sinha, S., Mittal, S., Bhat, S., & Baro, G. (2021). Effect of Nasal Dominance on Pulmonary Function Test and Heart Rate: A Pilot Study. *International Journal of Yoga*, *14*(2), 141–145. https://doi.org/10.4103/ijoy.IJOY_115_20

Slater, J., Joober, R., Koborsy, B. L., Mitchell, S., Sahlas, E., & Palmer, C. (2022). Can electroencephalography (EEG) identify ADHD subtypes? A systematic review. *Neuroscience & Biobehavioral Reviews*, *139*, 104752. https://doi.org/10.1016/j.neubiorev.2022.104752

Smith, A. M., & Czyz, C. N. (2023). Neuroanatomy, Cranial Nerve 2 (Optic). In *StatPearls*. StatPearls Publishing. http://www.ncbi.nlm.nih.gov/books/NBK507907/

Smith, J. C., Ellenberger, H. H., Ballanyi, K., Richter, D. W., & Feldman, J. L. (1991). Pre-Bötzinger Complex: A Brainstem Region That May Generate Respiratory Rhythm in Mammals. *Science (New York, N.Y.)*, *254*(5032), 726–729.

Soman, S. M., Vijayakumar, N., Thomson, P., Ball, G., Hyde, C., & Silk, T. J. (2023). Functional and structural brain network development in children with attention

deficit hyperactivity disorder. *Human Brain Mapping*, *44*(8), 3394–3409. https://doi.org/10.1002/hbm.26288

Soos, M. P., & McComb, D. (2023). Sinus Arrhythmia. In *StatPearls*. StatPearls Publishing. http://www.ncbi.nlm.nih.gov/books/NBK537011/

Sporns, O. (2016). *Networks of the Brain*. MIT Press.

Sporns, O., Honey, C. J., & Kötter, R. (2007). Identification and Classification of Hubs in Brain Networks. *PLoS ONE*, *2*(10), e1049. https://doi.org/10.1371/journal.pone.0001049

Stam, C. J., Nolte, G., & Daffertshofer, A. (2007). Phase lag index: Assessment of functional connectivity from multi channel EEG and MEG with diminished bias from common sources. *Human Brain Mapping*, *28*(11), 1178–1193. https://doi.org/10.1002/hbm.20346

Stettner, G. M., & Kubin, L. (2013). Antagonism of orexin receptors in the posterior hypothalamus reduces hypoglossal and cardiorespiratory excitation from the perifornical hypothalamus. *Journal of Applied Physiology (Bethesda, Md.: 1985)*, *114*(1), 119–130. https://doi.org/10.1152/japplphysiol.00965.2012

Strauß, A., Wöstmann, M., & Obleser, J. (2014). Cortical Alpha oscillations as a tool for auditory selective inhibition. *Frontiers in Human Neuroscience*, *8*. https://www.frontiersin.org/articles/10.3389/fnhum.2014.00350

Suarez, L. E., Yovel, Y., van den Heuvel, M. P., Sporns, O., Assaf, Y., Lajoie, G., & Misic, B. (2022). A connectomics-based taxonomy of mammals. *eLife*, *11*, e78635. https://doi.org/10.7554/eLife.78635

Teplan, M. (2002). FUNDAMENTALS OF EEG MEASUREMENT. *MEASUREMENT SCIENCE REVIEW*, *2*.

Tewarie, P., Schoonheim, M. M., Stam, C. J., Meer, M. L. van der, Dijk, B. W. van, Barkhof, F., Polman, C. H., & Hillebrand, A. (2013). Cognitive and Clinical Dysfunction, Altered MEG Resting-State Networks and Thalamic Atrophy in Multiple Sclerosis. *PLOS ONE*, *8*(7), e69318. https://doi.org/10.1371/journal.pone.0069318

Travel Adaptor for New Zealand. (2023). Electrical Safety First. Retrieved 17 October 2023, from https://www.electricalsafetyfirst.org.uk/guidance/advice-for-you/when-travelling/travel-adaptor-for-new-zealand/

Trevisan, M. E., Boufleur, J., Soares, J. C., Haygert, C. J. P., Ries, L. G. K., & Corrêa, E. C. R. (2015). Diaphragmatic amplitude and accessory inspiratory muscle activity in nasal and mouth-breathing adults: A cross-sectional study. *Journal of Electromyography and Kinesiology*, *25*(3), 463–468. https://doi.org/10.1016/j.jelekin.2015.03.006

Ushamohan, B., Rajasekaran, A. K., Belur, Y. K., Srinivasan, T., & Ilavarasu, J. V. (2020). Bhramari Pranayama as an aid to meditation: A review of classical yoga texts. *International Journal of Yoga - Philosophy, Psychology and Parapsychology*, *8*(2), 58–68.

van den Broek, S. P., Reinders, F., Donderwinkel, M., & Peters, M. J. (1998). Volume conduction effects in EEG and MEG. *Electroencephalography and Clinical Neurophysiology*, *106*(6), 522–534. https://doi.org/10.1016/S0013-4694(97)00147-8

van der Zwan, J. E., de Vente, W., Huizink, A. C., Bögels, S. M., & de Bruin, E. I. (2015). Physical activity, mindfulness meditation, or heart rate variability biofeedback for stress reduction: A randomized controlled trial. *Applied Psychophysiology and Biofeedback*, *40*(4), 257–268. https://doi.org/10.1007/s10484-015-9293-x

van Mierlo, P., Höller, Y., Focke, N. K., & Vulliemoz, S. (2019). Network Perspectives on Epilepsy Using EEG/MEG Source Connectivity. *Frontiers in Neurology, 10*. https://www.frontiersin.org/articles/10.3389/fneur.2019.00721

Vazquez, M., Jing, J., Dauwels, J., & Vialatte, F. (2013). Automated detection of paroxysmal gamma waves in meditation EEG. In *Acoustics, Speech, and Signal Processing, 1988. ICASSP-88., 1988 International Conference on* (p. 1196). https://doi.org/10.1109/ICASSP.2013.6637839

Vialatte, F. B., Bakardjian, H., Prasad, R., & Cichocki, A. (2009). EEG paroxysmal gamma waves during Bhramari Pranayama: A yoga breathing technique. *Consciousness and Cognition*, *18*(4), 977–988. https://doi.org/10.1016/j.concog.2008.01.004

Vinck, M., Oostenveld, R., van Wingerden, M., Battaglia, F., & Pennartz, C. M. A. (2011). An improved index of phase-synchronization for electrophysiological data in the presence of volume-conduction, noise and sample-size bias. *NeuroImage*, *55*(4), 1548–1565. https://doi.org/10.1016/j.neuroimage.2011.01.055

von Leupoldt, A., & Dahme, B. (2005). Cortical substrates for the perception of dyspnea. *Chest*, *128*(1), 345–354. https://doi.org/10.1378/chest.128.1.345

Watts, D. J., & Strogatz, S. H. (1998). Collective dynamics of 'small-world' networks. *Nature*, *393*(6684), Article 6684. https://doi.org/10.1038/30918

Weisz, N., Hartmann, T., Müller, N., Lorenz, I., & Obleser, J. (2011). Alpha Rhythms in Audition: Cognitive and Clinical Perspectives. *Frontiers in Psychology*, *2*, 73. https://doi.org/10.3389/fpsyg.2011.00073

Weitzberg, E., & Lundberg, J. O. N. (2002). Humming greatly increases nasal nitric oxide. *American Journal of Respiratory and Critical Care Medicine*, *166*(2), 144–145. https://doi.org/10.1164/rccm.200202-138BC

Williams, R. H., & Burdakov, D. (2008). Hypothalamic orexins/hypocretins as regulators of breathing. *Expert Reviews in Molecular Medicine*, *10*, e28. https://doi.org/10.1017/S1462399408000823

Winkler, I., Haufe, S., & Tangermann, M. (2011). Automatic Classification of Artifactual ICA-Components for Artifact Removal in EEG Signals. *Behavioral and Brain Functions*, *7*(1), 30. https://doi.org/10.1186/1744-9081-7-30

Xing, C.-Y., Tarumi, T., Liu, J., Zhang, Y., Turner, M., Riley, J., Tinajero, C. D., Yuan, L.-J., & Zhang, R. (2017). Distribution of cardiac output to the brain across the adult lifespan. *Journal of Cerebral Blood Flow & Metabolism*, *37*(8), 2848–2856. https://doi.org/10.1177/0271678X16676826

Xing, M., Tadayonnejad, R., MacNamara, A., Ajilore, O., DiGangi, J., Phan, K. L., Leow, A., & Klumpp, H. (2016). Resting-state Thata band connectivity and graph analysis in generalized social anxiety disorder. *NeuroImage : Clinical*, *13*, 24–32. https://doi.org/10.1016/j.nicl.2016.11.009

Yang, C. F., Kim, E. J., Callaway, E. M., & Feldman, J. L. (2020). Monosynaptic Projections to Excitatory and Inhibitory preBötzinger Complex Neurons. *Frontiers in Neuroanatomy*, *14*, 58. https://doi.org/10.3389/fnana.2020.00058

Yao, D., Qin, Y., Hu, S., Dong, L., Bringas Vega, M. L., & Valdés Sosa, P. A. (2019). Which Reference Should We Use for EEG and ERP practice? *Brain Topography*, *32*(4), 530–549. https://doi.org/10.1007/s10548-019-00707-x

Yokota, S., Oka, T., Asano, H., & Yasui, Y. (2016). Orexinergic fibers are in contact with Kölliker-Fuse nucleus neurons projecting to the respiration-related nuclei in the medulla oblongata and spinal cord of the rat. *Brain Research*, *1648*(Pt A), 512–523. https://doi.org/10.1016/j.brainres.2016.08.020

Young, J. K., Wu, M., Manaye, K. F., Kc, P., Allard, J. S., Mack, S. O., & Haxhiu, M. A. (2005). Orexin stimulates breathing via medullary and spinal pathways. *Journal of Applied Physiology (Bethesda, Md.: 1985)*, *98*(4), 1387–1395. https://doi.org/10.1152/japplphysiol.00914.2004

Yu, X., Fumoto, M., Nakatani, Y., Sekiyama, T., Kikuchi, H., Seki, Y., Sato-Suzuki, I., & Arita, H. (2011). Activation of the anterior prefrontal cortex and serotonergic system is associated with improvements in mood and EEG changes induced by Zen meditation practice in novices. *International Journal of Psychophysiology*, *80*(2), 103–111. https://doi.org/10.1016/j.ijpsycho.2011.02.004

Zaccaro, A., Piarulli, A., Laurino, M., Garbella, E., Menicucci, D., Neri, B., & Gemignani, A. (2018). How Breath-Control Can Change Your Life: A Systematic Review on Psycho-Physiological Correlates of Slow Breathing. *Frontiers in Human Neuroscience*, *12*, 353. https://doi.org/10.3389/fnhum.2018.00353

Zalesky, A., Fornito, A., & Bullmore, E. T. (2010). Network-based statistic: Identifying differences in brain networks. *NeuroImage*, *53*(4), 1197–1207. https://doi.org/10.1016/j.neuroimage.2010.06.041

Zheng, G., Qi, X., Li, Y., Zhang, W., & Yu, Y. (2018). A Comparative Study of Standardized Infinity Reference and Average Reference for EEG of Three Typical Brain States. *Frontiers in Neuroscience*, *12*. https://www.frontiersin.org/articles/10.3389/fnins.2018.00158

Zheng, M.-X., Shen, Y.-D., Hua, X.-Y., Hou, A.-L., Zhu, Y., & Xu, W.-D. (2018). Cortical Reorganization in Dual Innervation by Single Peripheral Nerve. *Neurosurgery*, *83*(4), 819–826. https://doi.org/10.1093/neuros/nyx474

Zuo, X.-N., Ehmke, R., Mennes, M., Imperati, D., Castellanos, F. X., Sporns, O., & Milham, M. P. (2012). Network centrality in the human functional connectome. *Cerebral Cortex (New York, N.Y.: 1991)*, *22*(8), 1862–1875. https://doi.org/10.1093/cercor/bhr269

Appendices

Appendix 1. Figures

Sensor space Alpha filtered

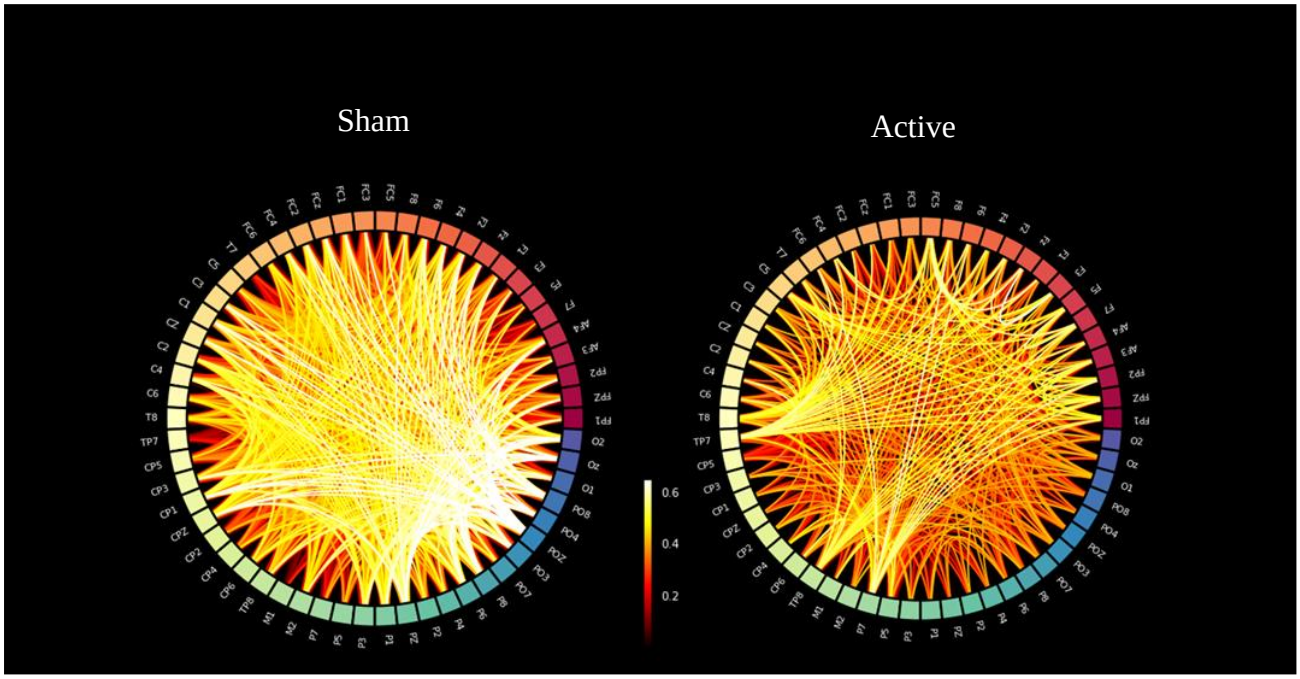

Active source space recontraction reorientated.

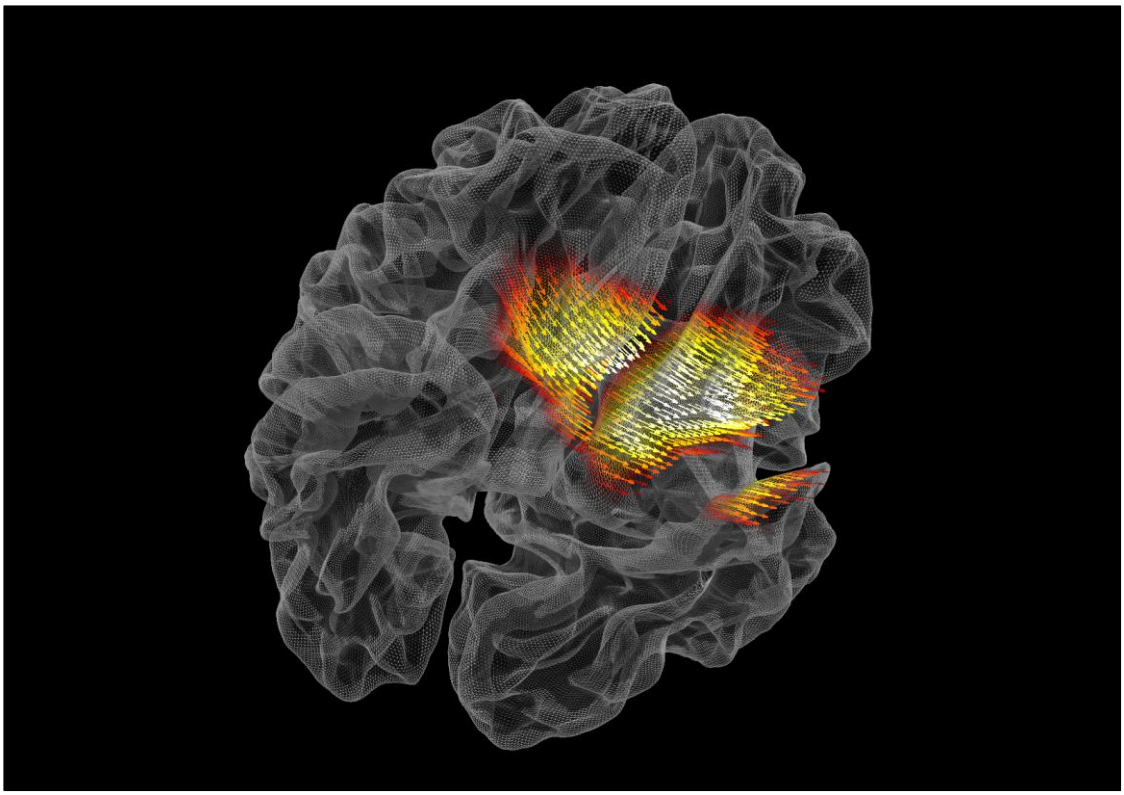

Appendix 2. Code

Author: Geet Vashista

```
import mne_bids

# import mne_connectivity

import os.path as op

import numpy as np

import matplotlib.pyplot as plt

import mne

from mne.datasets import fetch_fsaverage

from mne.beamformer import make_lcmv, apply_lcmv_epochs


plt.matplotlib.use('Qt5Agg')


# directory containing the data for all subjects + parameters for frequency bands and epoch time

tmin, tmax = (0, 60)

# freqs = (2, 5, 10, 20, 50)

# n_songs = 6

# n_electrodes = 64

# subject_ids = '757'
```

```
# Load the data for this subject - need to have subject_identifier when loading each

data_file = r'C:\Users\em17531\Desktop\Chip_EEG_data\Acquisition 01.dat'

raw = mne.io.read_raw_curry(data_file, preload=True, verbose=None)


# Setting line noise

raw.info['line_freq'] = 50


# Remove channels not used in analysis

raw.drop_channels(['VEOG', 'HEOG', 'EKG', 'EMG', 'Trigger'])


# Mark bad channels

# raw.info['bads'] = find_bad_channels(raw)


# BIDS standardization of the data (for storage)

bids_path = mne_bids.BIDSPath(subject='Chip',

                              task='breathing augmentation',

                              root=r'C:\Users\em17531\Desktop')


mne_bids.write_raw_bids(raw, bids_path=bids_path, allow_preload=True,

format='BrainVision', overwrite=True)
```

```
bids_path = mne_bids.BIDSPath(subject='Chip',
                              task='breathing augmentation',
                              root=r'C:\Users\em17531\Desktop')


raw_BIDS = mne_bids.read_raw_bids(bids_path)
raw_BIDS.load_data()
raw_BIDS.plot(block=True)
# Notch filter (50 Hz)
raw_notch = raw_BIDS.copy().notch_filter(np.arange(50, 500, 50))


# high pass filter set to 1 Hz (to 100 Hz)
raw_filtered = raw_notch.copy().filter(l_freq=1, h_freq=100)


# Virtual reference (average referencing here)
raw_avg_ref = raw_filtered.copy().set_eeg_reference(ref_channels='average')


# Interpolation of bad channels
#raw_interp = raw_avg_ref.interpolate_bads(reset_bads=False)


# downsample data from to 250 Hz
raw_downsampled = raw_avg_ref.resample(250, npad="auto")
```

```
#del raw

del raw_notch

del raw_filtered


# Independent Components Analysis (ICA) for artifact removal

ica = mne.preprocessing.ICA(n_components=20, random_state=0)

ica.fit(raw_downsampled)

ica.plot_sources(raw_downsampled, block=True)

ica.plot_components()


raw_ica = ica.apply(raw_downsampled.copy())

raw_ica.plot(block=True)


events = mne.events_from_annotations(raw_ica)


# if x.shape[0] == n_songs*2:

#     events, event_id = mne.events_from_annotations(raw_ica)

#

#     # extract our 6 epochs of interest (start of each song)

#     events2 = events[0 : : 2]
```

```
#

# else:

#     events, event_id = mne.events_from_annotations(raw_ica)

#     events = np.delete(events, 0, 0)

#     del event_id["8"]

#

#     # extract our 6 epochs of interest (start of each song)

#     events2 = events[0 : : 2]


# epoch data

picks = mne.pick_types(raw_ica.info, meg=False, eeg=True, stim=False, eog=False, exclude='bads')

epochs_org = mne.Epochs(raw_ica, events=events[0], event_id=events[1], proj=True, picks=picks, baseline=None, preload=True, tmin=tmin, tmax=tmax)


epochs_org.drop_channels(['F11', 'F12', 'FT11', 'FT12', 'CB1', 'CB2'])

evocked = epochs_org.average(method='mean',by_event_type=True)



# Calculate EEG connectivity, here wPLI (double check freqs!)

# con = mne_connectivity.spectral_connectivity_time(epochs, freqs=freqs, method='wpli', mode='multitaper',
```

```
#                                       fmin=(1., 4., 8., 13., 31), fmax=(3., 7., 12., 30., 100),

#                                       sfreq=ica.info['sfreq'], average=False)


# im = plt.imshow(con)

# plt.ylabel("Channels")

# plt.xlabel("Channels")

# plt.show()


# Download fsaverage files

fs_dir = fetch_fsaverage(verbose=True)

subjects_dir = op.dirname(fs_dir)


# The files live in:

subject = "fsaverage"

trans = "fsaverage"  # MNE has a built-in fsaverage transformation

src = op.join(fs_dir, "bem", "fsaverage-ico-5-src.fif")

bem = op.join(fs_dir, "bem", "fsaverage-5120-5120-5120-bem-sol.fif")



# Clean channel names to be able to use a standard 1005 montage

new_names = dict(
```

```
    (ch_name, ch_name.rstrip(".").upper().replace("Z", "z").replace("FP", "Fp"))
    for ch_name in epochs_org.ch_names
)
epochs_org.rename_channels(new_names)

# Read and set the EEG electrode locations, which are already in fsaverage's
# space (MNI space) for standard_1020:
montage = mne.channels.make_standard_montage("standard_1005")
epochs_org.set_montage(montage)
epochs_org.set_eeg_reference(projection=True)  # needed for inverse modeling

fwd = mne.make_forward_solution(
    epochs_org.info, trans=trans, src=src, bem=bem, eeg=True, mindist=5.0,
n_jobs=None
)

data_cov = mne.compute_covariance(epochs_org, tmin=0.01, tmax=0.25,
                                  method='empirical')
noise_cov = mne.compute_covariance(epochs_org, tmin=-0.2, tmax=0,
                                   method='empirical')
```

```
sel = mne.pick_channels(raw_ica.info['ch_names'], raw_ica.info['ch_names'])
epochs_org.pick(['eeg'])


filters_vec = make_lcmv(raw_ica.info, fwd, data_cov, reg=0.05,
                        noise_cov=noise_cov, pick_ori='vector',
                        weight_norm='unit-noise-gain', rank='info', reduce_rank=True)


# filters_Volvec = make_lcmv(raw_ica.info, fwd, data_cov, reg=0.05,
#                         noise_cov=noise_cov, pick_ori='vector',
#                         weight_norm='unit-noise-gain-invariant', rank=None)


# src = fwd['src']


stc_vec_org = apply_lcmv_epochs(epochs_org, filters_vec)
stc_vec_evo_0 = mne.beamformer.apply_lcmv(evocked[0], filters_vec)
stc_vec_evo_1 = mne.beamformer.apply_lcmv(evocked[1], filters_vec)
stc_vec_evo_2 = mne.beamformer.apply_lcmv(evocked[2], filters_vec)
# stc_Volvec = apply_lcmv_epochs(epochs_org, filters_Volvec)


#  visualization
mne.viz.set_3d_backend('notebook')
```

stc_vec_org.plot(hemi='both')

stc_vec.plot(hemi='both', views=['coronal', 'sagittal', 'axial'])

```
from matplotlib import pyplot as plt
import pathlib
import mne
import mne_connectivity
import numpy as np
import mne.stats
from scipy import stats
import scipy

directory = r'C:\Users\em17531\Desktop\Clean_data'
data = []

folder = pathlib.Path(directory).glob('*')
for file in folder:
    data.append(mne.read_epochs(file))

sham = evokeds[2].compute_psd()
buds = evokeds[1].compute_psd()
```

import pathlib

import mne

import numpy as np

import scipy

from scipy import stats

directory = r'C:\Users\em17531\Desktop\Clean_data'

data = []

folder = pathlib.Path(directory).glob('*')

for file in folder:

data.append(mne.read_epochs(file))

```
temp_master_buds = []
for i in data:
    temp = i[1].get_data()
    temp_master_buds.append(temp)



temp_master_sham = []
for i in data:
    temp = i[2].get_data()
    temp_master_sham.append(temp)
del temp

buds_master = np.array(temp_master_buds)
del temp_master_buds
sham_master = np.array(temp_master_sham)
del temp_master_sham

buds_master = np.mean(buds_master, axis= 1)
sham_master = np.mean(sham_master, axis= 1)

fs = 250
```

```
# Theta

fb = [4, 7]

passband = [fb[0] / (fs / 2.0), fb[1] / (fs / 2.0)]

passband = np.ravel(passband)

b, a = scipy.signal.butter(5, passband, "bandpass", analog=False, output="ba")


filtered_buds = scipy.signal.filtfilt(b, a, buds_master, axis=2)

filtered_sham = scipy.signal.filtfilt(b, a, sham_master, axis=2)


input_buds = np.mean(filtered_buds, axis=2)

input_sham = np.mean(filtered_sham, axis=2)


_, p_val_theta = stats.ttest_rel(input_buds,input_sham,axis=0,nan_policy='propagate')



# Alpha

fb = [8, 12]

passband = [fb[0] / (fs / 2.0), fb[1] / (fs / 2.0)]

passband = np.ravel(passband)
```

```
b, a = scipy.signal.butter(5, passband, "bandpass", analog=False, output="ba")


filtered_buds = scipy.signal.filtfilt(b, a, buds_master, axis=2)

filtered_sham = scipy.signal.filtfilt(b, a, sham_master, axis=2)


input_buds = np.mean(filtered_buds, axis=2)

input_sham = np.mean(filtered_sham, axis=2)


_, p_val_alpha = stats.ttest_rel(input_buds,input_sham,axis=0,nan_policy='propagate')



# Beta

fb = [13, 30]

passband = [fb[0] / (fs / 2.0), fb[1] / (fs / 2.0)]

passband = np.ravel(passband)

b, a = scipy.signal.butter(5, passband, "bandpass", analog=False, output="ba")


filtered_buds = scipy.signal.filtfilt(b, a, buds_master, axis=2)

filtered_sham = scipy.signal.filtfilt(b, a, sham_master, axis=2)


input_buds = np.mean(filtered_buds, axis=2)
```

```
input_sham = np.mean(filtered_sham, axis=2)


_, p_val_beta = stats.ttest_rel(input_buds,input_sham,axis=0,nan_policy='propagate')




# Extras


p_val_band = p_val_beta


temp_list = list(p_val_band)
index = []
for i in p_val_band:
    if i <= 0.05:
        index.append(temp_list.index(i))
print(index)




[print(p_val_band[i]) for i in index]
```

```
print(sham_temp[33])

print(buds_temp[33])

import numpy as np

import bct

from scipy import stats



# Load data by wave band

# Fill in the correct file path here


# buds_degree_centerality = bct.strengths_und(buds)

# buds_betweenness_centrality = bct.betweenness_wei(buds)

# buds_eig_centrality = bct.eigenvector_centrality_und(buds)

# buds_clust_coef = bct.clustering_coef_wu(buds)


# Source space

Beta_buds = np.load('Beta_buds_wpli.npy')

Beta_sham = np.load('Beta_sham_wpli.npy')


Alpha_buds = np.load('Alpha_buds_wpli.npy')

Alpha_sham = np.load('Alpha_sham_wpli.npy')
```

```
Theta_buds = np.load('Theta_buds_wpli.npy')

Theta_sham = np.load('Theta_sham_wpli.npy')


# Sensor space


Buds_master = np.load('sensor_space_buds.npy')

Sham_master = np.load('sensor_space_sham.npy')


Buds_master = np.mean(Buds_master, axis= 1)

Sham_master = np.mean(Sham_master, axis= 1)


Beta_buds = Buds_master[:, :, :, 1]

Beta_sham = Sham_master[:, :, :, 1]


Alpha_buds = Buds_master[:, :, :, 2]

Alpha_sham = Sham_master[:, :, :, 2]


Theta_buds = Buds_master[:, :, :, 3]

Theta_sham = Sham_master[:, :, :, 3]
```

```
del Buds_master

del Sham_master


# node strength


#### Theta #####

Theta_buds_strength_temp = []

for i in range(0, 14):

    temp_array = bct.strengths_und(Theta_buds[i, :, :])

    Theta_buds_strength_temp.append(temp_array)

    del temp_array

Theta_buds_strength = np.array(Theta_buds_strength_temp)

del Theta_buds_strength_temp


Theta_sham_strength_temp = []

for i in range(0, 14):

    temp_array = bct.strengths_und(Theta_sham[i, :, :])

    Theta_sham_strength_temp.append(temp_array)

    del temp_array

Theta_sham_strength = np.array(Theta_sham_strength_temp)

del Theta_sham_strength_temp
```

```
    # Zeroing negative phasing
Theta_sham_strength[Theta_sham_strength<0] = 0
Theta_buds_strength[Theta_buds_strength<0] = 0


    # Stats
T_val, p_val_theta = stats.ttest_rel(Theta_buds_strength, Theta_sham_strength)
np.nan_to_num(p_val_theta, copy=False, nan=1)
strength_Theta_fdc = stats.false_discovery_control(p_val_theta)


### Alpha ###


Alpha_buds_strength_temp = []
for i in range(0, 14):
    temp_array = bct.strengths_und(Alpha_buds[i, :, :])
    Alpha_buds_strength_temp.append(temp_array)
    del temp_array
Alpha_buds_strength = np.array(Alpha_buds_strength_temp)
del Alpha_buds_strength_temp


Alpha_sham_strength_temp = []
```

```
for i in range(0, 14):
    temp_array = bct.strengths_und(Alpha_sham[i, :, :])
    Alpha_sham_strength_temp.append(temp_array)
    del temp_array
Alpha_sham_strength = np.array(Alpha_sham_strength_temp)
del Alpha_sham_strength_temp

    # Zeroing negative phasing
Alpha_buds_strength[Alpha_buds_strength<0] = 0
Alpha_sham_strength[Alpha_sham_strength<0] = 0

# Stats
T_val, p_val_alpha = stats.ttest_rel(Alpha_buds_strength, Alpha_sham_strength)
np.nan_to_num(p_val_alpha, copy=False, nan=1)
strength_alpha_fdc = stats.false_discovery_control(p_val_alpha)

### Beta ####

Beta_buds_strength_temp = []
for i in range(0, 14):
    temp_array = bct.strengths_und(Beta_buds[i, :, :])
```

```
    Beta_buds_strength_temp.append(temp_array)
    del temp_array
Beta_buds_strength = np.array(Beta_buds_strength_temp)
del Beta_buds_strength_temp


Beta_sham_strength_temp = []
for i in range(0, 14):
    temp_array = bct.strengths_und(Beta_sham[i, :, :])
    Beta_sham_strength_temp.append(temp_array)
    del temp_array
Beta_sham_strength = np.array(Beta_sham_strength_temp)
del Beta_sham_strength_temp


    # Zeroing negative phasing
Beta_buds_strength[Beta_buds_strength<0] = 0
Beta_sham_strength[Beta_sham_strength<0] = 0


# Stats
T_val, p_val_beta = stats.ttest_rel(Beta_buds_strength, Beta_sham_strength)
np.nan_to_num(p_val_beta, copy=False, nan=1)
strength_Beta_fdc = stats.false_discovery_control(p_val_beta)
```

```
# Extras


band = p_val_beta


temp_list = list(band)

index = []

for i in band:

    if i <= 0.05:

        index.append(temp_list.index(i))

print(index)

print([band[i] for i in index])




temp = 0

for i in p_val_beta:

    if i <= 0.05:

        temp += 1

print(temp)


T_sham_temp = np.average(Theta_sham_strength, axis=0)
```

```
T_buds_temp = np.average(Theta_buds_strength, axis=0)

A_sham_temp = np.average(Alpha_sham_strength, axis=0)

A_buds_temp = np.average(Alpha_buds_strength, axis=0)

B_sham_temp = np.average(Beta_sham_strength, axis=0)

B_buds_temp = np.average(Beta_buds_strength, axis=0)


print(B_sham_temp[55])

print(B_buds_temp[55])

import numpy as np

import bct

from scipy import stats



# load data


Beta_buds = np.load('Beta_buds_wpli.npy')

Beta_sham = np.load('Beta_sham_wpli.npy')


Alpha_buds = np.load('Alpha_buds_wpli.npy')

Alpha_sham = np.load('Alpha_sham_wpli.npy')
```

```
Theta_buds = np.load('Theta_buds_wpli.npy')

Theta_sham = np.load('Theta_sham_wpli.npy')


# Load Senser data


Buds_master = np.load('sensor_space_buds.npy')

Sham_master = np.load('sensor_space_sham.npy')


Buds_master = np.mean(Buds_master, axis= 1)

Sham_master = np.mean(Sham_master, axis= 1)


Beta_buds = Buds_master[:, :, :, 1]

Beta_sham = Sham_master[:, :, :, 1]


Alpha_buds = Buds_master[:, :, :, 2]

Alpha_sham = Sham_master[:, :, :, 2]


Theta_buds = Buds_master[:, :, :, 3]

Theta_sham = Sham_master[:, :, :, 3]


del Buds_master
```

```
del Sham_master



# Betweenness


#### Theta #####

Theta_buds_Betweenness_temp = []

for i in range(0, 14):

    temp_array = bct.betweenness_wei(Theta_buds[i, :, :])

    Theta_buds_Betweenness_temp.append(temp_array)

    del temp_array

Theta_buds_Betweenness = np.array(Theta_buds_Betweenness_temp)

del Theta_buds_Betweenness_temp


Theta_sham_Betweenness_temp = []

for i in range(0, 14):

    temp_array = bct.betweenness_wei(Theta_sham[i, :, :])

    Theta_sham_Betweenness_temp.append(temp_array)

    del temp_array

Theta_sham_Betweenness = np.array(Theta_sham_Betweenness_temp)

del Theta_sham_Betweenness_temp
```

```
    # Zeroing negative phasing
# Theta_buds_Betweenness[Theta_buds_Betweenness<0] = 0
# Theta_sham_Betweenness[Theta_sham_Betweenness<0] = 0


    # Stats
T_val, p_val_theta = stats.ttest_rel(Theta_buds_Betweenness,
Theta_sham_Betweenness)
np.nan_to_num(p_val_theta, copy=False, nan=1)
strength_Theta_fdc = stats.false_discovery_control(p_val_theta)


### Alpha ###


Alpha_buds_Betweenness_temp = []
for i in range(0, 14):
    temp_array = bct.betweenness_wei(Alpha_buds[i, :, :])
    Alpha_buds_Betweenness_temp.append(temp_array)
    del temp_array
Alpha_buds_Betweenness = np.array(Alpha_buds_Betweenness_temp)
del Alpha_buds_Betweenness_temp
```

```
Alpha_sham_Betweenness_temp = []
for i in range(0, 14):
    temp_array = bct.betweenness_wei(Alpha_sham[i, :, :])
    Alpha_sham_Betweenness_temp.append(temp_array)
    del temp_array
Alpha_sham_Betweenness = np.array(Alpha_sham_Betweenness_temp)
del Alpha_sham_Betweenness_temp


    # Zeroing negative phasing
# Alpha_buds_Betweenness[Alpha_buds_Betweenness<0] = 0
# Alpha_sham_Betweenness[Alpha_sham_Betweenness<0] = 0


# Stats
T_val, p_val_alpha = stats.ttest_rel(Alpha_buds_Betweenness,
Alpha_sham_Betweenness)
np.nan_to_num(p_val_alpha, copy=False, nan=1)
strength_alpha_fdc = stats.false_discovery_control(p_val_alpha)


### Beta ####


Beta_buds_Betweenness_temp = []
```

```
for i in range(0, 14):
    temp_array = bct.betweenness_wei(Beta_buds[i, :, :])
    Beta_buds_Betweenness_temp.append(temp_array)
    del temp_array
Beta_buds_Betweenness = np.array(Beta_buds_Betweenness_temp)
del Beta_buds_Betweenness_temp


Beta_sham_Betweenness_temp = []
for i in range(0, 14):
    temp_array = bct.betweenness_wei(Beta_sham[i, :, :])
    Beta_sham_Betweenness_temp.append(temp_array)
    del temp_array
Beta_sham_Betweenness = np.array(Beta_sham_Betweenness_temp)
del Beta_sham_Betweenness_temp


    # Zeroing negative phasing
# Beta_buds_Betweenness[Beta_buds_Betweenness<0] = 0
# Beta_sham_Betweenness[Beta_sham_Betweenness<0] = 0


# Stats
T_val, p_val_beta = stats.ttest_rel(Beta_buds_Betweenness, Beta_sham_Betweenness)
```

```
np.nan_to_num(p_val_beta, copy=False, nan=1)

strength_Beta_fdc = stats.false_discovery_control(p_val_beta)



# Extras



band = p_val_alpha



temp_list = list(band)

index = []

for i in band:

    if i <= 0.05:

        index.append(temp_list.index(i))

print(index)

print([band[i] for i in index])




temp = 0

for i in strength_Beta_fdc:

    if i <= 0.05:

        temp += 1

print(temp)
```

```
T_sham_temp = np.average(Theta_sham_Betweenness, axis=0)

T_buds_temp = np.average(Theta_buds_Betweenness, axis=0)

A_sham_temp = np.average(Alpha_sham_Betweenness, axis=0)

A_buds_temp = np.average(Alpha_buds_Betweenness, axis=0)

B_sham_temp = np.average(Beta_sham_Betweenness, axis=0)

B_buds_temp = np.average(Beta_buds_Betweenness, axis=0)




print(T_sham_temp[56])

print(T_buds_temp[56])


import numpy as np

import bct

from scipy import stats


# buds_eig_centrality = bct.eigenvector_centrality_und(buds)


# load data


Beta_buds = np.load('Beta_buds_wpli.npy')
```

```
Beta_sham = np.load('Beta_sham_wpli.npy')


Alpha_buds = np.load('Alpha_buds_wpli.npy')

Alpha_sham = np.load('Alpha_sham_wpli.npy')


Theta_buds = np.load('Theta_buds_wpli.npy')

Theta_sham = np.load('Theta_sham_wpli.npy')


# Sensor space


Buds_master = np.load('sensor_space_buds.npy')

Sham_master = np.load('sensor_space_sham.npy')


Buds_master = np.mean(Buds_master, axis= 1)

Sham_master = np.mean(Sham_master, axis= 1)


Beta_buds = Buds_master[:, :, :, 1]

Beta_sham = Sham_master[:, :, :, 1]


Alpha_buds = Buds_master[:, :, :, 2]

Alpha_sham = Sham_master[:, :, :, 2]
```

```
Theta_buds = Buds_master[:, :, :, 3]

Theta_sham = Sham_master[:, :, :, 3]


del Buds_master

del Sham_master


# clustering coefficient


#### Theta #####

Theta_buds_eigenvector_temp = []

for i in range(0, 14):

    temp_array = bct.eigenvector_centrality_und(Theta_buds[i, :, :])

    Theta_buds_eigenvector_temp.append(temp_array)

    del temp_array

Theta_buds_eigenvector = np.array(Theta_buds_eigenvector_temp)

del Theta_buds_eigenvector_temp


Theta_sham_eigenvector_temp = []

for i in range(0, 14):

    temp_array = bct.eigenvector_centrality_und(Theta_sham[i, :, :])
```

```
    Theta_sham_eigenvector_temp.append(temp_array)
    del temp_array
Theta_sham_eigenvector = np.array(Theta_sham_eigenvector_temp)
del Theta_sham_eigenvector_temp

    # Zeroing negative phasing
# Theta_buds_Betweenness[Theta_buds_Betweenness<0] = 0
# Theta_sham_Betweenness[Theta_sham_Betweenness<0] = 0

    # Stats
T_val, p_val_theta = stats.ttest_rel(Theta_buds_eigenvector, Theta_sham_eigenvector)
np.nan_to_num(p_val_theta, copy=False, nan=1)
eigenvector_Theta_fdc = stats.false_discovery_control(p_val_theta)

### Alpha ###

Alpha_buds_eigenvector_temp = []
for i in range(0, 14):
    temp_array = bct.eigenvector_centrality_und(Alpha_buds[i, :, :])
    Alpha_buds_eigenvector_temp.append(temp_array)
    del temp_array
```

```
Alpha_buds_eigenvector = np.array(Alpha_buds_eigenvector_temp)
del Alpha_buds_eigenvector_temp


Alpha_sham_eigenvector_temp = []
for i in range(0, 14):
    temp_array = bct.eigenvector_centrality_und(Alpha_sham[i, :, :])
    Alpha_sham_eigenvector_temp.append(temp_array)
    del temp_array
Alpha_sham_eigenvector = np.array(Alpha_sham_eigenvector_temp)
del Alpha_sham_eigenvector_temp


    # Zeroing negative phasing
# Alpha_buds_Betweenness[Alpha_buds_Betweenness<0] = 0
# Alpha_sham_Betweenness[Alpha_sham_Betweenness<0] = 0


# Stats
T_val, p_val_alpha = stats.ttest_rel(Alpha_buds_eigenvector, Alpha_sham_eigenvector)
np.nan_to_num(p_val_alpha, copy=False, nan=1)
eigenvector_alpha_fdc = stats.false_discovery_control(p_val_alpha)


### Beta ####
```

```
Beta_buds_eigenvector_temp = []
for i in range(0, 14):
    temp_array = bct.eigenvector_centrality_und(Beta_buds[i, :, :])
    Beta_buds_eigenvector_temp.append(temp_array)
    del temp_array
Beta_buds_eigenvector = np.array(Beta_buds_eigenvector_temp)
del Beta_buds_eigenvector_temp


Beta_sham_eigenvector_temp = []
for i in range(0, 14):
    temp_array = bct.eigenvector_centrality_und(Beta_sham[i, :, :])
    Beta_sham_eigenvector_temp.append(temp_array)
    del temp_array
Beta_sham_eigenvector = np.array(Beta_sham_eigenvector_temp)
del Beta_sham_eigenvector_temp


    # Zeroing negative phasing
# Beta_buds_Betweenness[Beta_buds_Betweenness<0] = 0
# Beta_sham_Betweenness[Beta_sham_Betweenness<0] = 0
```

```
# Stats

T_val, p_val_beta = stats.ttest_rel(Beta_buds_eigenvector, Beta_sham_eigenvector)

np.nan_to_num(p_val_beta, copy=False, nan=1)

clustering_Beta_fdc = stats.false_discovery_control(p_val_beta)



# Extras



band = p_val_beta



temp_list = list(band)

index = []

for i in band:

    if i <= 0.05:

        index.append(temp_list.index(i))

print(index)

print([band[i] for i in index])




temp = 0

for i in p_val_beta:

    if i <= 0.05:
```

```
        temp += 1

print(temp)



T_sham_temp = np.average(Theta_sham_eigenvector, axis=0)

T_buds_temp = np.average(Theta_buds_eigenvector, axis=0)

A_sham_temp = np.average(Alpha_sham_eigenvector, axis=0)

A_buds_temp = np.average(Alpha_buds_eigenvector, axis=0)

B_sham_temp = np.average(Beta_sham_eigenvector, axis=0)

B_buds_temp = np.average(Beta_buds_eigenvector, axis=0)



print(B_sham_temp[268])

print(B_buds_temp[268])

import numpy as np

import bct

from scipy import stats



# buds_clust_coef = bct.clustering_coef_wu(buds)



# load data



Beta_buds = np.load('Beta_buds_wpli.npy')
```

```
Beta_sham = np.load('Beta_sham_wpli.npy')


Alpha_buds = np.load('Alpha_buds_wpli.npy')

Alpha_sham = np.load('Alpha_sham_wpli.npy')


Theta_buds = np.load('Theta_buds_wpli.npy')

Theta_sham = np.load('Theta_sham_wpli.npy')


# Load senser data


Buds_master = np.load('sensor_space_buds.npy')

Sham_master = np.load('sensor_space_sham.npy')


Buds_master = np.mean(Buds_master, axis= 1)

Sham_master = np.mean(Sham_master, axis= 1)


Beta_buds = Buds_master[:, :, :, 1]

Beta_sham = Sham_master[:, :, :, 1]


Alpha_buds = Buds_master[:, :, :, 2]

Alpha_sham = Sham_master[:, :, :, 2]
```

```
Theta_buds = Buds_master[:, :, :, 3]

Theta_sham = Sham_master[:, :, :, 3]


del Buds_master

del Sham_master



# clustering coefficient


#### Theta #####

Theta_buds_clustering_temp = []

for i in range(0, 14):

    temp_array = bct.clustering_coef_wu(Theta_buds[i, :, :])

    Theta_buds_clustering_temp.append(temp_array)

    del temp_array

Theta_buds_clustering = np.array(Theta_buds_clustering_temp)

del Theta_buds_clustering_temp


Theta_sham_clustering_temp = []

for i in range(0, 14):
```

```
    temp_array = bct.clustering_coef_wu(Theta_sham[i, :, :])
    Theta_sham_clustering_temp.append(temp_array)
    del temp_array
Theta_sham_clustering = np.array(Theta_sham_clustering_temp)
del Theta_sham_clustering_temp


    # Zeroing negative phasing
# Theta_buds_Betweenness[Theta_buds_Betweenness<0] = 0
# Theta_sham_Betweenness[Theta_sham_Betweenness<0] = 0


    # Stats
T_val, p_val_theta = stats.ttest_rel(Theta_buds_clustering, Theta_sham_clustering)
np.nan_to_num(p_val_theta, copy=False, nan=1)
clustering_Theta_fdc = stats.false_discovery_control(p_val_theta)


### Alpha ###


Alpha_buds_clustering_temp = []
for i in range(0, 14):
    temp_array = bct.clustering_coef_wu(Alpha_buds[i, :, :])
    Alpha_buds_clustering_temp.append(temp_array)
```

```
    del temp_array
Alpha_buds_clustering = np.array(Alpha_buds_clustering_temp)
del Alpha_buds_clustering_temp


Alpha_sham_clustering_temp = []
for i in range(0, 14):
    temp_array = bct.clustering_coef_wu(Alpha_sham[i, :, :])
    Alpha_sham_clustering_temp.append(temp_array)
    del temp_array
Alpha_sham_clustering = np.array(Alpha_sham_clustering_temp)
del Alpha_sham_clustering_temp


    # Zeroing negative phasing
# Alpha_buds_Betweenness[Alpha_buds_Betweenness<0] = 0
# Alpha_sham_Betweenness[Alpha_sham_Betweenness<0] = 0


# Stats
T_val, p_val_alpha = stats.ttest_rel(Alpha_buds_clustering, Alpha_sham_clustering)
np.nan_to_num(p_val_alpha, copy=False, nan=1)
clustering_alpha_fdc = stats.false_discovery_control(p_val_alpha)
```

```
### Beta ####


Beta_buds_clustering_temp = []
for i in range(0, 14):
    temp_array = bct.clustering_coef_wu(Beta_buds[i, :, :])
    Beta_buds_clustering_temp.append(temp_array)
    del temp_array
Beta_buds_clustering = np.array(Beta_buds_clustering_temp)
del Beta_buds_clustering_temp


Beta_sham_clustering_temp = []
for i in range(0, 14):
    temp_array = bct.clustering_coef_wu(Beta_sham[i, :, :])
    Beta_sham_clustering_temp.append(temp_array)
    del temp_array
Beta_sham_clustering = np.array(Beta_sham_clustering_temp)
del Beta_sham_clustering_temp


    # Zeroing negative phasing
# Beta_buds_Betweenness[Beta_buds_Betweenness<0] = 0
# Beta_sham_Betweenness[Beta_sham_Betweenness<0] = 0
```

```
# Stats

T_val, p_val_beta = stats.ttest_rel(Beta_buds_clustering, Beta_sham_clustering)

np.nan_to_num(p_val_beta, copy=False, nan=1)

clustering_Beta_fdc = stats.false_discovery_control(p_val_beta)



# Extras



band = p_val_theta



temp_list = list(band)

index = []

for i in band:

    if i <= 0.05:

        index.append(temp_list.index(i))

print(index)

print([band[i] for i in index])



temp = 0

for i in p_val_alpha:
```

```
    if i <= 0.05:
        temp += 1
print(temp)


T_sham_temp = np.average(Theta_sham_clustering, axis=0)
T_buds_temp = np.average(Theta_buds_clustering, axis=0)
A_sham_temp = np.average(Alpha_sham_clustering, axis=0)
A_buds_temp = np.average(Alpha_buds_clustering, axis=0)
B_sham_temp = np.average(Beta_sham_clustering, axis=0)
B_buds_temp = np.average(Beta_buds_clustering, axis=0)


print(B_sham_temp[283])
print(B_buds_temp[283])
```